

Summer 8-2022

## Inspection of Flexible Fillers in Post-Tensioned Bridges

Carley Gonzalez  
gonzac46@my.erau.edu

Follow this and additional works at: <https://commons.erau.edu/edt>



Part of the [Civil Engineering Commons](#), and the [Structural Engineering Commons](#)

---

### Scholarly Commons Citation

Gonzalez, Carley, "Inspection of Flexible Fillers in Post-Tensioned Bridges" (2022). *PhD Dissertations and Master's Theses*. 675.

<https://commons.erau.edu/edt/675>

This Thesis - Open Access is brought to you for free and open access by Scholarly Commons. It has been accepted for inclusion in PhD Dissertations and Master's Theses by an authorized administrator of Scholarly Commons. For more information, please contact [commons@erau.edu](mailto:commons@erau.edu).

INSPECTION OF FLEXIBLE FILLERS IN POST-TENSIONED BRIDGES

By

Carley Nicole Barbara Gonzalez, E.I.T.

A Thesis Submitted to the College of Engineering, Department of Civil Engineering  
In Partial Fulfillment of the Requirements for the Degree of  
Master of Science in Civil Engineering

August 2022  
Embry-Riddle Aeronautical University  
Daytona Beach, Florida

INSPECTION OF FLEXIBLE FILLERS IN POST-TENSIONED BRIDGES

by

Carley Gonzalez

This thesis was prepared under the direction of the candidate's Thesis Committee Chair, Dr. Jeff Brown, Professor and Program Coordinator, Daytona Beach Campus; and Thesis Committee Members Dr. Dan Su, Professor, Daytona Beach Campus; and Dr. Ghada Ellithy, Professor, Daytona Beach Campus; and has been approved by the Thesis Committee. It was submitted to the Department of Civil Engineering in partial fulfillment of the requirements for the degree of Master of Science in Civil Engineering

Thesis Review Committee:

---

Jeff Brown, Ph.D.  
Committee Chair

---

Dan Su, Ph.D., P.E.  
Committee Member

---

Ghada Ellithy, Ph.D., P.E.  
Committee Member

---

Jeff Brown, Ph.D.  
Graduate Program Coordinator,  
Civil Engineering

---

Ashok Gurjar, Ph.D.  
Department Chair,  
Civil Engineering

---

Jim Gregory, Ph.D.  
Dean, College of Engineering

---

Christopher Grant, Ph.D., P.E.  
Associate Vice President of Academics

---

Date

## ACKNOWLEDGEMENTS

This research has been an adventure from beginning to end, I have made so many new friends and have had some awesome experiences. There are so many people for me to thank for supporting me throughout my journey.

First, I would like to thank the best advisor out there which is Dr. Brown, if it wasn't for his influence I would not be where I am today and I can't thank him enough for all the guidance he has given me over the years.

I would also like to thank the Civil Engineering Department; everyone has been so amazing and helpful throughout my time here at Embry-Riddle Aeronautical University (ERAU). Special thanks to Rosa who works so hard to keep the department running smoothly.

Next, I would like to thank my committee members Dr. Su and Dr. Ellithy, who have been super helpful in the development of this research and keeping me on track.

I would also like to thank all my friends and family who have supported me throughout the years, with special thanks to Chris who reviewed my thesis multiple times to ensure no mistakes made it through.

I would also like to thank the Florida Department of Transportation (FDOT) for not only funding this research but providing useful resources and awesome people who assisted in the research process. Big thanks to the Federal Highway Administration (FHWA) and ERAU for providing funding to make this project possible.

Finally, I would like to thank the wonderful folks at Advent Health who stitched me up after an unfortunate lab accident.

## ABSTRACT

The Florida Department of Transportation (FDOT) is currently pushing toward the use of flexible fillers (FF) in new post-tensioned (PT) bridges. Flexible fillers have several advantages compared to the currently used cementitious grouts (CG) and can offer longer-lasting structures by providing better corrosion protection and allowing for replaceable tendons, which reduces the overall maintenance costs over the structure's lifespan. Due to these fillers being used in new bridges, FDOT needs effective nondestructive evaluation (NDE) methods to employ in their biennial inspections. There are currently numerous NDE methods available to inspectors that have been used to identify defects in PT bridges that use CG, but the NDE methods identified in this study are specifically for PT bridges that use FFs. These methods are Visual Inspections, Radiography, and Thermoelasticity. After an extensive literature review, these methods became the most promising and feasible to perform given the resources available. It was found that visual inspections and radiography are both highly effective methods in evaluating these bridges, whereas thermoelasticity was not as successful. Visual examinations are currently performed on all bridge inspections, but it is important to identify visual indicators that are unique to PT bridges that use FF. Radiography is also an effective method in identifying defects, however there are some major drawbacks, such as the price and accessibility to the internal components of the bridge. Thermoelasticity also seemed like a promising NDE method due to its success in the mining industry, but after completing tests in the lab it was found that the results were inconsistent and inconclusive, therefore this method would not be beneficial to employ in the field. Based on the testing performed in this study, visual inspections and radiography are both recommended methods to use in future bridge inspections and more research should be conducted to create standardized inspection procedures for inspectors.

## TABLE OF CONTENTS

<b>CHAPTER 1: INTRODUCTION</b> .....	1
<b>1.1 Background</b> .....	1
<b>1.2 What is NDE:</b> .....	1
<b>1.3 What are PT bridges</b> .....	2
<b>1.4 Cementitious Grouts Vs. Flexible Filler</b> .....	5
<b>1.5 Tendon Failures in Post-Tensioned Bridges</b> .....	7
<b>1.5.1 Niles Channel Bridge</b> .....	8
<b>1.5.2 Mid Bay Bridge</b> .....	8
<b>1.5.3 Ringling Bridge</b> .....	9
<b>1.5.4 Roosevelt Bridge</b> .....	10
<b>CHAPTER 2: LITERATURE REVIEW</b> .....	12
<b>2.1 Ground Penetrating Radar (GPR):</b> .....	12
<b>2.2 Infrared Thermography (IRT):</b> .....	14
<b>2.3 Electrical Capacitance Tomography (ECT)</b> .....	14
<b>2.4 Magnetic Flux Leakage (MFL)</b> .....	16
<b>2.5 Impact Echo (IE):</b> .....	16
<b>2.6 Ultrasonic Tomography (UST):</b> .....	19
<b>2.7 Ultrasonic Echo (USE)</b> .....	20
<b>2.8 Sonic/Ultrasonic Pulse Velocity (SPV-UPV)</b> .....	20
<b>2.9 Low Frequency Ultrasound (LFUT)</b> .....	21
<b>2.10 Sounding</b> .....	22
<b>2.11 Visual Testing (VT)</b> .....	23
<b>2.12 Borescope (Bor):</b> .....	24
<b>2.13 Electrochemical Impedance Spectroscopy (EIS)</b> .....	25
<b>2.14 Radiography Methods</b> .....	26
<b>2.15 Conclusion</b> .....	27
<b>CHAPTER 3: VISUAL INSPECTIONS</b> .....	28
<b>3.1 Visual Indicators for Cementitious Grout vs Flexible Filler</b> .....	28
<b>3.2 Bridge Inspections</b> .....	29
<b>3.2.1 Seabreeze Bridge Inspection</b> .....	30
<b>3.2.2 Broadway Bridge Inspection</b> .....	32
<b>3.3 Inspection Guide:</b> .....	35

3.3.1 Three-Span Segmental Bridge .....	35
3.3.2 C-Pier .....	37
3.3.3 Straddle Bent Pier .....	38
3.4 Conclusion .....	40
<b>CHAPTER 4: RADIOGRAPHY .....</b>	<b>41</b>
4.1 Specimens.....	41
4.2 Equipment .....	45
4.3 Data Collection:.....	47
4.4 Results:.....	47
4.4.1 POSKOM PXM-20BT:.....	47
4.4.2 YXLON:.....	52
4.5 Conclusion:.....	56
<b>CHAPTER 5: THERMOELASTICITY .....</b>	<b>58</b>
5.1 Introduction.....	58
5.2 Finite Element Analysis (FEA) .....	60
5.2.1 Model Geometry.....	60
5.2.2 Material Properties .....	61
5.2.3 Boundary Conditions.....	61
5.2.4 Mesh Refinement Study.....	62
5.2.5 Results .....	64
5.3 Experimental Validation .....	65
5.3.1 Block geometry.....	65
5.3.2 Experimental setup .....	66
5.3.3 Testing parameters .....	67
5.3.4 Results .....	67
<b>CHAPTER 6: CONCLUSION.....</b>	<b>71</b>
6.1 Summary of Findings .....	71
6.2 Recommendations .....	71
6.3 Future Work.....	72
<b>CHAPTER 7: REFERENCES.....</b>	<b>74</b>
Acronyms .....	776
Appendix.....	77

## Table of Figures

<b>Figure 1: Reinforced concrete beam with no Prestressing.....</b>	<b>2</b>
<b>Figure 2: Pre-Tensioning vs. Post-Tensioning.....</b>	<b>4</b>
<b>Figure 3: Seabreeze Bridge (Left), Broadway Bridge (Right) .....</b>	<b>5</b>
<b>Figure 4: Duct filled with CG (Left) (FHWA, 2014), Duct filled with FF (Right) (Hamilton et al. 2017) .....</b>	<b>7</b>
<b>Figure 5: Corrosion of strands in the anchorage (Left), Anchorage of the Failed Tendon with Water Staining from the Leaking Expansion Joint (Right) (FDOT, 2002) .....</b>	<b>8</b>
<b>Figure 6: Tendon failures on the Mid-Bay Bridge (FDOT, 2002) .....</b>	<b>9</b>
<b>Figure 7: StructureScan Mini HR GPR unit (Left), GPR unit inspecting the external tendons (Right) (Hurlebaus, Hueste, Karthik, and Terzioglu, 2016).....</b>	<b>13</b>
<b>Figure 8: Sensor head (Top), Examples of the composite images gathered by the ECT device (Bottom) (Hurlebaus, Hueste, Karthik, and Terzioglu, 2016) .....</b>	<b>135</b>
<b>Figure 9: Reflected wave energy propagating through a duct .....</b>	<b>137</b>
<b>Figure 10: (Left) Shows the IE scanner test head, (Middle) Shows the PC data acquisition platform, (Right) Shows the IE device in use on an external duct (Hurlebaus, Hueste, Karthik, and Terzioglu, 2016) .....</b>	<b>18</b>
<b>Figure 11: (Left) A1040 MIRA device, (Right) results from the deviator blocks (left is defect key and right is the UST scan) (Hurlebaus, Hueste, Karthik, and Terzioglu, 2016). ..</b>	<b>19</b>
<b>Figure 12: SPV testing system along with impulse hammer, data acquisition system PC and ultrasonic transducer (Left), Photograph showing location of source impact and receiver for SPV testing (Right) (Hurlebaus, Hueste, Karthik, and Terzioglu, 2016) .....</b>	<b>21</b>
<b>Figure 13: Visual testing of an external tendon (Left) and end cap (Right) in PT Girder Specimen (Hurlebaus, Hueste, Karthik, and Terzioglu, 2016) .....</b>	<b>23</b>
<b>Figure 14: Depicts the borescope access port and the equipment used (Hurlebaus, Hueste, Karthik, and Terzioglu, 2016) .....</b>	<b>24</b>
<b>Figure 15: Images provided by the borescope inspection inside the external tendons depicting corrosion of the strands (Hurlebaus, Hueste, Karthik, and Terzioglu, 2016) ....</b>	<b>245</b>
<b>Figure 16: Localized corrosion damage for internal tendon in Stuart, FL (Roustan and Erblat, 2020 &amp; Detman and Rodriguez, 2020) .....</b>	<b>29</b>
<b>Figure 17: Seabreeze Bridge .....</b>	<b>30</b>
<b>Figure 18: Example of cracking (Left) and efflorescence (Right) from the eastbound Seabreeze Bridge Inspection .....</b>	<b>31</b>
<b>Figure 19: Impact Echo NDE performed on Seabreeze Bridge .....</b>	<b>32</b>
<b>Figure 20: Broadway Bridge.....</b>	<b>33</b>
<b>Figure 21: External ducts that were repaired from previous intrusive NDE inspection (Left) Rust stains on external tendon (Right).....</b>	<b>33</b>
<b>Figure 22: Ultrasonic Pulse Velocity (UPV) Testing .....</b>	<b>34</b>
<b>Figure 23: Electrical Impedance Inspection.....</b>	<b>34</b>
<b>Figure 24: Three-Span Segmental Bridge .....</b>	<b>35</b>
<b>Figure 25: Cracks due to tension in the middle of the span.....</b>	<b>36</b>
<b>Figure 26: Anchorage Region, protruding strands/defects (Right).....</b>	<b>37</b>
<b>Figure 27: Post-Tensioned C-Pier .....</b>	<b>37</b>



<b>Figure 28: Post-Tensioned C-Pier with cracks</b> .....	38
<b>Figure 29: Post-Tensioned Straddle Bent pier</b> .....	39
<b>Figure 30: Post-Tensioned Straddle Bent pier with cracks</b> .....	39
<b>Figure 31: Anchorage assembly</b> .....	42
<b>Figure 32: Anchorage mock-up showing varied strand and grip locations for testing</b> .....	42
<b>Figure 33: Type 5 Anchorage (FDOT SDG)</b> .....	43
<b>Figure 34: Filled External Tendon Mock-up</b> .....	44
<b>Figure 35: Internal Duct Large Scale Specimen (FDOT Project BDV31 977-93)</b> .....	45
<b>Figure 36: POSKOM PXM-20BT</b> .....	46
<b>Figure 37: YXLON</b> .....	47
<b>Figure 38: POSKOM PXM-20BT Setup</b> .....	48
<b>Figure 39: Specimen 1 Anchorage Cap Results: Images collected from POSKOM PXM-20BT from different angles</b> .....	49
<b>Figure 40: External Duct Mockup: Filled Anchorage Cap Results</b> .....	49
<b>Figure 41: Internal Specimen: Anchorage Cap Results</b> .....	50
<b>Figure 42: Anchorage Mockup: Duct Results</b> .....	51
<b>Figure 43: Specimen 2: Filled Duct Results</b> .....	52
<b>Figure 44: Anchorage Mockup: Trumpet Results</b> .....	52
<b>Figure 45: YXLON X-Ray Machine on Internal Duct Specimen</b> .....	53
<b>Figure 46: YXLON Machine on Internal Specimen Anchorage Cap</b> .....	54
<b>Figure 47: Internal Duct Specimen: Duct without strands</b> .....	55
<b>Figure 48: Internal Duct Specimen: Duct with strands 1ft away from end block (Left) and 5ft away from end block (Right)</b> .....	56
<b>Figure 49: Test setup and experimental typical result for thermal conductivity variations in rock specimens due to axial stress (Demirci, 2004)</b> .....	59
<b>Figure 50: Model Geometry</b> .....	60
<b>Figure 51: ANSYS Concrete Properties</b> .....	61
<b>Figure 52: Model Geometry &amp; Boundary Conditions</b> .....	62
<b>Figure 53: Mesh Refinement Study</b> .....	63
<b>Figure 54: .01 m Mesh Size</b> .....	63
<b>Figure 55: <math>k=.75 \text{ W/m } ^\circ\text{C}</math> (left), <math>k=2 \text{ W/m } ^\circ\text{C}</math> (Right)</b> .....	64
<b>Figure 56: Surface Temperature Profiles for Different Thermal Conductivities at T=5 min</b> .....	65
<b>Figure 57: Block that was tested on (Left), Identical block to show reinforcing (Right)</b> .....	66
<b>Figure 58: Testing Setup</b> .....	67
<b>Figure 59: Experiment 1 vs 2</b> .....	68
<b>Figure 60: Experiment 3 vs 4</b> .....	69
<b>Figure 61: Experiments 1-4</b> .....	70

## **CHAPTER 1: INTRODUCTION**

### **1.1 Background**

The purpose of this research is to determine effective nondestructive evaluation (NDE) methods for post-tensioned (PT) bridges using flexible fillers (FF). Historically, PT systems in bridge applications have relied on cementitious grouts (CG). Traditional grouts provide corrosion protection in much the same way as concrete protects mild reinforcement and prestressing steel in conventional concrete structures. For the case of internal ducts, CGs also provide a bond between the grouted tendon and the surrounding concrete. The wax or grease used in flexible filler systems provide corrosion protection by maintaining a physical barrier between the PT strands and corrosion-inducing elements (e.g., water). Unlike CG systems, FFs always result in an unbonded tendon. Due to these differences, it is important to develop an inspection protocol that works specifically for PT bridges using FFs.

### **1.2 What is NDE:**

Nondestructive testing is any kind of testing that is performed on the structure that does not cause permanent harm or require excessive repairs (e.g., visual inspections, radiography, etc.). There are many different NDE methods in use today that have been developed over the years, but all these methods are currently being geared towards CG instead of FF. Of these methods, none of them have been proven effective for evaluating bridges using CG. Most of these methods require a more intrusive inspection after the initial NDE is performed. As a result of this lapse in effective techniques, FDOT has transitioned to FF and still requires effective NDE methods to use on these bridges. After an extensive literature review and multiple conversations with FDOT, four main methods were determined to be the most promising and feasible to research given the project

timeline and resources: visual inspections, radiography, thermoelasticity, and ultrasound. This thesis focuses on visual inspections, radiography, and thermoelasticity.

### 1.3 What are PT bridges

Post-tensioned bridges rely upon a post-tensioning force to counteract the loads that are applied on the bridge. When a transverse load is applied to a beam, it creates compressive stresses on the top and tensile stresses on the bottom as shown in Figure 1. Prestressing and post-tensioning apply an additional compressive force along the axis of the member that generates a state of compression rather than tension, allowing a higher load capacity. It is important to keep as much of the bridge in compression as possible, according to AASHTO LRFD Bridge Design Specifications Section 5.9.2.3 “Stress Limits for Concrete”, very little to no tension stresses are allowed. Table 5.9.2.3b-1 “Tensile Stress Limits in Prestressed Concrete at Service Limit State after Losses” (AASHTO LRFD 8) explains each bridge scenario and the allowable tension stresses, ranging from no tension allowed to .6 ksi depending on the bridge type and environmental conditions (Table 1).

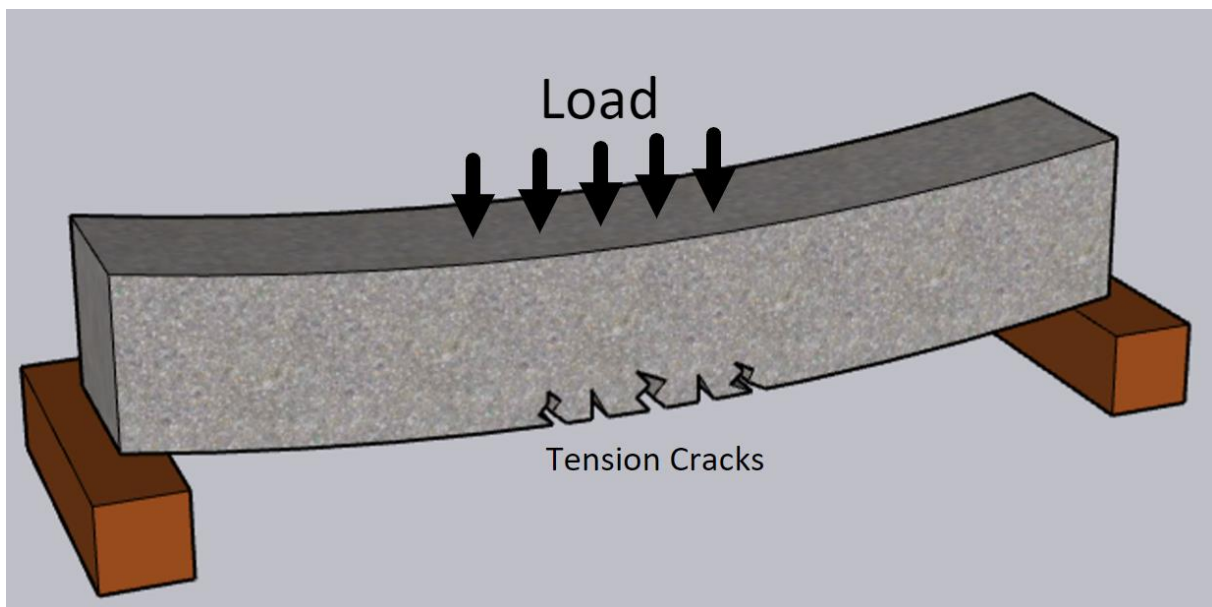


**Figure 1: Reinforced concrete beam with no Prestressing**

**Table 1: Tensile Stress Limits in Prestressed Concrete at Service Limit State after Losses  
(Table 5.9.2.3.2b-1 AASHTO LRFD Bridge Specifications)**

Bridge Type	Location	Stress Limit
<p>Other Than Segmentally Constructed Bridges</p> <p>These limits may be used for normal weight concrete with concrete compressive strengths for use in design up to 15.0 ksi and lightweight concrete up to 10.0 ksi.</p>	<p>Tension in the Precompressed Tensile Zone, Assuming Uncracked Sections</p> <ul style="list-style-type: none"> <li>For components with bonded prestressing tendons or reinforcement that are subjected to not worse than moderate corrosion conditions</li> <li>For components with bonded prestressing tendons or reinforcement that are subjected to severe corrosive conditions</li> <li>For components with unbonded prestressing tendons</li> </ul>	<p><math>0.19\lambda\sqrt{f'_c} \leq 0.6</math> (ksi)</p> <p><math>0.0948\lambda\sqrt{f'_c} \leq 0.3</math> (ksi)</p> <p>No tension</p>
<p>Segmentally Constructed Bridges</p> <p>These limits may be used for normal weight concrete with concrete compressive strengths for use in design up to 15.0 ksi and lightweight concrete up to 10.0 ksi.</p>	<p>Longitudinal Stresses through Joints in the Precompressed Tensile Zone</p> <ul style="list-style-type: none"> <li>Joints with minimum bonded auxiliary reinforcement through the joints sufficient to carry the calculated longitudinal tensile force at a stress of <math>0.5 f_y</math>; internal tendons or external tendons</li> <li>Joints without the minimum bonded auxiliary reinforcement through joints</li> </ul>	<p><math>0.0948\lambda\sqrt{f'_c} \leq 0.3</math> (ksi)</p> <p>No tension</p>
	<p>Transverse Stresses</p> <ul style="list-style-type: none"> <li>Tension in the transverse direction in precompressed tensile zone</li> </ul>	<p><math>0.0948\lambda\sqrt{f'_c} \leq 0.3</math> (ksi)</p>
	<p>Stresses in Other Areas</p> <ul style="list-style-type: none"> <li>For areas without bonded reinforcement</li> <li>In areas with bonded reinforcement sufficient to resist the tensile force in the concrete computed assuming an uncracked section, where reinforcement is proportioned using a stress of <math>0.5 f_y</math>, not to exceed 30.0 ksi</li> </ul>	<p>No tension</p> <p><math>0.19\lambda\sqrt{f'_c}</math> (ksi)</p>

There are two methods of prestressing: pre-tensioning and post-tensioning. In pre-tensioning, the steel tendons are stressed before the concrete is cast, whereas post-tensioning occurs after the concrete has been placed (Figure 2).

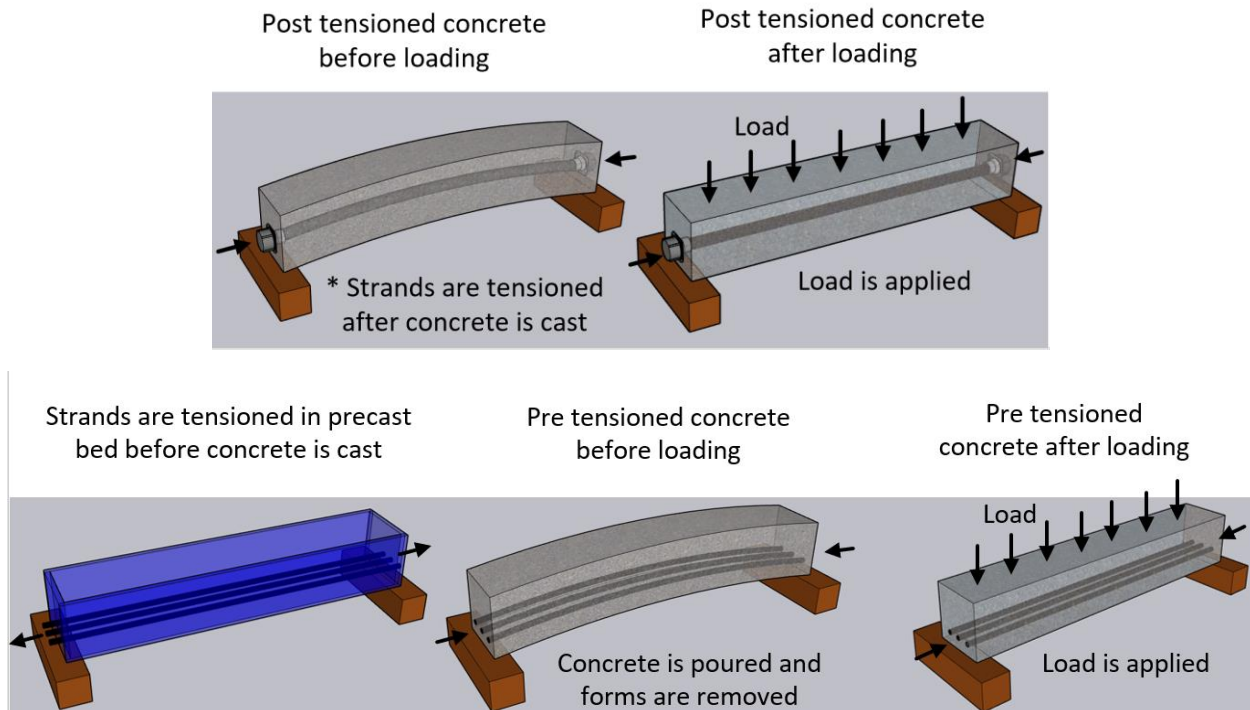


**Figure 2: Pre-Tensioning vs. Post-Tensioning**

There are two different kinds of post-tensioning ducts utilized in bridges: internal and external ducts. Internal ducts are embedded within the structure, which makes them difficult to access and inspect. This topic is explained more in the Radiography Section. External ducts are not embedded in the concrete, allowing for easier less intrusive inspections. External ducts are preferred by inspectors, allowing for a clear visual when performing field inspections. The differences can be seen below in Figure 3, which were taken from the Seabreeze and Broadway bridges, located in Daytona Beach, Florida. Both the eastbound and the westbound Seabreeze bridges are constructed with internal ducts, whereas the Broadway bridge utilizes external ducts. Both types of ducts run along the length of the bridge girders in these two examples. The Broadway bridge's external ducts allow for easy access, whereas the ducts utilized in the Seabreeze bridges are instead embedded in concrete.



**Figure 3: Seabreeze Bridge (Left), Broadway Bridge (Right)**

Both internal and external tendons are effective in counteracting the loads applied on the bridge. Thus, both types of tendons would be effective in supporting the structure. Issues will arise if a loss of this prestressing force occurs, which is why bridge inspections are performed every 2 years. With a loss of prestress or post-tensioning force, cracks and possible overall failure of the structure can occur. Current inspectors are extensively trained to look for any possible faults before they become larger problems. At this time, inspectors are trained on bridges that use CG instead of FF, therefore it is important to create methods that work well for these newly designed FF bridges.

#### **1.4 Cementitious Grouts Vs. Flexible Filler**

If proper mixing and injection procedures are not followed, cementitious grouts can undergo a process known as “bleed-water segregation,” meaning that the water from the concrete mix will separate from the solids after the grout is injected into the duct. This water then interacts with the steel strands and induces corrosion. FFs consist entirely of either grease or polycrystalline wax. This wax/grease can coat each individual strand creating a barrier from any moisture that could be introduced into the duct.

To incorporate FF into a duct, the material is heated and then pumped into the ducts; this requires extensive training of the personnel that would be installing/filling these ducts. FDOT currently has a training program that instructs the workers on how to properly fill/construct the ducts. FF is brought to the site as a solidified wax, where it is then heated and installed, whereas CG requires

the cement to be both brought and mixed with water on-site. This leads to more factors that can influence the grout quality, such as the amount of water added. Sometimes, more water is required to allow for fluid grout that will smoothly be pumped into the ducts. This excess water can lead to insufficient grout that does not fully protect the strands. Excess chlorides could also be introduced into this grout on-site depending on external environmental conditions. Due to FF being a wax or grease that is premade and sent to the site, the only thing that the workers need to focus on is the heat and pumping the material into the ducts avoiding possible voids. Having the material premixed and ready to go on-site is one less factor introduced into the construction process that could affect tendon quality.

FFs also allow for replaceable tendons, making maintenance easier to perform and more economical throughout the structure's life span. With CG, the tendon is bonded within the cement, which makes repairs difficult to perform. As these strands are encased in solid grout, it is not only difficult to inspect but to replace them as well. The entire tendon/duct would need to be removed if any defects are present, meaning an entirely new duct would need to take its place. This is a costly repair and, in most cases, requires temporary shutdown of the bridge while these repairs are made, which leads to major traffic disruptions. In the case of FF, if one or more strands need repair, it is possible to replace the tendon without replacing the entire duct. The tendon is removed, and more FF is pumped in once it has been replaced and re-tensioned. FF is more costly to initially install due to the material being more expensive compared to CG but makes for easier maintenance in the long run.

Due to FF being a softer material than CG, it provides no structural rigidity. Because of this, CG is required in locations that are subjected to the impact of live loads, such as the top slab transverse/longitudinal tendons in segmental box girders. (SDG Section 1.11.5 “Tendon Design”).

Although FF is not allowed in these locations, it is the preferred material for any other tendon within the bridge due to its replaceability and corrosion protection.



**Figure 4: Duct filled with CG (Left) (FHWA, 2014), Duct filled with FF (Right) (Hamilton et al. 2017)**

**Table 2: Cementitious Grout vs. Flexible Filler**

<b>Cementitious Grouts</b>	<b>Flexible Fillers</b>
<ul style="list-style-type: none"> <li>• Bonded System (not replaceable)</li> <li>• Can corrode over time from either poor grouting practice or defective grout materials</li> <li>• Initial installation is cheaper, but inspection costs increase overtime if defects occur</li> </ul>	<ul style="list-style-type: none"> <li>• Unbonded system (replaceable)</li> <li>• Extended Service Life</li> <li>• Minimize corrosion</li> <li>• Wax repels water and provides better protection for the strands</li> <li>• Commonly found in the Nuclear Industry</li> </ul>

### 1.5 Tendon Failures in Post-Tensioned Bridges

Corrosion of PT tendons has become a reoccurring issue in the state of Florida. This type of failure has been demonstrated in multiple bridges throughout the state. The examples that will be covered in this report include the Niles Channel Bridge, Mid-Bay Bridge, Ringling Bridge, and Roosevelt Bridge.



### 1.5.1 Niles Channel Bridge

The 1999 biennial inspection of the Niles Channel Bridge led to the discovery of failed longitudinal PT tendons. In this case, the boot connecting the duct to the steel pipe at the expansion joint was opened which led to active corrosion of the PT strands in the tendon (FDOT, 2002). This tendon was then quickly replaced to avoid further damage to the bridge. Once removed, inspectors noticed voids and pitting of the strands within the failed tendon. This failure was attributed to bleed water segregation initially, but after further investigation they learned that ocean salt spray was leaking into the expansion joints onto the anchorages and then into the duct, thus further corroding the strands/anchorages. After this incident, FDOT worked to better understand PT bridges and performed multiple different NDE methods such as MFL & Impact Echo to identify any other voids/defects that could be present within the bridge. After this incident, FDOT worked to control the grout quality and grouting techniques to further prevent possible voids in future ducts.



**Figure 5: Corrosion of strands in the anchorage (Left), Anchorage of the Failed Tendon with Water Staining from the Leaking Expansion Joint (Right) (FDOT, 2002)**

### 1.5.2 Mid Bay Bridge

The annual inspection of the Mid-Bay Bridge in August 2000 resulted in the discovery of two failed tendons. The failure in the first tendon occurred in the free length of the duct and consisted

of isolated corrosion which was caused by a breach in the duct, allowing for excess moisture to enter (FDOT 2002). The second tendon failed due to corrosion that occurred in the anchor head, similar to the Niles Channel Bridge failure. The Mid-Bay bridge failure led to emergency inspections consisting of visual assessments, sounding of the ducts, borescope investigations, MFL, and vibration testing (FDOT,2002). After more in-depth inspections, 11 corroded tendons were discovered and quickly replaced. This incident led to additional precautions from FDOT including the use of prebagged grout and extensive inspections during construction.



**Figure 6: Tendon failures on the Mid-Bay Bridge (FDOT, 2002)**

### **1.5.3 Ringling Bridge**

The next example of defective grout in the state of Florida is the Ringling Bridge located in Sarasota. This incident is explained in “Development of Quality Assurance and Quality Control System for Post Tensioned Segmental Bridges in Florida: Case of Ringling Bridge – Phase II”. In 2011, two external PT tendons failed in the Ringling Bridge after only 8 years of service. The cause of this failure was deemed to be the severe corrosion of steel strands resulting from deficient grouting conditions. This grout became a highly segregated material which occurred over time, creating a high moisture content along with a high sulfate content. This moisture/high sulfate combination worked together to corrode the strands within the duct. This failure led to a more

extensive evaluation leading to the discovery of corrosion in fifteen other steel tendons which were then replaced throughout 2011-2012. Luckily these issues were addressed before failure of the structure occurred. This bridge would have benefited from FFs in initial construction which would have helped prevent corrosion within the ducts.

#### **1.5.4 Roosevelt Bridge**

A more recent failure occurred in 2020 in Stuart, Fl. The Roosevelt Bridge is a segmental concrete PT bridge which has been in service for 24 years. Span 1 of the South Bound bridge experienced tendon failures. FDOT then collected grout and concrete specimens for testing and found a high chloride content of 30 pounds per cubic yard (pcy) in the areas surrounding the failure (FDOT, 2021). The chloride content is 1.0 pcy for protected grout not exposed to external chlorides. After learning of the high chloride content, FDOT then cored multiple locations to determine the source of the high chlorides. Visual observations revealed efflorescence on the joints/closure pores throughout the bridge. This then led to the conclusion that water penetrated the PT system during rain events and later evaporated leaving chlorides behind. These chlorides accumulated over time and led to the overall corrosion and failure of these tendons. Moving forward, FDOT worked to seal the deck which prevents additional rainwater from entering the system, but there are still chlorides present within the ducts that pose a concern. Due to the overwhelming number of chlorides that have already entered the system, more frequent inspections will be necessary to ensure the structural health of this bridge. If FFs were used instead, it might have better protected these strands. Rainwater entering the closure pours is still a significant issue that would affect the anchorage regions negatively, however the FFs would have made for easier repairs and allow for easier tendon replacement.

After multiple incidents in FL linking CG to corrosion, FDOT has clear motivation to move towards a better material such as FF. As previously mentioned, it is now important to identify effective NDE methods to determine the structural health of existing and future bridges that utilize FFs instead of CG's.

## **CHAPTER 2: LITERATURE REVIEW**

An extensive literature review was conducted at the beginning of this research to determine the most effective NDE methods available. This literature review summarizes the different NDE methods researched and is mostly encompassed of material retrieved by two main studies. The first study conducted by Dr. Hurlebaus in 2016 at Texas A&M University funded by NCHRP and the second study completed by Dr. Azizinamini in 2017 at FIU funded by FDOT. Both studies focused on multiple NDE methods for internal and external ducts which is explained more in the following sections.

### **2.1 Ground Penetrating Radar (GPR):**

Ground Penetrating Radar (GPR) consists of emitting electromagnetic pulses from an antenna and analyzing these reflected pulses (Hurlebaus, Hueste, Karthik, and Terzioglu, 2016). These reflections are a result of changes in the materials electrical conductivity. GPR is sensitive to metallic materials such as metal ducts or mild reinforcement but can detect the location of these metallic materials present within the beam. Due to the sensitivity that this method experiences with metallic materials, it is not able to detect any strand breakages or grout defects within metal ducts, however it is somewhat effective on HDPE ducts. In the study “Condition Assessment of Bridge Post-Tensioning and Stay Cable Systems Using NDE Methods” GPR was performed on internal and external ducts (filled with CG) along with anchorages and two deviators in a PT girder specimen. To perform this study, the StructureScan Mini HR GPR unit was utilized and has a 2.6 GHz antenna, which can scan through up to 16” of concrete. This device can be seen in Figure 7 below. To scan the external duct, wooden supports were added along the side to account for the circular shape and ensure accurate results.



**Figure 7: StructureScan Mini HR GPR unit (Left), GPR unit inspecting the external tendons (Right) (Hurlebaus, Hueste, Karthik, and Terzioglu, 2016)**

In this study, GPR was able to accurately show the profile of the metal ducts due to the strong reflections they produce, however the scans were not able to detect any strand or grout defects within the ducts as expected. The HDPE duct profiles were also identified when using GPR but produced weaker reflections when compared to the metal ducts. GPR produced more promising results while scanning the external tendons and was capable of detecting voids along with some water infiltration in the ducts. When used upon the deviator region, the metal ducts were detected, yet none of the defects in the ducts were identified.

Some major findings of this method concluded that GPR is not effective for identifying grout or strand defects in internal metal or HDPE ducts. However, it was effective in identifying the location of these ducts, which is useful information for performing other methods such as impact echo and ultrasonic tomography. This method is more advanced than some of the other methods and can be performed quickly. GPR is effective in detecting both compromised grout and voids in external and internal HDPE ducts, but is unable to detect corrosion, cable breaks, and water infiltration. Due to the limitations of this method, GPR was not pursued for further investigation.

## **2.2 Infrared Thermography (IRT):**

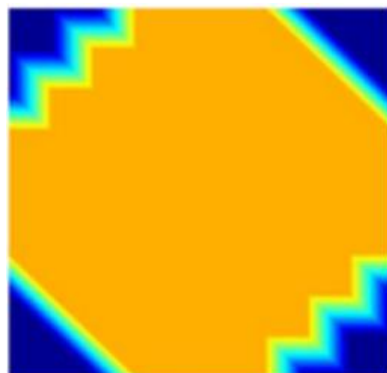
IRT is an imaging technique that can translate thermal energy emissions to a temperature map (Hurlebaus, Hueste, Karthik, and Terzioglu, 2016). One limitation of IRT is its dependency on the ambient temperature surrounding the specimen, optimal results are obtained during the day when the temperature changes rapidly compared to overnight. There are two types of IRT: Passive and Active. Passive IRT relies on the heating and cooling of the sun at different times of the day, whereas Active IRT uses a controlled heat source.

IRT utilizes an infrared camera to detect voids of the filler material within an external PT duct. This is done by recognizing the differences in the heat map provided by the camera's image of the duct with areas of less heat indicating a void. This method would only work on external tendons as it would be difficult to read the heat map of a duct that is embedded in concrete; the camera would not be able to pick up the voids within the grout of an embedded duct. This method works upon the principle that air will not conduct heat through the duct wall as well as a filler material would, meaning that the heat map image would be able to show the inspector these voids. This is quickly becoming a popular method of NDE as it is relatively cheap and does not require extensive knowledge to identify voids within the ducts (Azizinamini, 2017). That said, this method does not indicate if there is damage to the tendon within the duct nor does it indicate the severity of the damage. This method can be effectively used as a simple first pass inspection method that will require more advanced NDE techniques to pinpoint the issues in the areas flagged by IRT.

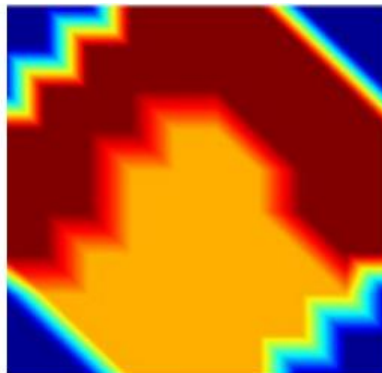
## **2.3 Electrical Capacitance Tomography (ECT)**

ECT has been primarily used and tested in the oil industry where these sensors are used to analyze the flow of crude oil through pipelines, mainly identifying air pockets/voids in the flow. This method works by measuring the capacitance of the object below the sensor head. The sensor head

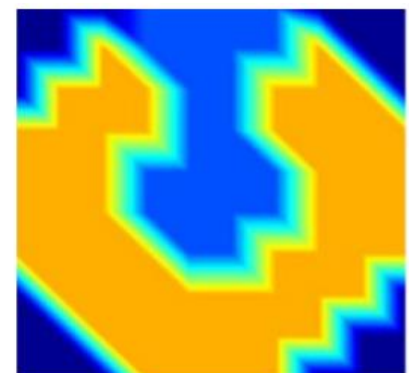
consists of multiple electrode sensors, which through iterative scans, make a composite image showing the zones of different capacitance (Hurlebaus, Hueste, Karthik, and Terzioglu, 2016). Due to this method being effective in determining voids in pipelines, it should also be effective in identifying voids in PT ducts. Hurlebaus used ECT to inspect a PT girder and found that this method is only effective in external ducts, and even then, did not perform well in detecting compromised grout, voids, and water infiltration. Below is a set of images from this study, along with the sensor head that was used.



No faults



Red indicates moisture  
(water/bleeding grout)



Blue indicates  
air void

**Figure 8: Sensor head (Top), Examples of the composite images gathered by the ECT device (Bottom) (Hurlebaus, Hueste, Karthik, and Terzioglu, 2016)**



ECT seems to be a promising method in identifying grout defects in external non-metallic ducts, but with current technology, it yields inaccurate results. These tests were performed on a CG filled duct, so how this method would differ on an FF duct is unknown. Due to the uncertainties regarding the effectiveness of this method, ECT was not further investigated.

#### **2.4 Magnetic Flux Leakage (MFL)**

MFL is a promising method in locating steel section loss due to corrosion, strand/wire pitting or breakage. This NDE method uses the interaction between magnetic fields and matter to inspect distress in ferrous materials. There are two kinds of MFL: Active and Residual. Active involves subjecting a ferrous material to a strong magnetic field induced by a portable magnet which induces flux paths in the material. In locations that experience section loss, there is a “leak” in the magnetic field. This leak is then measured by a magnetic field detector and can determine the location of section loss. In Residual MFL, the ferrous material is brought to full magnetic saturation (to erase magnetic history), then the magnet is removed, and the sensors are passed over to detect the residual magnetic field (Hurlebaus, Hueste, Karthik, and Terzioglu, 2016).

Azizinamini found that MFL is a promising method in detecting physical discontinuity in strands, but additional factors such as other ferromagnetic sources (mild reinforcement & steel ducts) and masking effects lead to complicated signals that are difficult to decipher. MFL is found to be an extremely promising method when inspecting external tendons and is a method that could be expanded upon for NDE of ducts with FF.

#### **2.5 Impact Echo (IE):**

Another common NDE method utilized by bridge inspectors is Impact Echo (IE), this method involves hitting the concrete surface with a small impactor/impulse hammer and analyzing the reflected wave energy with a displacement or accelerometer receiver mounted on the surface near

the impact joint (Hurlebaus, Hueste, Karthik, and Terzioglu, 2016). This method can detect voids in metal and HDPE internal ducts. The impact device can measure the wave energy which is depicted below. A fully grouted duct will emit a current passing straight through the duct, while a voided duct will behave differently and veer off.

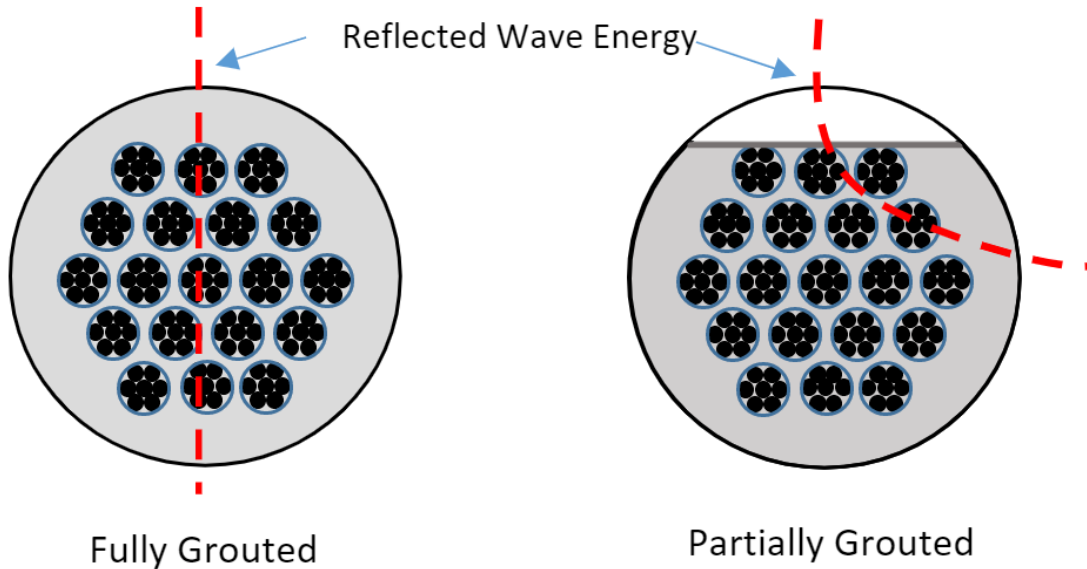


**Figure 9: Reflected wave energy propagating through a duct**

In the study, “Condition Assessment of Bridge Post-Tensioning and Stay Cable Systems Using NDE Methods,” the IE method was utilized on an internal and external PT girder system using an Impact Echo Scanner test head and a PC data acquisition platform as seen below. Once GPR was performed to determine the location of the ducts, an impact echo test was performed at 6” intervals as determined by the inspector.



**Figure 8: (Left) Shows the IE scanner test head, (Middle) Shows the PC data acquisition platform, (Right) Shows the IE device in use on an external duct (Hurlebaus, Hueste, Karthik, and Terzioglu, 2016)**

In this study, the IE testing was effective in determining voids in the external and internal ducts up to 3.3 ft deep, but not in the anchorages due to the minimum cover depth of 5 ft. Limitations of this method include accurately detecting voids in smaller diameter internal ducts with a large cover and identifying the presence of water or soft grout. This method is also more effective in metal ducts rather than HDPE ducts.

Another study with similar findings is “Durability of Precast Segmental Bridges” According to this study, IE is the most effective method for determining grout conditions in internal metal ducts, which coincides with the previously mentioned study. This study also emphasized the need for a skilled operator to analyze the results, which is a limitation to the method.

This study noted the first large scale use of IE occurring in 1997 on a 14-span precast segmental bridge, which consisted of internal metal grouted ducts. IE was able to accurately detect voids throughout the ducts and confirmed with the use of a borescope. The ducts had severe grout loss along with no grout in some places. Due to the use of IE, the inspectors were able to accurately determine grout loss and if repairs were required.

## 2.6 Ultrasonic Tomography (UST):

Ultrasonic Tomography (UST) consists of reflecting ultrasonic waves at a material and measuring the change in acoustic impedance to identify grout defects in internal ducts. In the study “Condition Assessment of Bridge Post-Tensioning and Stay Cable Systems using NDE Methods” UST was tested upon a 75’ long PT bridge girder along the anchorages and deviators. The device used for this test was the A1040 MIRA as seen in Figure 12 which has many applications such as the identification of voids, rebar, cracks, and substance filled cavities.



**Figure 91: (Left) A1040 MIRA device, (Right) results from the deviator blocks (left is defect key and right is the UST scan) (Hurlebaus, Hueste, Karthik, and Terzioglu, 2016)**

Due to the size of the specimen, data was collected in sections and later combined to be analyzed. Concrete being a nonhomogeneous material required the need for obtaining sample velocities and then averaging the results for each section. This method was unable to identify grout defects in the internal ducts, with difficulties inspecting metal ducts. UST was able to identify the location of the internal ducts and proved to be more effective when used upon HDPE ducts. UST was also incapable of locating defects in the anchorage zones of the PT system.

## **2.7 Ultrasonic Echo (USE)**

Ultrasonic NDE methods consists of a group of sensors emitting a stress pulse into the specimen which travels along the beam. As these waves propagate through, the area of varying impedance is reflected upon the waves. These waves are then captured by the group of sensors (Hurlebaus, Hueste, Karthik, and Terzioglu, 2016). In USE NDE testing, the specimen is excited by a pulse in an inaudible ultrasonic range, and the reflected portions of the pulse are then evaluated. These reflections occur when the pulse interfaces with metal (such as mild reinforcement, or metal ducts) and with air (voids). When using USE, multiple measurements along the specimen are required to gain the full picture of where the reinforcement is located.

To perform this method, a control unit and a probe is necessary. The unit is responsible for generating the electronic pulse, which is then led to the probe through a coaxial cable. In the study performed by Hurlebaus, no coupling agents were used, and the probes were made of 24 single transducers. 12 transducers were used as a transmitter while the other 12 served as a receiver, creating constant and even coupling. In this study, a variety of different duct and tendon defects were simulated, but it was found that USE is not capable of detecting grout defects in internal ducts and is incapable of detecting strand and grout defects in the anchorage regions. Although this method is ineffective in locating grout defects, it is still promising in locating reinforcement/duct locations.

## **2.8 Sonic/Ultrasonic Pulse Velocity (SPV-UPV)**

SPV-UPV is another ultrasonic method similar to USE & UST. This method consists of impacting one side of the specimen with an instrumented hammer while recording the signal on the other side (Hurlebaus, Hueste, Karthik, and Terzioglu, 2016). By evaluating the arrival of this signal, the material velocity can then be calculated. Hurlebaus performed this NDE method on a deck and

pylon anchorages to assess internal grouting conditions. This testing required a source and a receiver which can be seen below.

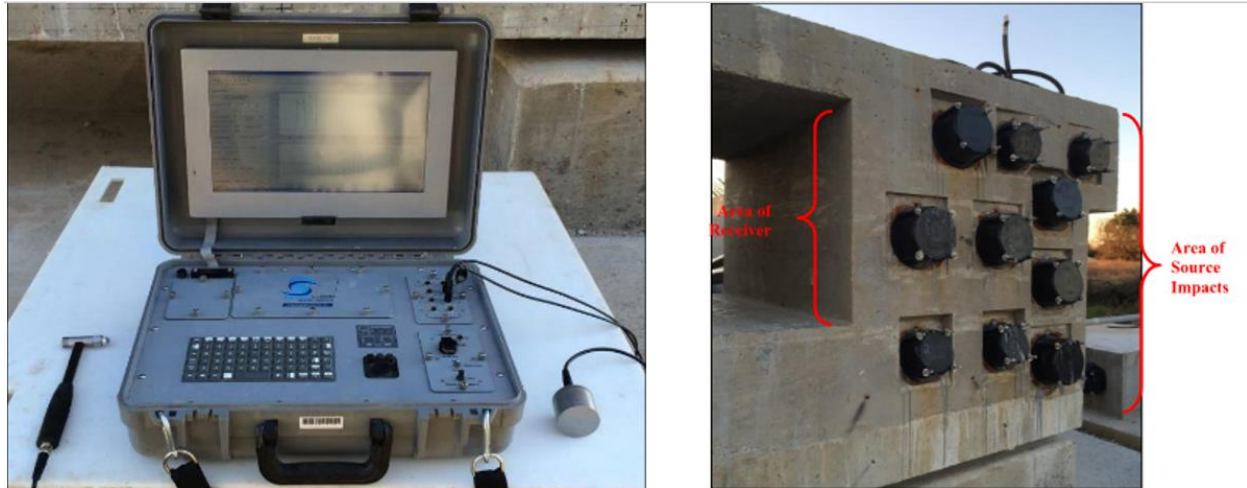


**Figure 102: SPV testing system along with impulse hammer, data acquisition system PC and ultrasonic transducer (Left), Photograph showing location of source impact and receiver for SPV testing (Right) (Hurlebaus, Hueste, Karthik, and Terzioglu, 2016)**

SPV tomography was unable to detect any voided ducts/cross sections in this study. It is believed that the small size of anomalies within the specimen led to the lack of results, as the imaging capabilities of this method were unable to detect these, therefore there is not conclusive data available on whether this method would be effective in future inspections.

## **2.9 Low Frequency Ultrasound (LFUT)**

LFUT is another ultrasonic NDE method available. This method is different from the others, as it is designed to generate and receive low frequency ultrasonic waves in a pitch-catch fashion, which propagates through the duct (Hurlebaus, Hueste, Karthik, and Terzioglu, 2016). By analyzing these waves, grout defects such as voids and water infiltration can be detected. In the study performed by Hurlebaus, both a stay cable specimen and external duct specimen were analyzed. This method was found to be effective in detecting the grout defects as expected. This study also concluded that LFUT is an effective method in evaluating external HDPE ducts, but not internal.

This method was not effective on internal or external metal ducts. A limitation of this method is that while it can detect air voids, it is unable to decipher between the severity of these voids. Therefore, further NDE methods would be required to determine more thorough results regarding how severe these defects are, thus this method was not chosen for further investigation.

## **2.10 Sounding**

Mechanical sounding is used in tangent with visual inspections, if an abnormality is visually apparent to the inspector, they will then conduct this method. Sounding is only effective for external tendons and consists of the inspector tapping along various points on the duct and listening for sound differences. An experienced inspector is trained to hear the dull/hollow sound that indicates the presence of voids. One downfall of this method is that it is not always accurate and is a loose indication of voids within the tendons. If an inspector suspects voids from performing this method, they will then be prompted to perform a more in-depth inspection. This method is also unable to detect soft grout or smaller voids/defects.

The sounding experiment in the paper “Condition Assessment of Bridge Post-Tensioning and Stay Cable Systems Using NDE Methods” where the testing of six external post-tensioned ducts along with the end caps and anchorages was performed. The spacing between the taps was determined to be 2”, which is at the discretion of the inspector. This method was found to be consistent for different trials and inspectors when conducted on HDPE ducts, but not metal ducts. As previously mentioned, this method is only effective for detecting voids in the grout, the testing only further proved this limitation. This method was also ineffective in determining any kind of defects in the anchorages but is mostly reliable for identifying grout condition in the end caps.

The accuracy of this method depends upon the experience of the inspectors. Because of this, there can be discrepancies between different inspectors' opinions, which usually results and a more in-depth inspection.

### 2.11 Visual Testing (VT)

Visual testing is effective in detecting grout defects, corrosion, or any kind of deterioration that could negatively affect the structure. Visual testing is effective for internal and external tendons, however internal tendons pose more difficulties of accessibility to the tendon resulting in VT being less common in these scenarios. In terms of external ducts, visual testing is one of the more common methods utilized to detect abnormalities. Visual testing consists of opening the duct or end cap in areas that are a cause for concern and looking inside to determine the state of the strands. Images of this can be seen below from the study “Condition Assessment of Bridge Post-Tensioning and Stay Cable Systems Using NDE Methods”.

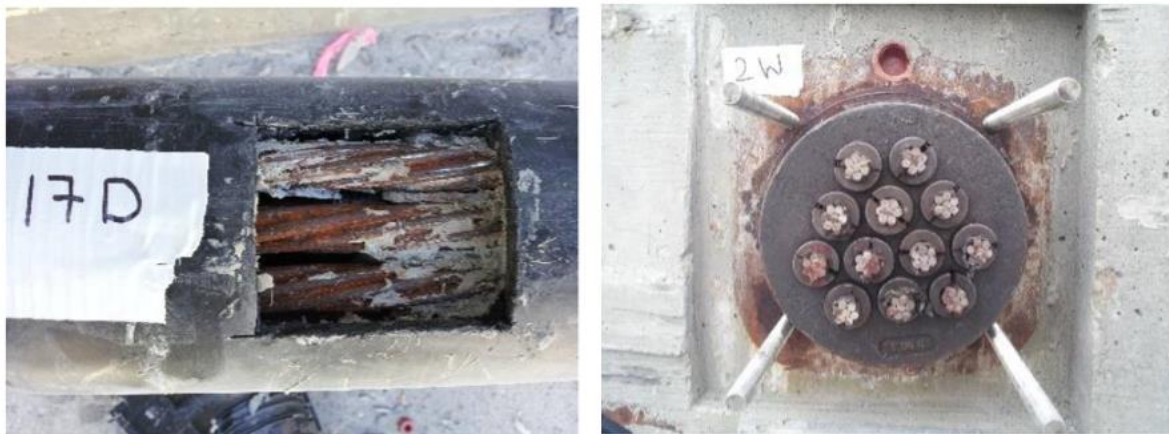


**Figure 113: Visual testing of an external tendon (Left) and end cap (Right) in PT Girder Specimen (Hurlebaus, Hueste, Karthik, and Terzioglu, 2016)**

In this study, the end cap inspections were performed by removing the cap and carefully inspecting the grouting conditions. A downside of this method is that it is more invasive than the other methods while also being more time consuming. It is not feasible to perform this method on a large



number of ducts/caps throughout the bridge, as it cannot identify the specific location of a defect until the later stages of deterioration when there are more apparent visual indicators on the outside of the duct. This method works in tangent to mechanical sounding, which is how the location of this testing was decided. VT is not effective in detecting early stages of grout/strand deterioration which is why it is always coupled with another NDE technique.

### **2.12 Borescope (Bor):**

Another tool that is utilized by bridge inspectors is the Borescope. This method is more invasive than some of the other NDE techniques, so it is sometimes referred to as a semi-destructive method, as it requires creating an access port for the borescope to enter through. This method is effective for determining voids and corrosion in both internal and external systems. This method is deployed once sounding or visual testing is completed and detects degradation of the grout or strands. This method allows the inspector to observe the corrosion or voids within the duct by running the borescope inside the system. In the study, “Condition Assessment of Bridge Post-Tensioning and Stay Cable Systems Using NDE Methods” the inspectors drilled access holes and used an Olympus IPLEX SX ii system as seen below.



**Figure 124: Depicts the borescope access port and the equipment used (Hurlebaus, Hueste, Karthik, and Terzioglu, 2016)**

In this study, four external ducts were investigated along with the anchorages. The borescope was able to show voids, water infiltration defects, and corrosion of the strands which can be seen in the images below. This method is a more accurate representation of what is occurring within the ducts, which allows the inspectors to see the state of the tendons and decide on how, where, and if repairs are necessary to keep the structural integrity of the bridge.

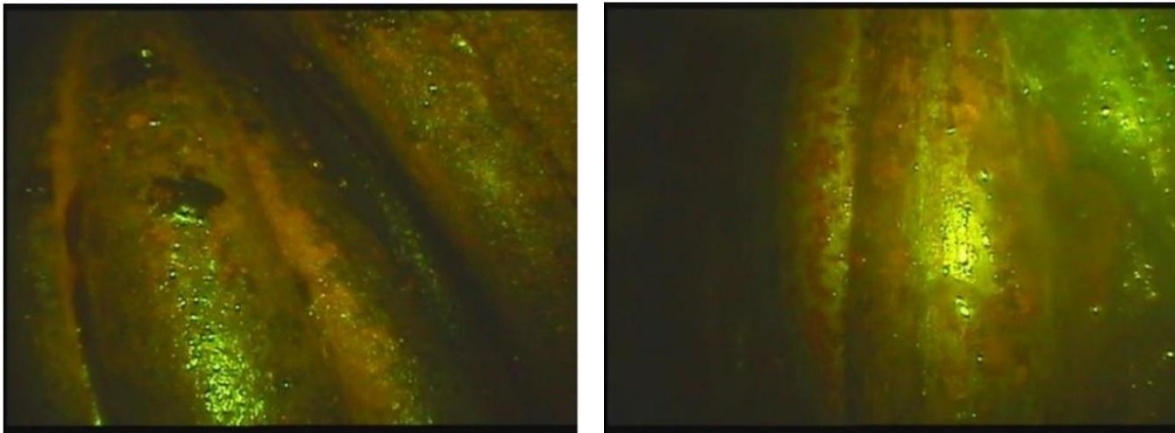


**Figure 15: Images provided by the borescope inspection inside the external tendons depicting corrosion of the strands (Hurlebaus, Hueste, Karthik, and Terzioglu, 2016)**

Some limitations of this method include the inability to identify the amount of voided area between congested strands. The borescope requires a void to enter the duct/anchorages, and the sight is limited to where the main voids are located.

### **2.13 Electrochemical Impedance Spectroscopy (EIS)**

EIS is an impedance technique that applies a low-amplitude voltage to the steel specimen under multiple frequencies. The impedance of the concrete-steel interface can then be calculated by measuring the changes in phase shift and signal amplitude (Azizimini, 2012). One limitation with this method is that it requires highly qualified operators and advanced processing of the data to evaluate the results. In the study performed by Hurlebaus, EIS was performed on an external PT girder specimen to determine corrosion defects. Corrosion was induced on multiple strands to test

if this method is effective in detecting these defects. To perform this testing, small holes were drilled into the duct so that there was access to the grout. This is not preferred as an NDE method, because these holes would then have to be repaired by the inspector and could leave weak points allowing access to external substances entering the duct. After performing this testing, it was found that EIS is effective in determining the location of the defects, but similar to other methods, was not able to detect the severity of the damage.

#### **2.14 Radiography Methods**

Radiography is a very useful NDE method that allows inspectors to get a clear visual of what is happening within the ducts. This method is capable of detecting strand breakage, corrosion, compromised grout, and voided regions in internal and external ducts. A limitation of this method is the expensive equipment and having trained personnel that know how to use it. This method also requires access to two sides of the specimen, making internal tendons more difficult to image. While this method can show defects, it is not able to show the depth of these anomalies unless images are taken from multiple perspectives. In the study “Improved Inspection Techniques for Steel Prestressing/Post-tensioning Stand,” Azizimini identified Radiography as a promising NDE method for PT bridges. Radiographic inspection was carried out at the Zarate Bridge in Argentina upon the grouted internal ducts. By performing this testing, severe voiding was found within the bridge’s ducts, which alerted the inspectors to perform necessary repairs. Due to the success this method had with the grouted ducts; it is worth exploring how well this method could perform on FF ducts.

Azizimini identified this as a promising NDE method that is applicable to both internal and external ducts. This method is further explored in this report and due to its effectiveness on the CG

ducts radiography methods should translate well to FF ducts. More on this method is explained in Chapter 4.

## **2.15 Conclusion**

After reviewing multiple NDE methods that have been effective for CG, several methods were identified as promising for use on FF ducts. These promising methods being Visual inspections, Radiography, Thermoelasticity, and Ultrasonic Testing. Three of these methods will be further explained in this report: Visual Inspections, Radiography and Thermoelasticity. This literature review was useful in identifying the available NDE methods along with learning their strengths and limitations. By performing this review, it was possible to determine these promising methods and move forward with the project.

## CHAPTER 3: VISUAL INSPECTIONS

Visual inspections are the first check that inspectors perform when inspecting any kind of bridge in the field. It is important to get a clear visual of the bridge and know what kinds of defects to look out for. This is the simplest NDE method to perform, as it is performed at every inspection. Current inspectors know what small defects/indicators to look out for when inspecting bridges that use CG, but as FDOT moves towards PT bridges that use FF, there are different indicators that inspectors need to look for.

### 3.1 Visual Indicators for Cementitious Grout vs Flexible Filler

Due to FF tendons being unbonded, as compared to those bonded with CG, they will behave differently at failure. For example, corrosion of the strands in a CG system can lead to cracking of the grout, which will extend to the duct surface. With an unbonded duct, corrosion of one strand will lead to deformation of the FF within the duct and will not show externally. Another major difference between bonded and unbonded systems is the way loss of prestressing force will occur. In a bonded system, if localized corrosion occurs, the effective prestressing force will only be lost in the immediate vicinity of the corrosion damage, whereas in a unbonded system, if localized corrosion occurs, loss of this prestress force will be distributed along the entire length of the structure.

FFs are often used in conjunction with HDPE ducts, meaning that the severity and visibility of visual indicators will be different from those of metal ducts. It is often found that the tendons are corroded from the outside in, so the ferrous duct is corroded first, then the strand within. With the HDPE ducts being used, this process will change and the normal visual indicators for cementitious grouted bridges using metal ducts may not hold true.

An example of a bonded system failure is the Roosevelt Bridge in Stuart, FL. In 2020, this bridge experienced corrosion damage due to a poorly constructed closure pour (as previously stated in Chapter 1) and, as a result, showed some severe visual indicators such as those in figure 16 below.



**Figure 13: Localized corrosion damage for internal tendon in Stuart, FL (Roustan and Erblat, 2020 & Detman and Rodriguez, 2020)**

This distinction between bonded and unbonded systems is important for inspectors to make when performing their inspections due to the major behavioral differences between these two systems.

### **3.2 Bridge Inspections**

To get a clear understanding of how these inspections are performed, FDOT allowed the team to shadow some inspections in Daytona Beach, FL. The inspectors explained that approximately 80% of the inspection process is visual and that by observing the appearance of the various structural elements, an inspector can infer the condition of that element. Flaws such as cracking, surface corrosion, pitting, etc. can be observed visually. More advanced forms of visual inspections can be performed with the use of technology, such as fiberscopes, borescopes, magnifying glasses, video monitoring equipment, and robotic crawlers, however this sometimes requires small holes to be made into the duct, which is not preferred. Visual inspections are inexpensive and easy to do, but do not provide reliable information regarding structural elements out of view (such as

internal tendons). This will always be the first step in an inspection, and with the knowledge of specific visual indicators, an inspector knows where to conduct more intrusive inspections. Visual indicators are the most often used method to find damage to bridges during routine biennial inspections such as the ones the team shadowed. These methods include identifying cracks, water ingress, rust spots, efflorescence, damage to anchorage blocks or caps, and in the worst-case separation of bridge segments. Though these methods do not give initial insight into the underlying issues that cause these indicators, it does allow for the inspector to understand where to focus more time intensive NDE methods. Most of these indicators are caused by some degree of corrosion to the reinforcement of the bridge, whether that is corrosion to mild reinforcing steel, or the PT strands themselves often requires further investigation.

### **3.2.1 Seabreeze Bridge Inspection**

Seabreeze Bridge is a PT segmental box girder bridge in Daytona Beach. During an inspection on the eastbound section of this bridge, insight was gained on the normal operating procedures of FDOT inspectors.



**Figure 14: Seabreeze Bridge**

Examples of visual indicators found during the Seabreeze Bridge inspection are shown in Figure 18 below. There was some cracking that appeared, along with efflorescence. Efflorescence is a white salt residue that occurs as moisture migrates up to the surface of the concrete. This white substance is the calcium salts from within the concrete that traveled up with the excess moisture. Now efflorescence isn't necessarily always an indication of major defects within the bridge, it does indicate moisture intrusion, which can usually lead to corrosion of any reinforcement within the bridge.



**Figure 15: Example of cracking (Left) and efflorescence (Right) from the eastbound Seabreeze Bridge Inspection**

As previously stated, visual indicators such as those shown above are used to identify problem areas that later need to be analyzed in greater detail, either by some NDE method or by an invasive visual method. One NDE method that was utilized during the inspection on the Seabreeze Bridge is acoustic sounding, which consisted of tapping the bridge with mallets and listening for variations in the reverberations to help identify areas of higher stress or cracking. Similar to the visual methods, this is also used to flag areas of interest which can later be further investigated using visual inspections that are then followed up by a more in depth NDE method. By performing this



method, the inspectors identified areas of the bridge that required more in-depth testing, which led to the IE testing that was performed. This IE testing was used to evaluate the closure pours and can be seen in Figure 19. The device used for this testing was a tool developed by Vector Corrosion Services who performed this inspection. The impactor was used to propel a stainless-steel BB into the concrete surface, while ultrasound transducers were positioned adjacent to the point of impact. The data acquisition system can also be seen in the figure. This IE testing required highly skilled operators that were extensively trained to use this equipment. The set-up for this equipment was minimal and lightweight, however it required constant power and a pressurized nitrogen source for the impactor.

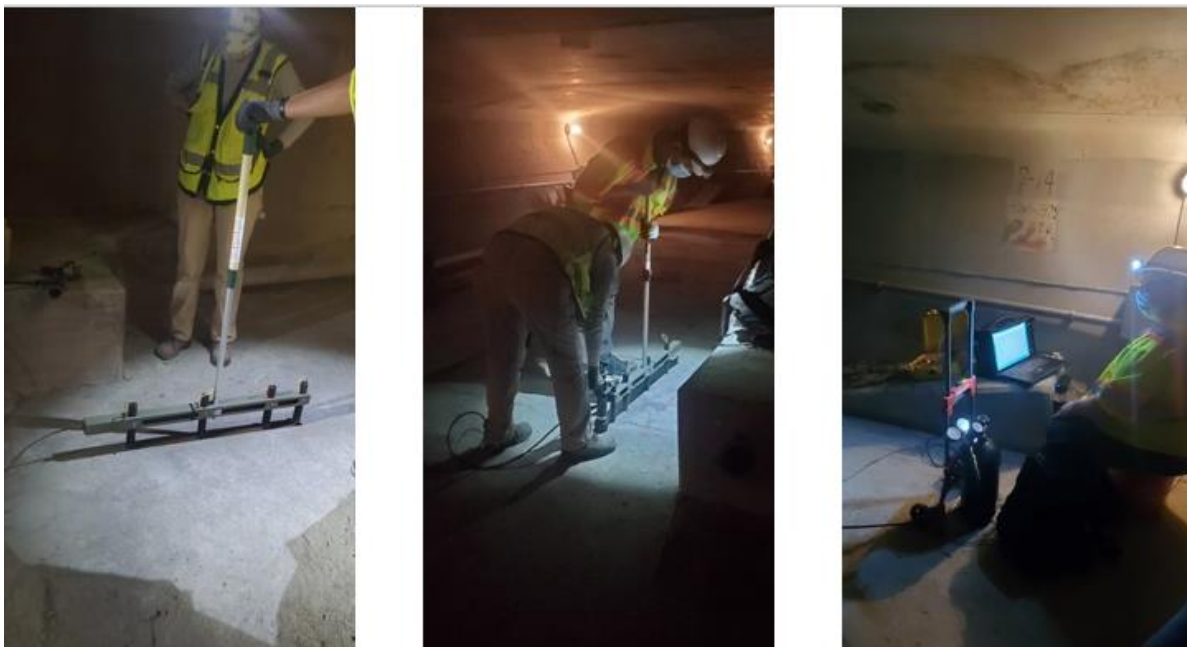


**Figure 16: Impact Echo NDE performed on Seabreeze Bridge**

### **3.2.2 Broadway Bridge Inspection**

Broadway Bridge is another PT segmental box girder bridge in Daytona Beach, FL. The main difference between the Broadway Bridge and Seabreeze Bridge is that Broadway has external tendons. These external tendons allowed for easier access and a more in-depth visual inspection allowing a clear visual of the ducts and any possible defects.



**Figure 17: Broadway Bridge**

Images from this inspection can be seen in Figure 21 below. A clear rust stain could be seen on one of the tendons, which was a cause of slight concern from the inspectors and led to a more in-depth inspection.

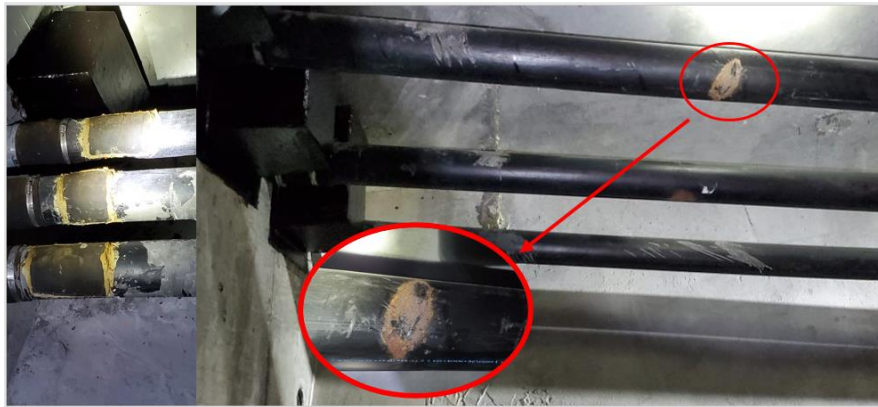


**Figure 18: External ducts that were repaired from previous intrusive NDE inspection (Left) Rust stains on external tendon (Right)**

After identifying these rust stains and other indicators mentioned by the inspectors, two more NDE methods were performed: ultrasonic pulse velocity (UPV) and electrical impedance (EI) which are both common methods currently used on external tendons.

UPV testing involves an ultrasonic transducer and receiver that are positioned on opposite sides of the tendon. Multiple scans are then recorded at different angles at one-foot intervals along the

length of the tendon as shown in Figure 22 below. This NDE testing requires trained operators to identify any possible defects or abnormalities.



**Figure 19: Ultrasonic Pulse Velocity (UPV) Testing**

The other NDE method performed on Broadway Bridge was electrical impedance. This testing was performed by a research group from the University of South Florida. The device used has been developed from multiple FDOT sponsored research projects. As shown in Figure 23, the sensor device is clamped over the tendon. The operator then rotates the device around the tendon at multiple one-foot intervals along the tendon. The other operator works to run the data acquisition system (small laptop). This device is then able to show a cross section of the tendon where these scans were performed. The tendon appears as a green area, while areas of concern within the duct (such as air voids, water voids, and defective grout) appear as different colors.

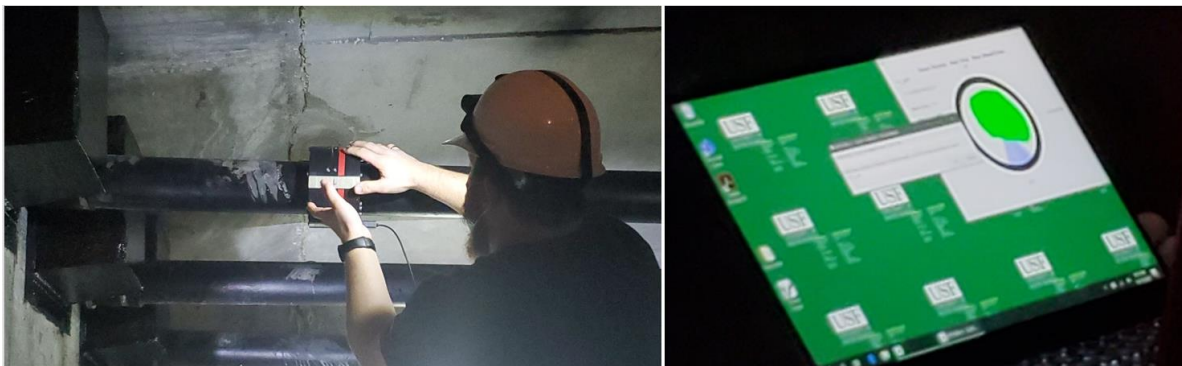


**Figure 20: Electrical Impedance Inspection**

### **3.3 Inspection Guide:**

To assist inspectors, a small inspection guide has been created to point out some visual indicators to look for when inspecting a PT bridge that uses FF. This guide will focus on a 3-span segmental bridge, C-Pier, and a Straddle Bent Pier. These are common structural elements that would use FFs and would need to be assessed by the inspectors. The guide will include special considerations for the anchorage region, as well as areas where cracking may occur due to post tensioning losses. A simplified 3-D model will be shown for each structure type to illustrate the overall geometry of the structure and the configuration of the PT system. The models will be used to highlight areas of concern for cracking or other indicators that the inspectors should lookout for in the FF systems.

#### **3.3.1 Three-Span Segmental Bridge**

The first Structure type this guide will focus on is a three-span segmental bridge. This structure can be seen in Figure 24 below.

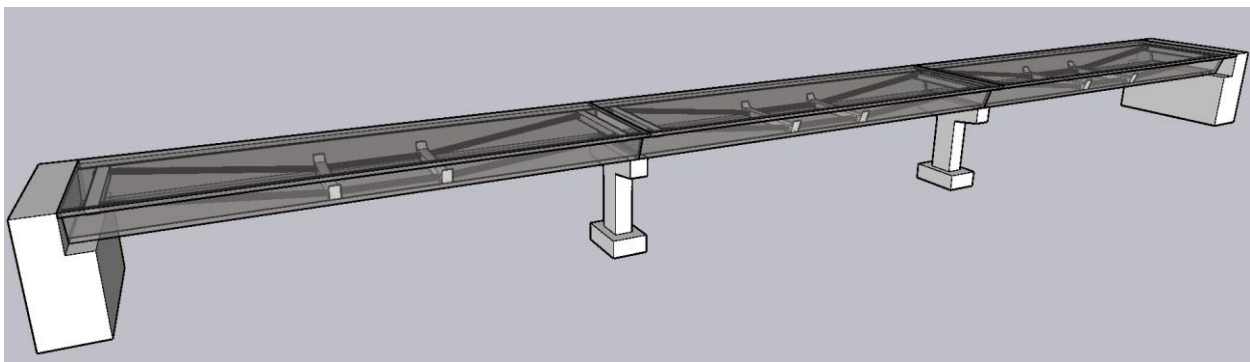


**Figure 21: Three-Span Segmental Bridge**

The first indicator to look for in this structure would be the cracking in the critical bending regions. Due to this being an unbonded system, the cracks would appear along the length of the structure instead of in a localized location. It is important to investigate the middle of the span, as once the load is applied on the bridge, this is where tension will be experienced. If loss of prestress force occurs, these tensile forces from the applied live load will not be counteracted, thus resulting in

high tensile stresses in the bottom of the beam. This will lead to cracking that should be apparent to the inspector.

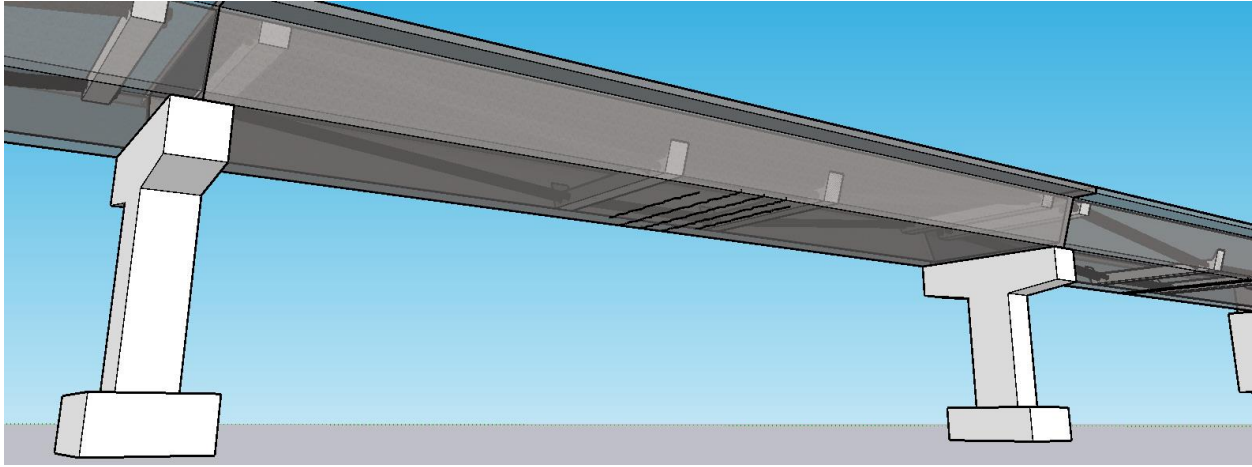


**Figure 22: Cracks due to tension in the middle of the span**

Another place the inspectors need to check is the closure pours. From experience with other PT bridge failures, these are critical locations that need to be evaluated. If these closure pours are not properly constructed, they will degrade over time, allowing for excess moisture and chlorides to enter the bridge. This excess moisture will corrode any mild reinforcement, or worse, the PT strands. If this moisture enters the duct, in theory the FF should coat the strands to protect them and repel the water, but the worst-case scenario would be a void in the filler allowing this moisture to penetrate the strands. This would corrode the strands and lead to loss of prestressing force, and as previously mentioned would result in cracks forming. Indicators at the closure pour could also include efflorescence due to the moisture in the concrete.

The anchorage regions should also be closely inspected. If a filler is leaking or any protruding strands are present, it would be cause for concern. If the strands/wedge grips corrode, this could lead to the strands moving in the cap region which would be noticed by the inspector. In severe cases, the strands could even penetrate the cap wall indicating severe damage (Figure 26). To

perform a more in-depth visual inspection, the inspector could remove the cap but this is not preferred due to possible time constraints of the inspection process. Most structures utilizing FF would use a Type 5 anchorage protection system which allows for a clear visual of the cap.

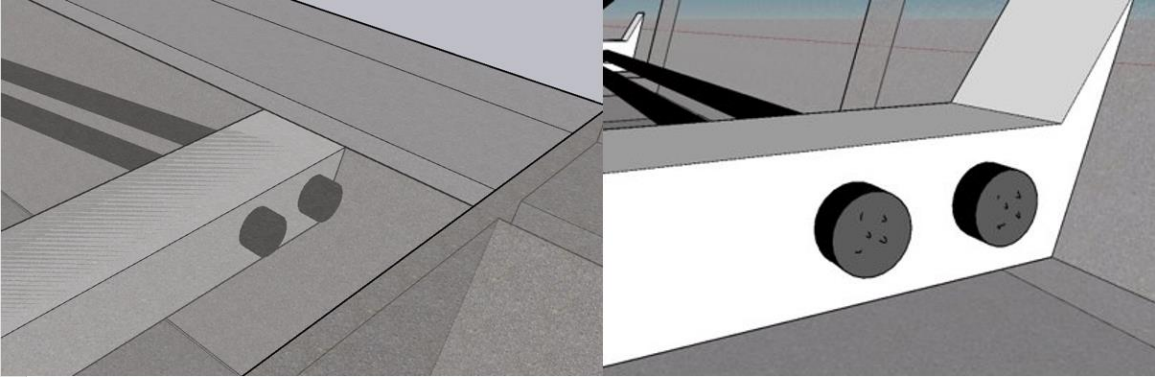


**Figure 23: Anchorage Region, protruding strands/defects (Right)**

**3.3.2 C-Pier**

The next structure type that is included in this guide is the C-Pier. This pier type is useful in bridge locations that span over other roadways where the use of a traditional pier is not possible. This pier type has internal post tensioning ducts to allow for the distribution of the load required to support the bridge.

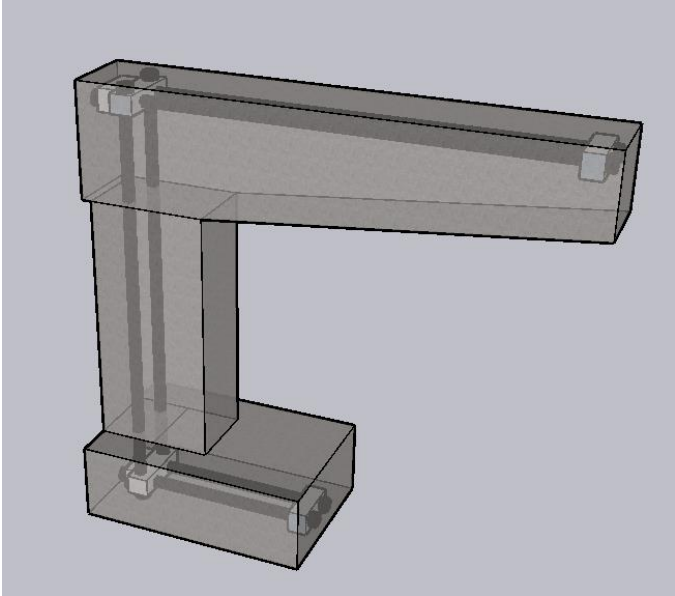


**Figure 24: Post-Tensioned C-Pier**

Similar to the three-span segmental bridge, if loss of prestressing force occurs, cracking would appear along the length of the structure as shown in Figure 28 below. These cracks would appear in the regions experiencing high tensile stresses.

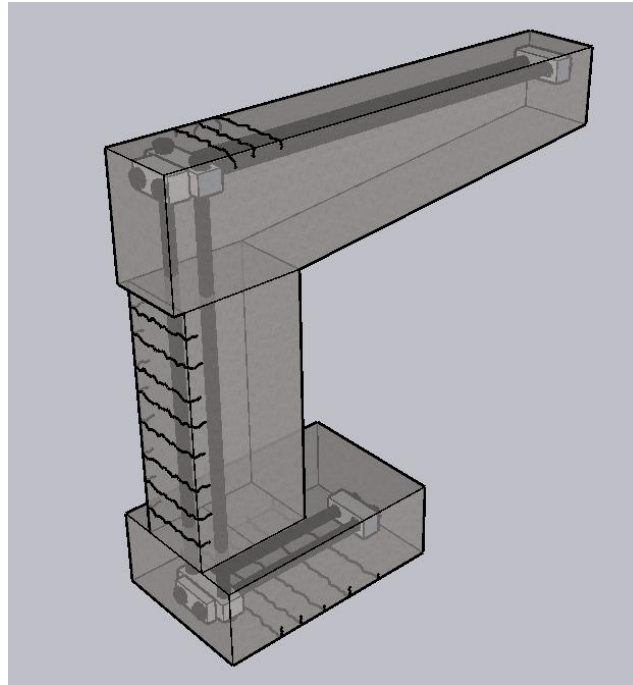


**Figure 25: Post-Tensioned C-Pier with cracks**

The PT duct anchorage region should also be evaluated, if any filler is leaking or any protruding strands are present, the inspector should perform a more in-depth inspection to determine the issue and how to mitigate the damage.

### **3.3.3 Straddle Bent Pier**

The final structure type that will be included in this guide is the straddle bent pier. Similar to the C-pier, the straddle bent pier as shown in Figure 29 is also utilized in confined bridge construction where the placement of a traditional pier is not possible. This pier type can span over roadways to support the bridge without disrupting the road below.

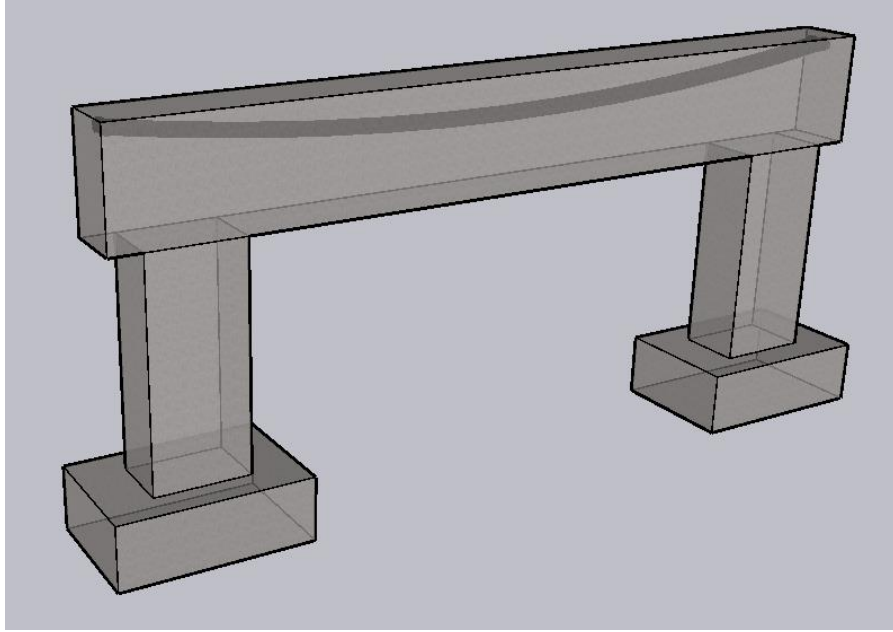


**Figure 26: Post-Tensioned Straddle Bent pier**

Inspection for this structure should be carried out similarly to the segmental bridge and the C-pier. The high moment regions should be carefully inspected for cracking along with the anchorage regions. Locations of where cracking could occur can be seen in Figure 30 below.

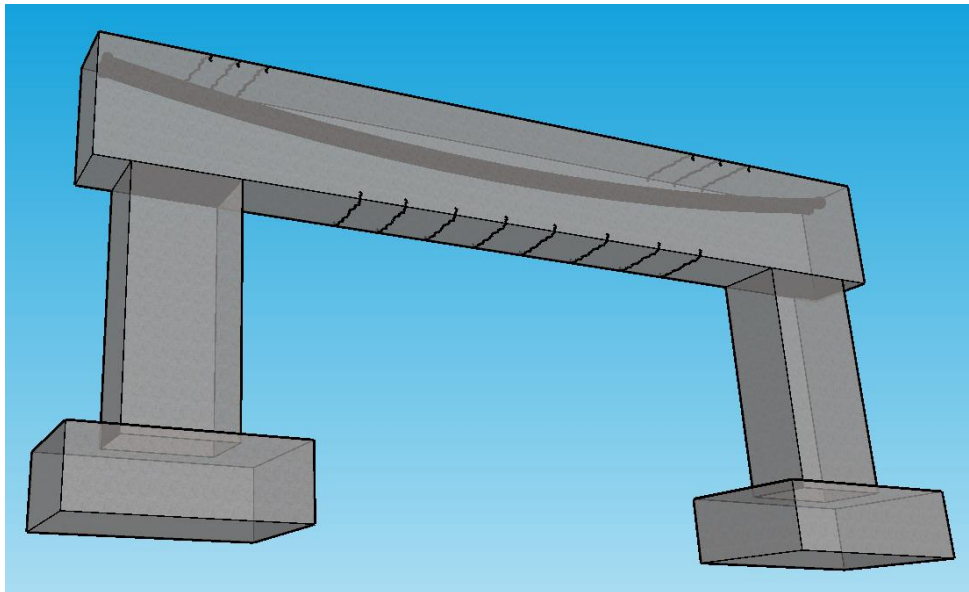


**Figure 27: Post-Tensioned Straddle Bent pier with cracks**



### **3.4 Conclusion**

This guide will be useful in identifying defects of the three structure types mentioned. Inspectors will benefit from knowing what kinds of indicators to look out for when inspecting these unbonded systems when compared to the bonded CG systems. This is a working guide, as more PT bridges are constructed with FF, any possible indicators of damage should be noted by inspectors for future inspections.

## CHAPTER 4: RADIOGRAPHY

Radiographic testing was performed in October 2021 at the Florida Department of Transportation Marcus H. Ansley Structures Research Center in Tallahassee, Florida. The goal of this testing was to determine if radiography is an effective NDE method for internal ducts, external ducts, and anchorage regions.

### 4.1 Specimens

This testing was performed on a variety of specimens to replicate different portions of the PT beam that would be evaluated in the field.

**Table 3: Specimen Summary**

Specimen 1	Small scale mock-up tendon
Specimen 2	Full-scale external mock-up tendon
Specimen 3	Prestressed girder with internal duct (no tendon)
Specimen 4	Prestressed Girder with internal duct (with tendon)

The first specimen is a full-scale anchorage mockup made of a VSL ECI 6-19 anchorage system (Figure 31). This specimen consists of the trumpet, anchorage plate, wedge plate and end cap. To represent a post-tensioned duct, the wedge plate was loaded with 16 strands that extended through the trumpet region.

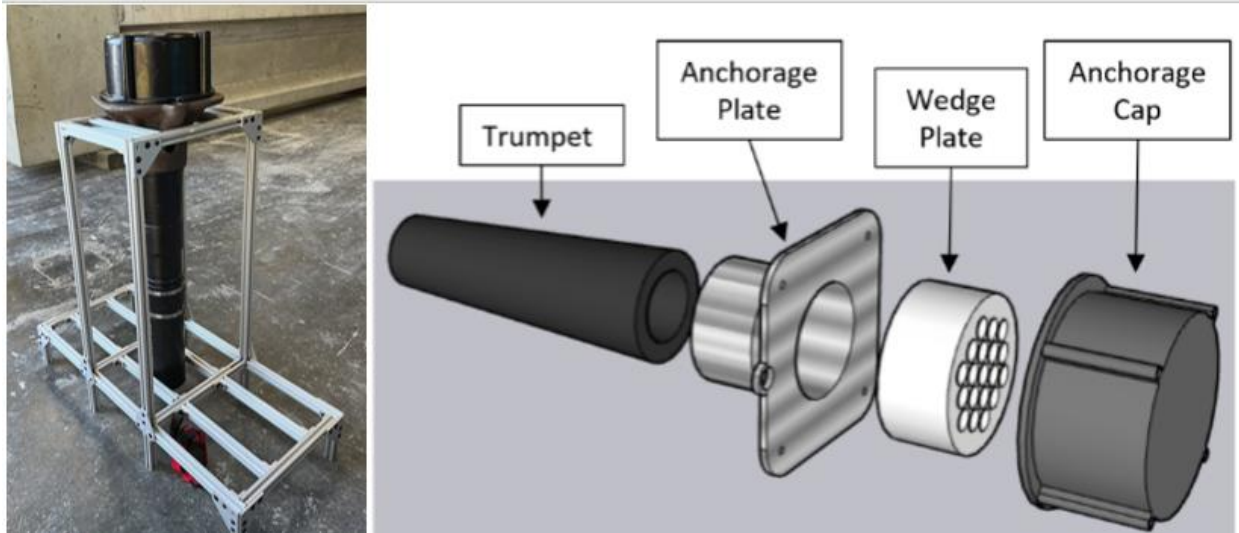


**Figure 28: Anchorage assembly**

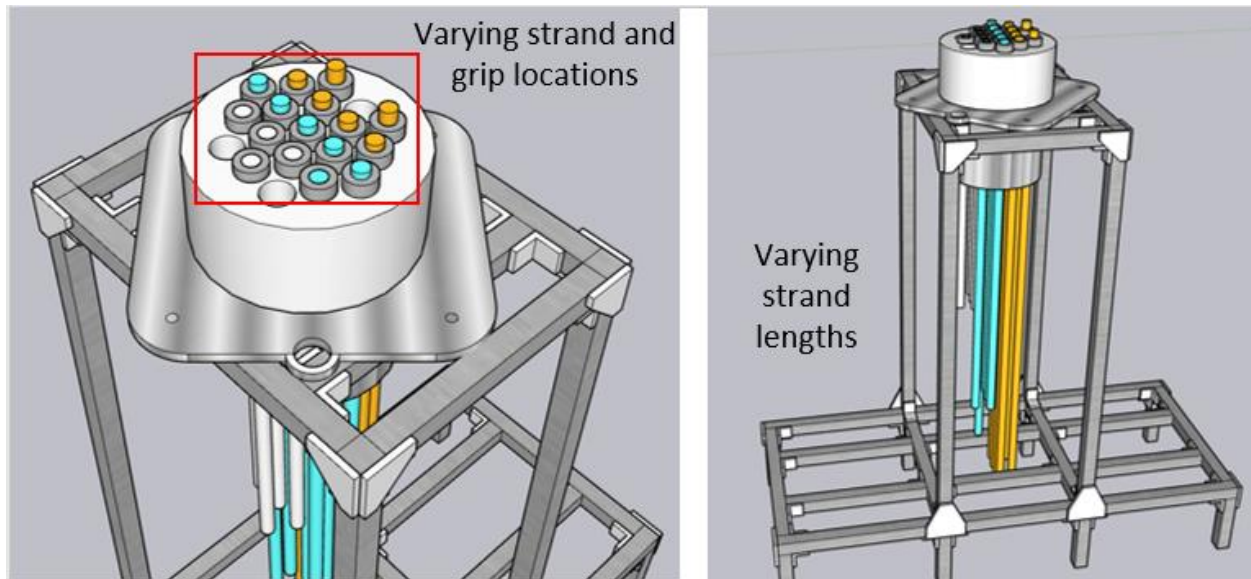


**Figure 29: Anchorage mock-up showing varied strand and grip locations for testing**

This mockup simulates a Type 5 anchorage protection detail, which has been commonly used in PT bridges with FFs. This anchorage type allows for more accessibility to the cap compared to other anchorage protection details as mentioned in the previous chapter.

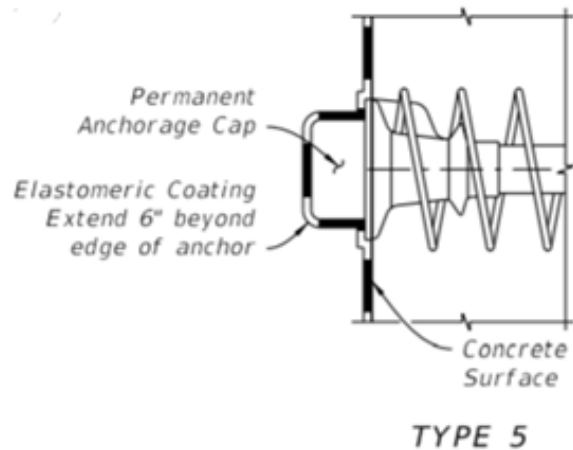


**Figure 30: Type 5 Anchorage (FDOT SDG)**

By imaging through the anchorage cap, the inspector can fully assess the cap without removing it. This is preferred by FDOT due to the removal of the cap being a time-consuming tedious task for the inspector. The cap is a good place to investigate for loss of PT force, if the strand and grip locations are off, then it indicates that the inspector may need to perform more in-depth inspections along the length of the duct to determine what is causing the issue. Because of this, imaging through the caps is an important part of this research to see if it is possible to detect any defects from radiographic images.

The second specimen that was tested on is an external tendon mockup filled with FF. This was created at the FDOT structures laboratory and is used for training on how to fill these ducts in the field. This specimen mimics a real duct and acts as a filled external duct for testing purposes. By testing on a filled duct, it is possible to determine if radiography will be effective in imaging through the FF to see the strands within.



**Figure 31: Filled External Tendon Mock-up**

The third and fourth specimen(s) that were tested on are both internal duct systems. Specimen 3 has an empty duct without strands while Specimen 4 has strands. These beams were repurposed from another FDOT project (BDV31 977-93) by Dr. Consolazio and Dr. Hamilton which can be seen in the figure below. As previously mentioned, the major challenge with inspecting internal ducts is that they are embedded in concrete. This is problematic since radiographic equipment has limits on how thick of a concrete cover it can image through. The deeper these ducts are embedded into the concrete, the more difficult it will be to get a clear image. The cross section of this specimen can be seen in Figure 35 below, showing a 10” web that the equipment must image through. Also, to perform these tests, the imaging plate must be on one side of the beam, where the radiographic source is on the other. If the beam is too thick, or difficult to access, this leads to more obstacles in performing this testing.

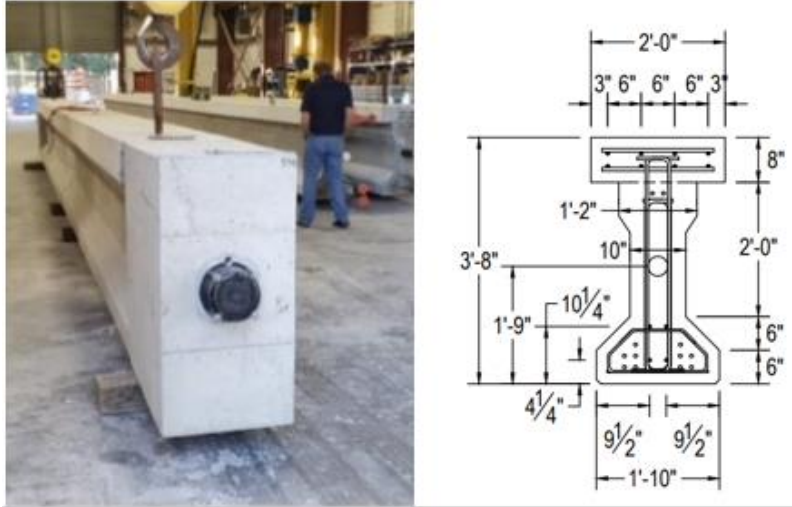


**Figure 32: Internal Duct Large Scale Specimen (FDOT Project BDV31 977-93)**

By testing different specimens, it was possible to determine the effectiveness of radiography on key parts of the PT beam to see how this method could be employed in the field.

#### **4.2 Equipment**

To determine the best radiographic setup, two different X-Ray machines were utilized. The first setup included the POSKOM PXM-20BT which is a low power (60-80 kV, 1.3-1.6mAs) portable X-Ray machine used by equine hospitals to assess their patients. This device is lightweight (~20lbs), user-friendly, and requires minimal setup. As this machine only needs a 120-volt electrical outlet, it is easy to use on any site; there are even models that run on battery making them even more portable for hard-to-access sites. This machine is low power, thus minimal PPE is necessary due to this equipment being used on equines and must be safe for veterinarians and their patients. Due to the simplicity of this device along with its portability, it seemed like a feasible option that could be employed on regular bridge inspections. The major drawback with this machine is its limited power and thus its inability to image through concrete.



**Figure 33: POSKOM PXM-20BT**

The other setup is the YXLON X-Ray machine, which is a higher power (250kV, 2.4mAs) industrial machine that can image through up to 12” of concrete. YXLON would be ideal for assessing internal tendons but requires more setup and safety precautions. As this is an industrial machine, it is more powerful compared to the POSKOM PXM-20BT and requires more equipment and power to run. YXLON is also much larger than the POSKOM PXM-20BT and is less portable, which requires more planning to effectively inspect the bridge. While this machine can image through up to 12” concrete, a 30’ radius is required from the machine to the operator to allow for a safe distance from the strong radiation source. In some cases, it would be necessary to close the bridge to perform the inspections, which is not ideal or feasible.



**Figure 34: YXLON**

#### **4.3 Data Collection:**

Images were collected from each of the specimens previously listed. The POSKOM PXM-20BT imaged through the anchorage mockup (Specimen 1), external duct specimen (Specimen 2), and through numerous end caps while the YXLON imaged through the end caps and internal duct specimens (Specimens 3 & 4). The results from these tests are described in the following section.

#### **4.4 Results:**

##### **4.4.1 POSKOM PXM-20BT:**

As previously mentioned, this is a low-power portable device. This device can be seen in action in Figure 38 below.





**Figure 35: POSKOM PXM-20BT Setup**

#### **4.4.1.1 Anchorage Cap (Specimens 1, 2, & 4)**

This machine produced promising results when imaging through the anchorage cap region. The following images would allow the inspector to determine strand and grip locations along with any other defaults within the cap, such as voids or corrosion. This inspection method could be carried out as a quick additional test to the current inspections to ensure that the cap region is free of faults. The anchorage mockup (Specimen 1) had strands of varying heights to simulate damage, which is clearly shown in the following images and proves that this method would be effective in the field.

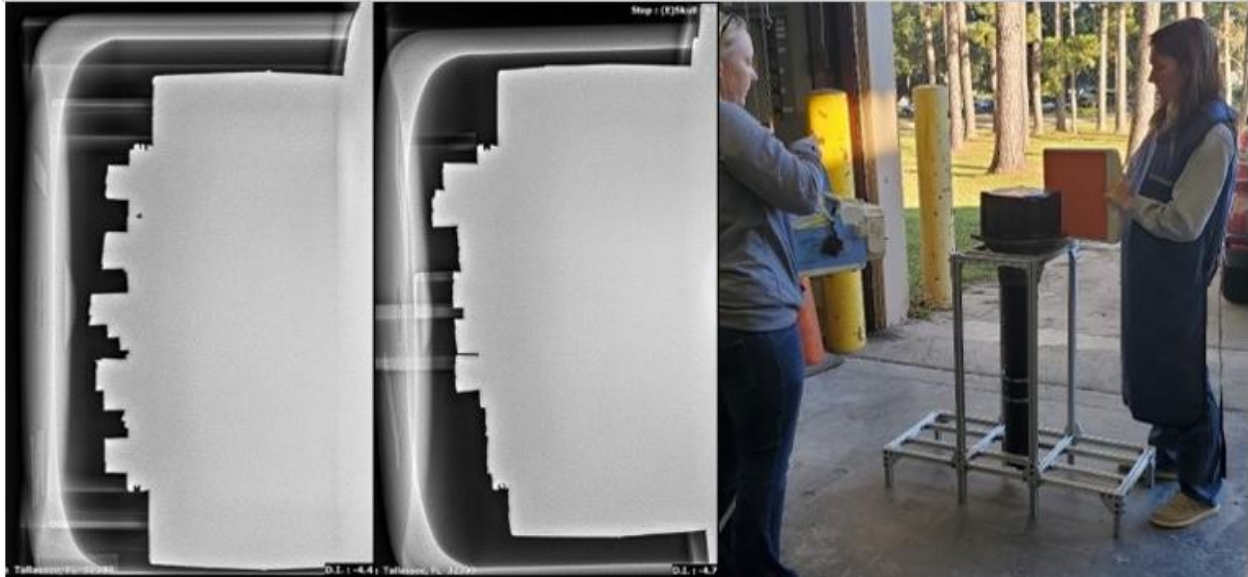


**Figure 36: Specimen 1 Anchorage Cap Results: Images collected from POSKOM PXM-20BT from different angles**

When used on the cap of Specimen 2, the images clearly depict the filled cap and would show the inspector any voids or defects. The FF is easily imaged through and does not disrupt the image quality in these photos. More research should be conducted on filled ducts to ensure the accuracy of this method due to this being the only filled specimen tested on in this project. The assumption can be made that tendons filled with CG would be more difficult to image through making it difficult to see the strands/wedge grips as clearly.

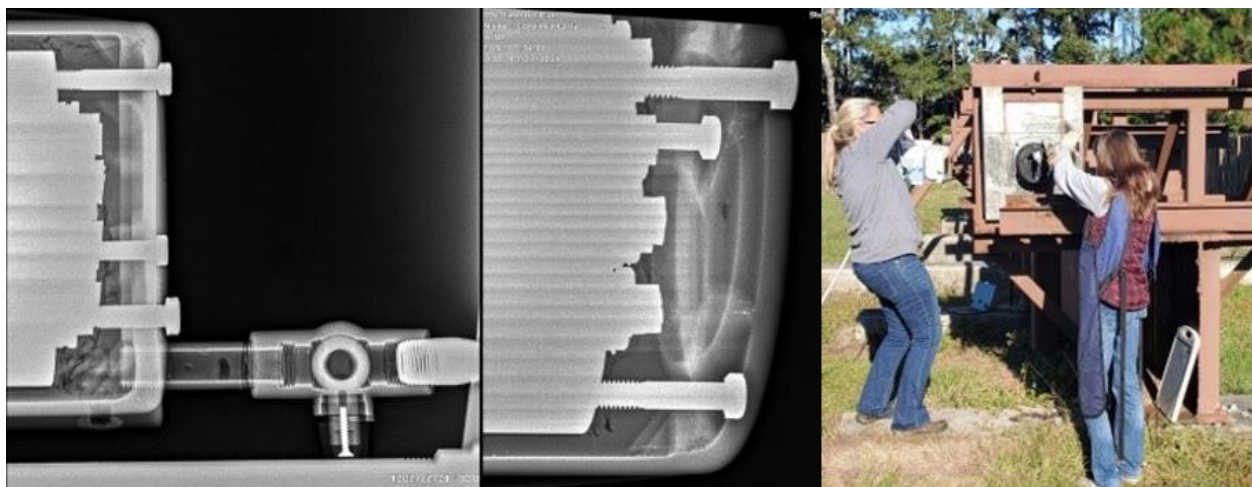


**Figure 37: External Duct Mockup: Filled Anchorage Cap Results**

The next test was performed on the full-scale internal specimen cap. Like the other cap images, the machine had no difficulty imaging through the cap and provided the inspector with a clear image depicting the inside of the cap.

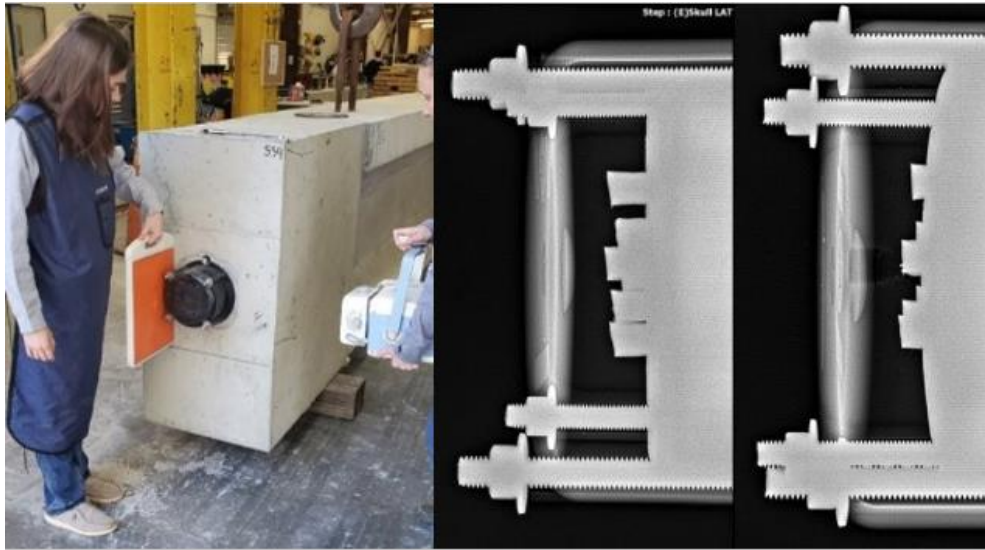


**Figure 38: Internal Specimen: Anchorage Cap Results**

#### **4.4.1.2 Internal Specimen (Specimens 3 & 4):**

The POSKOM PXM-20BT setup was not adequate for the inspection of internal ducts. This machine had difficulties imaging through 4” of concrete, thus is not suitable to image through full scale beams. The image below shows the attempt to image through concrete with this machine. Only a light visible outline of the strands is shown. Therefore, this machine is not recommended for the inspection of internal duct systems.



**Figure 39: Anchorage Mockup: Duct Results**

#### **4.4.1.3 External Specimen (Specimens 1 & 2):**

The POSKOM PXM-20BT had no difficulties imaging through the external duct system and yielded promising results. When tested on the filled external duct system, it was possible to see small voids in the filler along with the group of strands. One concern that was raised is that it is difficult to see each individual strand when they are grouped together in the tendon, making it challenging to see individual strands or detect possible corrosion within the strand bundle.



**Figure 40: Specimen 2: Filled Duct Results**

When tested on the trumpet of the anchorage mockup, the results were similar to those from the other external duct specimen photos. The images clearly show the strands, but it is difficult to decipher the strands from one another when all bundled together in the duct region. In this mockup, the strands were cut at various lengths/heights to test if the images would be able to show these height differences. The following images show these results.

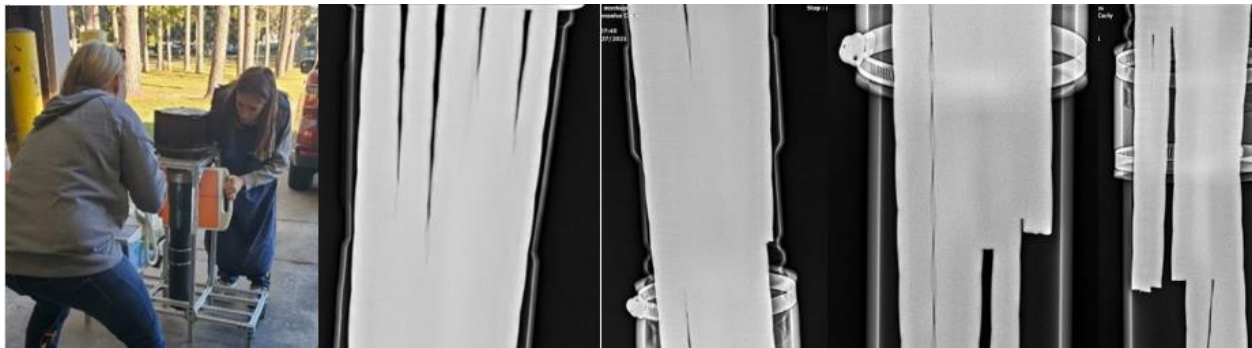


**Figure 41: Anchorage Mockup: Trumpet Results**

#### 4.4.2 YXLON:

The images below show the setup of the YXLON machine on the internal duct specimen. The imaging plate is on the left, while the radiation source is on the right.



**Figure 42: YXLON X-Ray Machine on Internal Duct Specimen**

#### **4.4.2.1 Anchorage Cap (Specimen 4):**

Due to the high power of the YXLON X-Ray machine, the images through the cap were slightly over exposed resulting in the “grayed” image of the cap seen below. Reducing exposure time could have prevented these overexposed images which should be explored in future testing. Fortunately, even with being over exposed, it is still possible to see the outline of the strand and grip locations. For inspection purposes this would be adequate in inspecting the cap and informing the inspector of any faults occurring within the cap.



**Figure 43: YXLON Machine on Internal Specimen Anchorage Cap**

#### **4.4.2.2 Internal Specimen:**

The YXLON X-Ray is capable of imaging through 12” of concrete, which can be seen in the following images.

#### **Empty Duct without strands (Specimen 3):**

These are the images produced of the internal specimen with an empty duct. The machine was able to show the duct location along with the mild reinforcement.

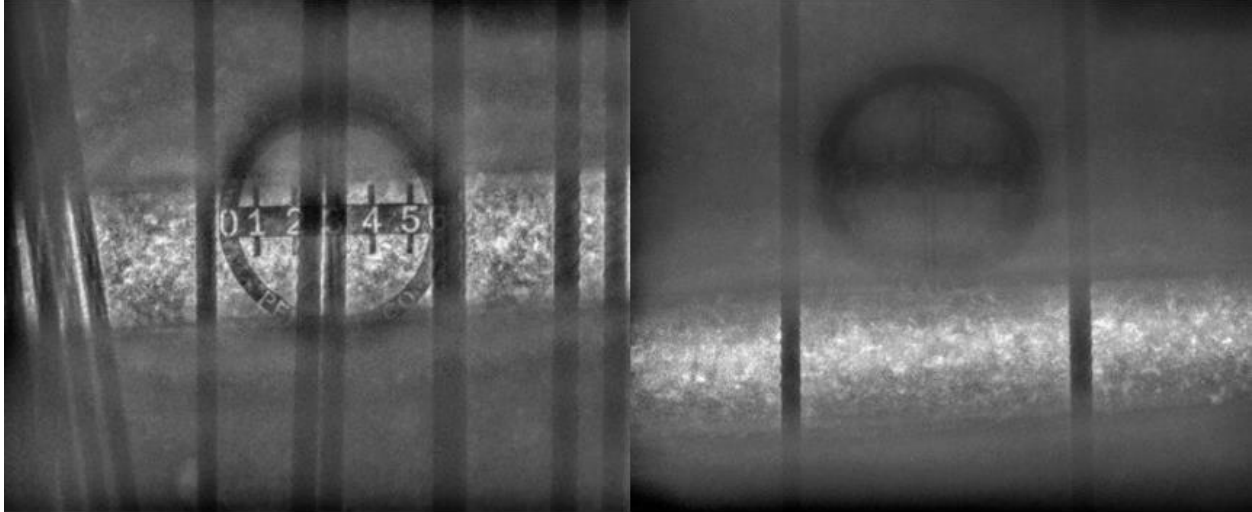


**Figure 44: Internal Duct Specimen: Duct without strands**

**Duct with strands (Specimen 4)**

The following images are of the internal specimen with the strand-filled duct (no filler). The machine was able to show mild reinforcement along with the strands. This is a 12-strand wedge plate only filled to half capacity, which is why the strand bundle isn't as concentrated as compared to the external specimen. Due to there being less strands, the YXLON was able to show a detailed image showing the individual wires that make up the strands. This method would be able to detect voids, and possibly corrosion of these strands in the field. One downfall of this technique on the internal specimens is that only one angle of the ducts can be imaged through due to how the duct is situated within the beam.





**Figure 45: Internal Duct Specimen: Duct with strands 1ft away from end block (Left) and 5ft away from end block (Right)**

#### **4.4.2.3 External Specimen (Specimen 2):**

Due to technical difficulties and weather conditions, testing of the external specimen with the YXLON equipment was not possible, but the assumption can be made that this equipment would work well due to the promising results on the other specimens there was collected. Although, due to the overexposed images that were produced when imaging through the anchorage cap, the external duct images might be slightly overexposed as well.

#### **4.5 Conclusion:**

At this point, radiography is a promising NDE method to consider when inspecting PT bridges that use FF. This method can detect voids, strand breakages, corrosion and other defects that can be present within the anchorage caps along with internal and external ducts (Table 4). By integrating radiography testing with the current biennial inspections, it will allow for inspectors to have a clear view of the internal working of these ducts/anchorage caps. There are some limitations, however, that must be considered when implementing this method, such as cost, ensuring a strong enough radiation source, and operator training/safety. This equipment on its own is already rather costly, pairing that with the highly skilled operator, the cost of this testing can become expensive rather

quickly depending on the specific project. To use this equipment, the operators must be extensively trained and must work with the inspector to ensure that the proper points of interest throughout the bridge are being inspected. Also, the higher power equipment, such as the industrial YXLON machine, requires extensive safety protocols including a 30' radius around the imaged area that must be blocked off. Due to the harmful effects of radiography, it is important to ensure a safe distance away from the source. When performing these tests, it might be necessary to close the bridge, which is not preferred as it will cause delays and upset the flow of traffic. Overall, radiography has proved to be a promising method but faces some challenges when implemented in the field.

**Table 4: Effectiveness of Radiographic NDE**

	Anchorage		Internal Duct				External Duct			
	Wedge grip seating	Strand-end location	Tendon Location in Duct	Broken Strand	Broken Wire	Void in Filler	Tendon Location in Duct	Broken Strand	Broken Wire	Void in Filler
<b>POSKOM PXM-20BT</b>	Recommended	Recommended	Not Recommended	Not Recommended	Not Recommended	Not Recommended	Recommended	Method works, but not recommended	Method works, but not recommended	Needs more research
<b>YXLON</b>	Recommended	Recommended	Method works, but not recommended	Method works, but not recommended	Method works, but not recommended	Needs more research	Recommended	Method works, but not recommended	Method works, but not recommended	Needs more research

Legend	
Recommended	Recommended
Method works, but not recommended	Method works, but not recommended
Not Recommended	Not Recommended
Needs more research	Needs more research

## CHAPTER 5: THERMOELASTICITY

### 5.1 Introduction

Thermoelasticity describes the behavior of a material as it expands and contracts with fluctuating temperatures. Thermoelasticity also describes changes in thermal conductivity as a function of stress level. This concept can be used to monitor the stress levels of concrete by analyzing the temperature of the surface as the material heats and cools. By analyzing the diurnal heating cycles that concrete bridges experience from the sun's heating, this could be used to analyze stress levels and ensure that the post-tensioning is still functioning.

This concept has been derived from previous studies and its uses within the mining industry. The design of HVAC systems for mining operations are highly dependent on the thermal properties of the rock formations surrounding the mine shafts. This is explained in the study “Thermal conductivity of rocks and its variation with uniaxial and triaxial stress”, which is a study that focused on characterizing the variation of thermal conductivity in rock structures as a function of the triaxial state of stress. This study consisted of measuring the thermal conductivity of multiple rock specimens as they were subjected to varying degrees of triaxial stress. This setup can be seen in Figure 49 below. The results of this testing found that for the zero-confinement condition, the thermal conductivity increased from  $5\text{W/m}^{\circ}\text{C}$  to approximately  $8.25\text{W/m}^{\circ}\text{C}$  when 1450 psi of compressive stress was applied. This shows that there is a possible correlation between the stress levels within the specimen and the thermal conductivity.

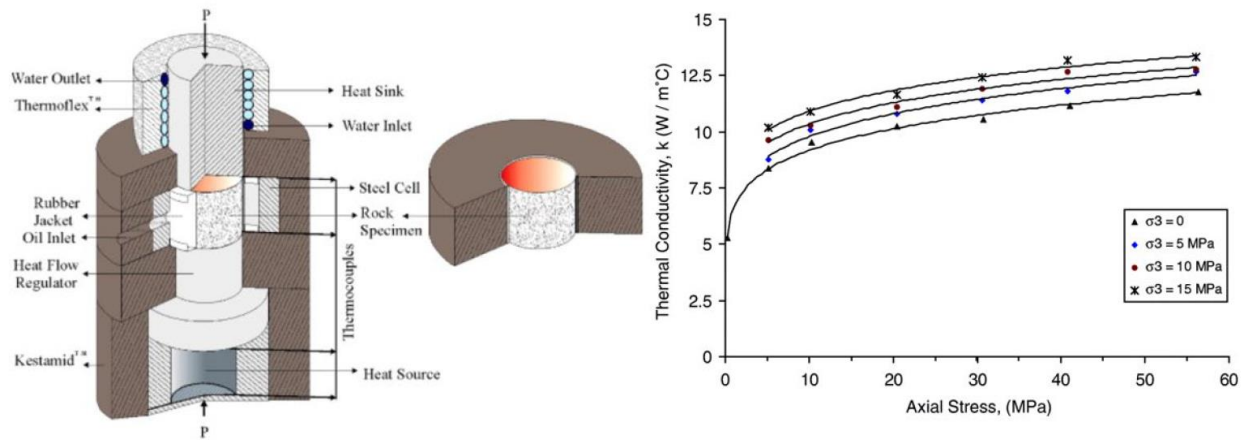


**Figure 46: Test setup and experimental typical result for thermal conductivity variations in rock specimens due to axial stress (Demirci, 2004)**

Assuming that concrete will exhibit similar variations in thermal conductivity when loading is applied, it should be possible to evaluate the stress level at critical locations in the PT bridge. There was also other research found that implies that the thermal conductivity of concrete can change as a result of mechanically induced damage such as cracking (Demirci, 2004). Thus, indicating that concrete should have a change thermal conductivity value under different stress levels.

These thermal conductivity values can be measured and estimated to identify the stress state of the concrete. This method could be useful in the areas surrounding the anchorage blisters to determine if the tendon has lost a significant level of post tensioning force.

The diurnal temperature effects on the overall stress level in the PT element may also be assessed at critical locations by making direct measurements of thermal conductivity. The diurnal changes can be compared to the expected value at the specific location which will give an indication of whether or not an appropriate level of post tensioning is being maintained in the structure. If the thermal conductivity is found to be lower than usual, the inspector could then assume that loss of PT force is occurring due to the lower stress levels that the concrete is experiencing.

Although this method seemed promising when completing initial research on the subject, after conducting numerous tests there was no evidence found that there is a correlation between the thermal conductivity and stress in concrete. As the results from these tests were inconsistent, this theory could not be proven.

### 5.2 Finite Element Analysis (FEA)

To determine the effectiveness of this method, an ANSYS model was created to establish a baseline for the small-scale testing. This is a simple way to analyze how the heat should propagate through the concrete while limiting external variables that could affect the results.

#### 5.2.1 Model Geometry

This model consisted of a simple 12"x 3.5"x 4.75" concrete block, to simulate the specimens that would be tested on. The model can be seen in Figure 50 below. The circular ring on the bottom represents the heating lamp and where the heat will be applied in the model. The vertical line is where the temperature will be measured as the surface heats and cools.

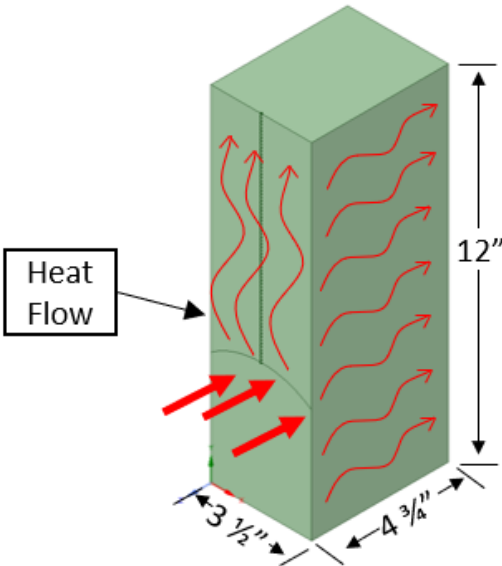
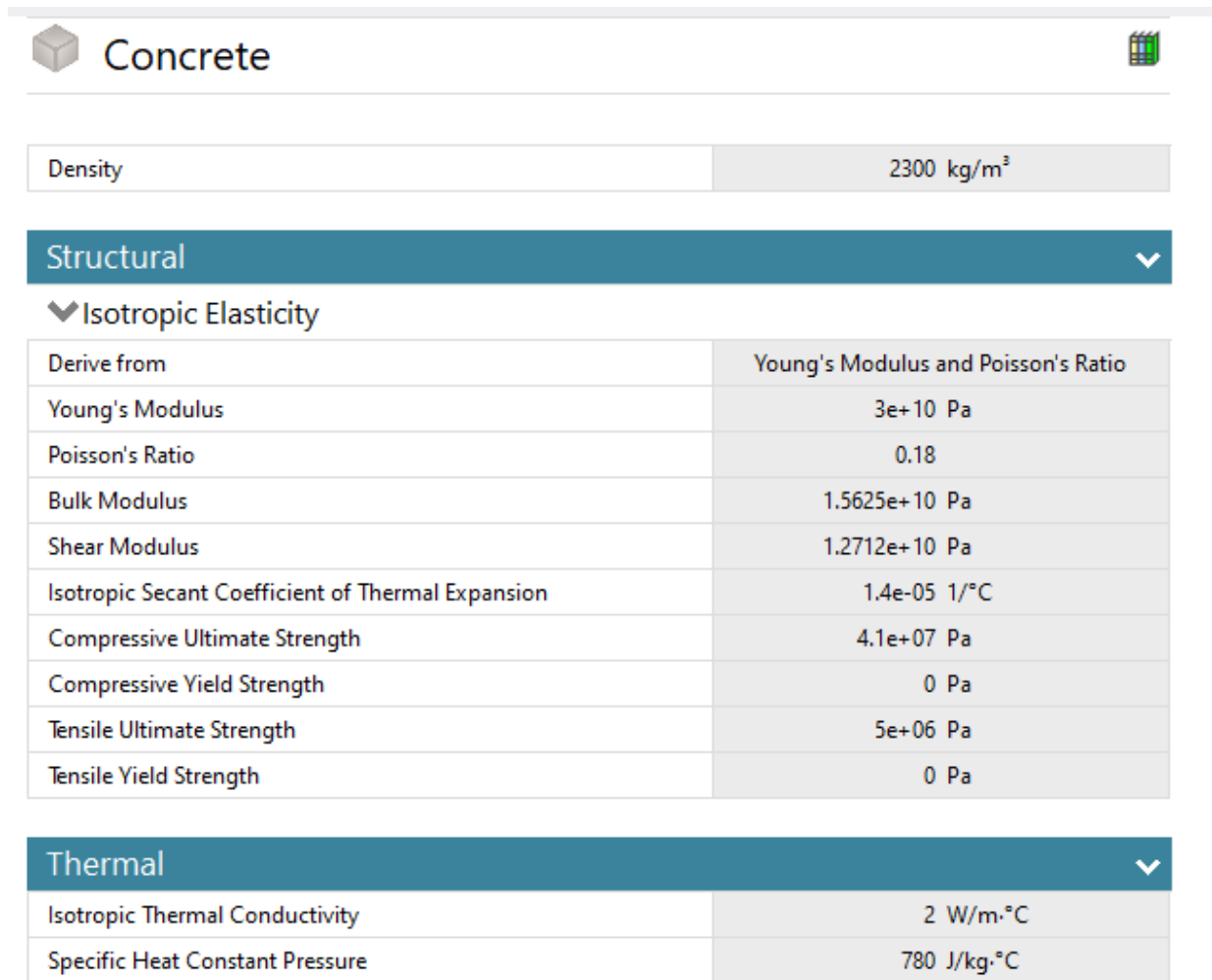


Figure 47: Model Geometry

## 5.2.2 Material Properties

The material that these tests will be performed on is concrete, so the ANSYS material properties for concrete were used. For this model the thermal conductivity (k) was varied from .75W/m °C to 2W/m °C to simulate the non-loaded specimen (lower thermal conductivity) and the loaded specimen (higher thermal conductivity). This will be explained more in the following sections.



The image shows the ANSYS material properties interface for Concrete. It includes a header with a cube icon and the word 'Concrete'. Below this, there is a table for Density (2300 kg/m³). A 'Structural' section is expanded to show 'Isotropic Elasticity' properties in a table. A 'Thermal' section is also expanded to show 'Isotropic Thermal Conductivity' (2 W/m·°C) and 'Specific Heat Constant Pressure' (780 J/kg·°C).

Concrete	
Density	2300 kg/m <sup>3</sup>
<b>Structural</b>	
▼ Isotropic Elasticity	
Derive from	Young's Modulus and Poisson's Ratio
Young's Modulus	3e+10 Pa
Poisson's Ratio	0.18
Bulk Modulus	1.5625e+10 Pa
Shear Modulus	1.2712e+10 Pa
Isotropic Secant Coefficient of Thermal Expansion	1.4e-05 1/°C
Compressive Ultimate Strength	4.1e+07 Pa
Compressive Yield Strength	0 Pa
Tensile Ultimate Strength	5e+06 Pa
Tensile Yield Strength	0 Pa
<b>Thermal</b>	
Isotropic Thermal Conductivity	2 W/m·°C
Specific Heat Constant Pressure	780 J/kg·°C

**Figure 48: ANSYS Concrete Properties**

## 5.2.3 Boundary Conditions

The initial temperature was set to 22°C as that is the general ambient temperature of the concrete surface of the specimens in the lab. This analysis consisted of a 5-minute heating period and a 10-minute cool down period for a total of 15 min (900 sec) to match the tests that will be performed

on the specimen in the lab. The lamp outline was drawn on the block to show where the heat source would be applied to as shown in the figure below. The blue portion is where the heat was applied, and the yellow portion is the area that is being measured. A convection boundary was applied on the front face where the heat would be propagating through.

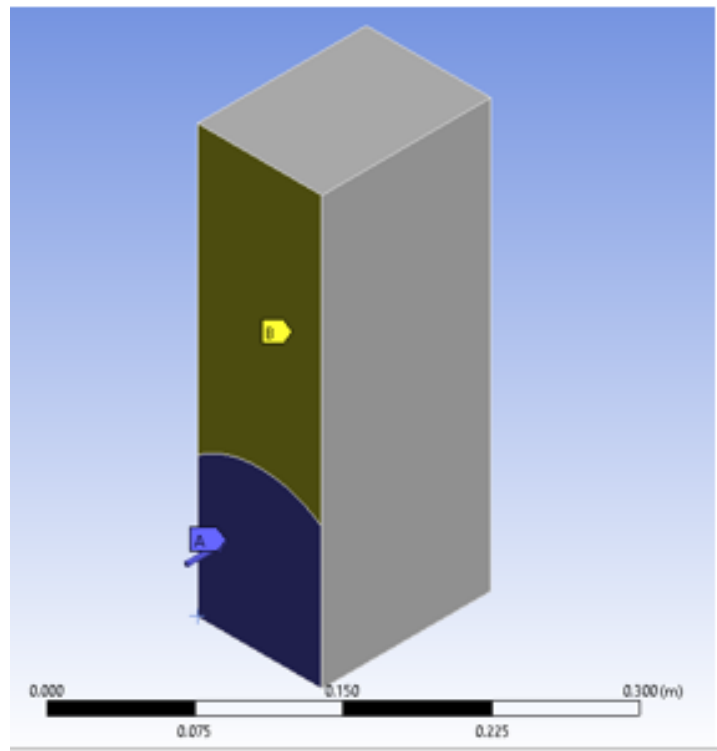


**Figure 49: Model Geometry & Boundary Conditions**

#### **5.2.4 Mesh Refinement Study**

A mesh refinement study was conducted to determine the best mesh size to perform this analysis. Multiple mesh sizes were analyzed, ranging from .003 m to .02 m. To choose the most effective mesh size, multiple runs were made with each size to see the coarsest mesh that could be used without compromising analysis results. A finer mesh would yield more precise analysis results, but too fine of a mesh would result in the analysis taking too long to complete and would sometimes freeze the system and ruin the analysis. A very coarse mesh results in a quick analysis but is not considered as precise.

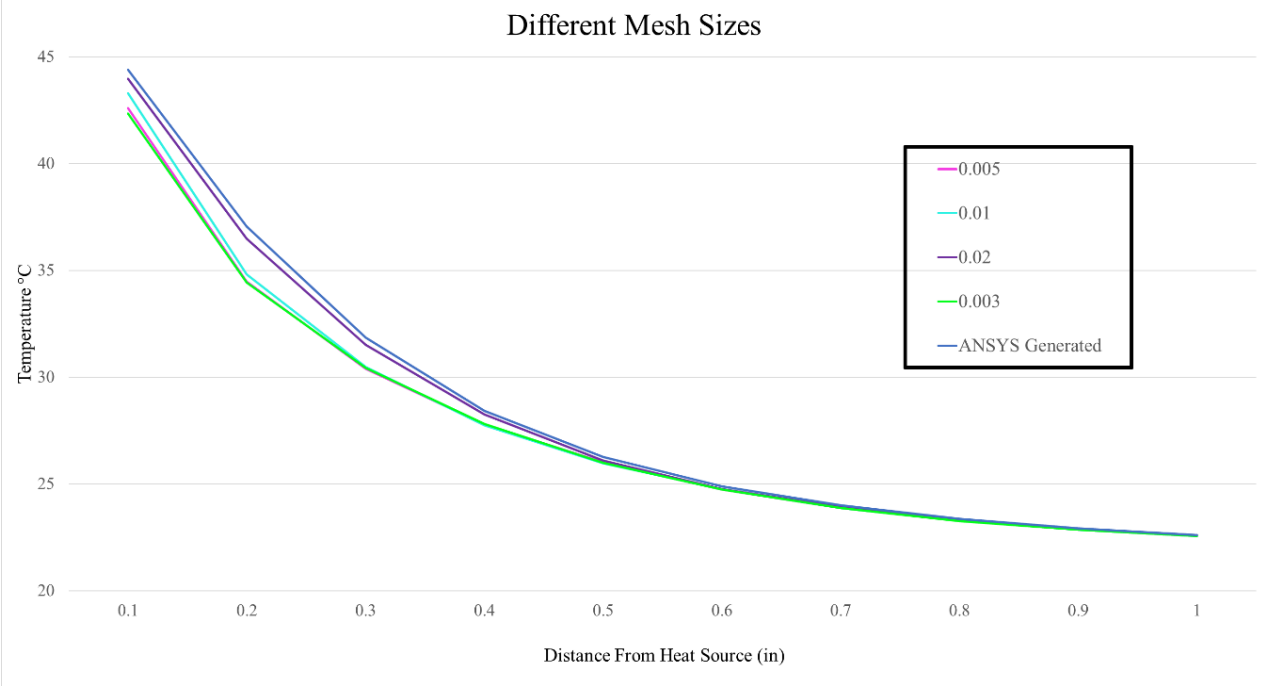


**Figure 50: Mesh Refinement Study**

After performing multiple tests with varying mesh sizes, a mesh size of .01 m was chosen. This allowed for the analyses too be completed in a reasonable time frame and yielded precise results.

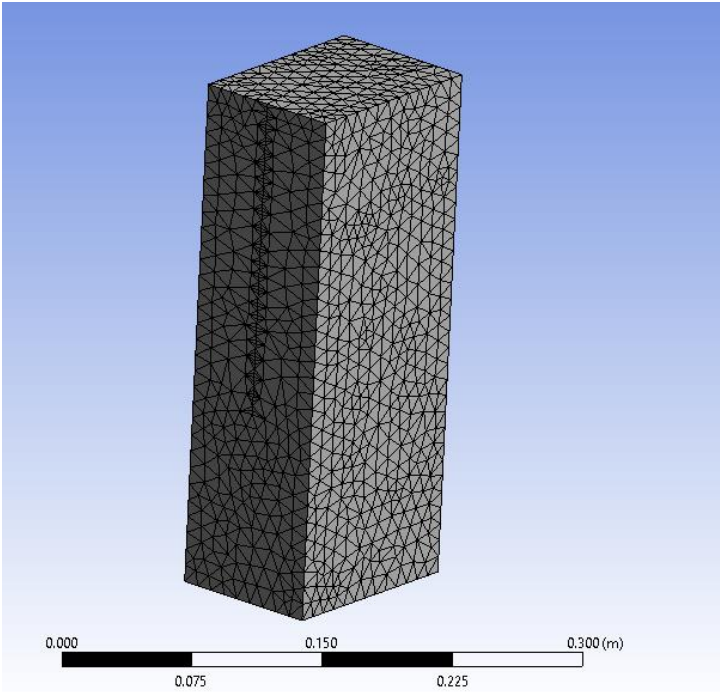


**Figure 51: .01 m Mesh Size**



### 5.2.5 Results

The same test was run twice with varying thermal conductivity values of  $.75 \text{ W/m } ^\circ\text{C}$  and  $2 \text{ W/m } ^\circ\text{C}$ . Concrete is said to have a higher thermal conductivity when the stress is higher, so the thermal conductivity of  $.75 \text{ W/m } ^\circ\text{C}$  simulates no load applied while the  $2 \text{ W/m } ^\circ\text{C}$  simulates what should be experienced when a load is applied. A visual representation of how the heat propagated through the concrete with the varying thermal conductivity can be seen in Figure 55 below.

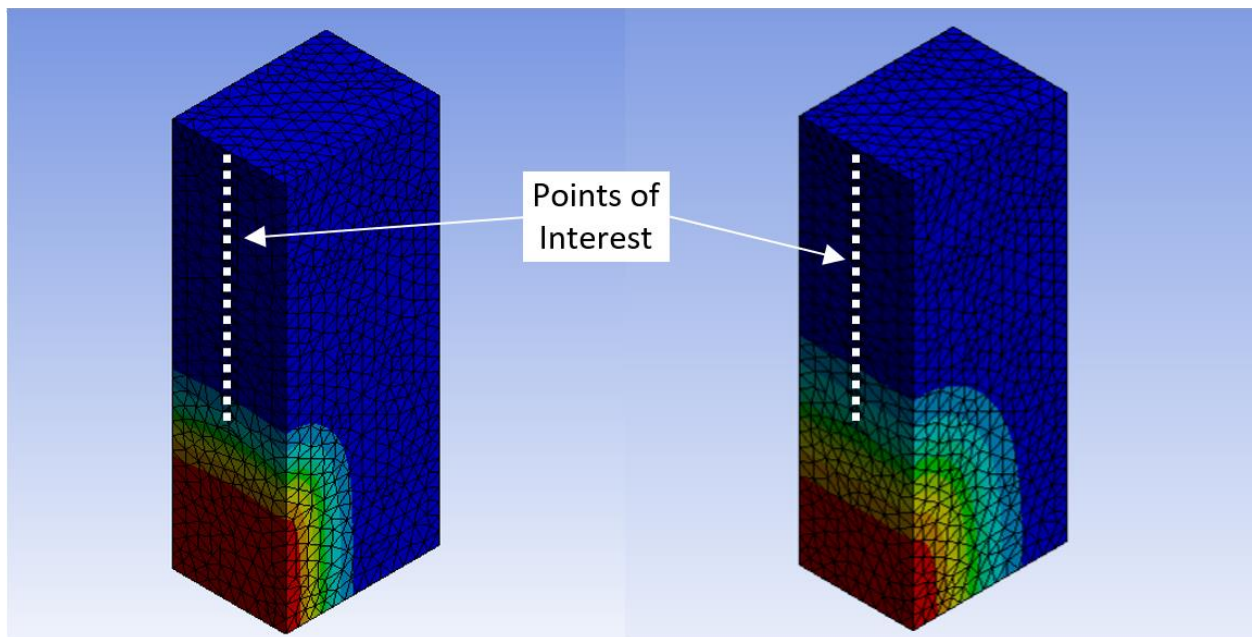


**Figure 52:  $k=.75 \text{ W/m } ^\circ\text{C}$  (left),  $k=2 \text{ W/m } ^\circ\text{C}$  (Right)**

The following graph shows the temperature at  $T=5 \text{ min}$  (beginning of cooldown period) and compares the different thermal conductivity values. As shown in the graph, the initial temperature right next to the heat source is consistently lower for the  $k=2 \text{ W/m } ^\circ\text{C}$  test. Meaning that the loaded tests should correlate with these results and should experience a lower temperature when compared to the unloaded test. The higher thermal conductivity means that the heat will propagate through the specimen faster thus resulting in a cooler specimen. As the distance increases from the heat

source, both tests show that the temperature reaches the starting temp of 22 °C at a distance of 2” away.

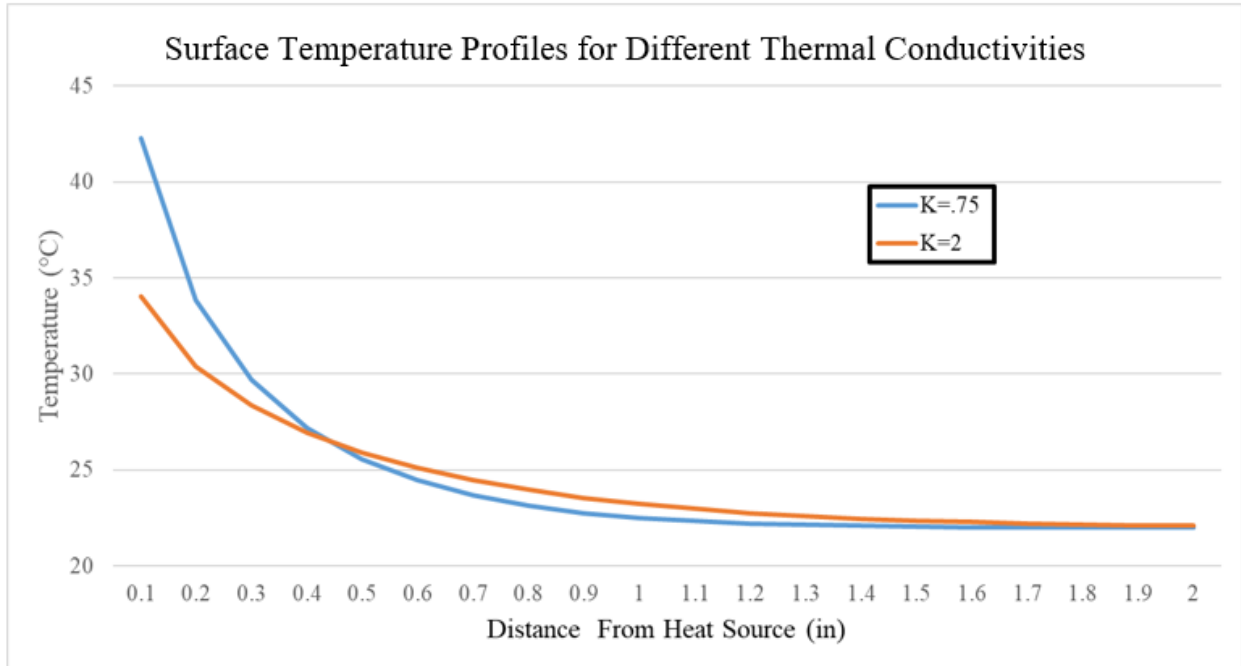


**Figure 53: Surface Temperature Profiles for Different Thermal Conductivities at T=5 min**

### 5.3 Experimental Validation

The next step consisted of testing on small blocks within the lab to validate the results from the ANSYS model. The goal was to determine if a relationship could be made between the thermal conductivity and stress levels in the concrete as hypothesized.

#### 5.3.1 Block geometry

The concrete block tested on can be seen in Figure 57 below. This block was made using QUIKRETE 5000 concrete mix and achieves 5000 psi after 28 days. This block also has four #3 bars of mild reinforcing steel and  $\frac{1}{8}$  in diameter stirrups spaced at  $1 \frac{3}{4}$  in to simulate transverse reinforcement.

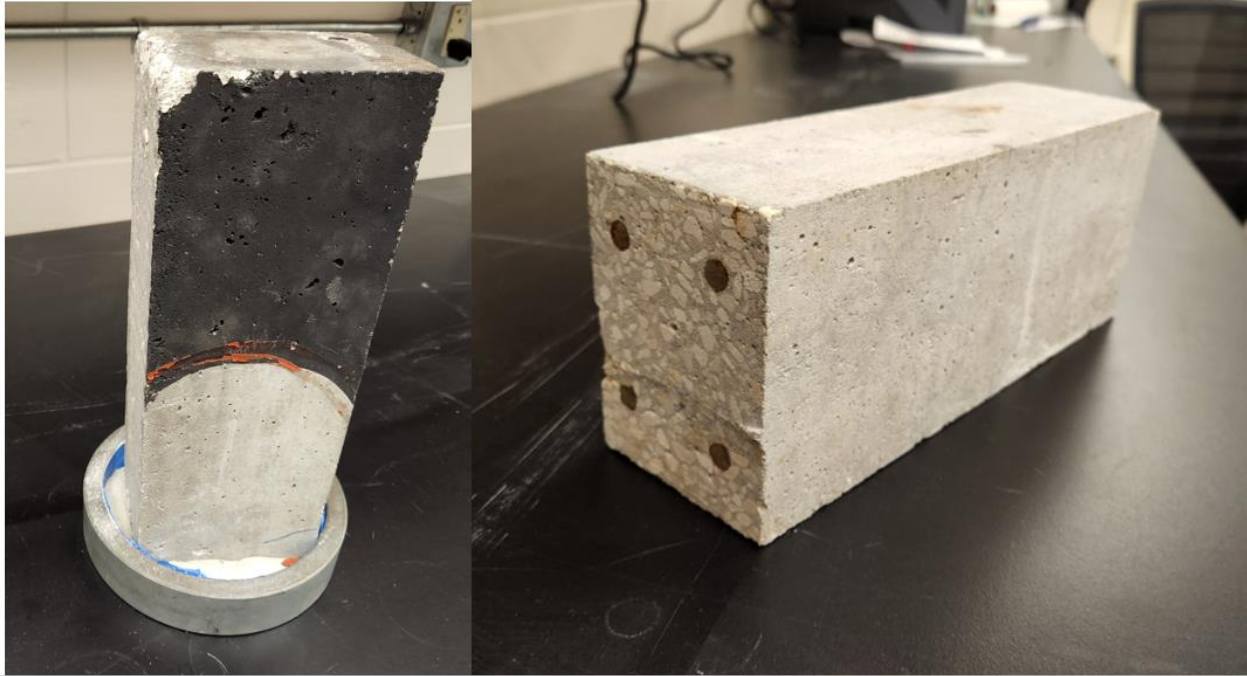


**Figure 54: Block that was tested on (Left), Identical block to show reinforcing (Right)**

### **5.3.2 Experimental setup**

The testing machine is the Tinius Olsen Super “L” Universal Testing Machine (Model 398 Display & CHM 496 Controller) and was used to apply a constant load of 15 kips to the specimen for the loaded tests. The heating source is a 250-watt heating lamp, and the camera is a FLIR A600-Series Infrared Camera. This entire setup can be shown in Figure 58 below. At first, neoprene pads were placed on the top and bottom of the specimen in the testing machine, but after multiple tests, it was realized that they were contracting as the load was applied, thus moving the specimen in the loaded tests, and altering the results. To avoid this, a rigid non-shrink grout was used to adhere the specimen to the base plate, thus avoiding the beam moving down when the load is applied and ensuring that the specimen does not move between tests. A frame was constructed from 80/20 steel to hold the camera and lamp in place onto the machine so that the camera and the lamp did not move between testing. To create a seal between the lamp and the concrete surface, rubber sealant was added to create a shield from the heat source and the surface that was being studied.

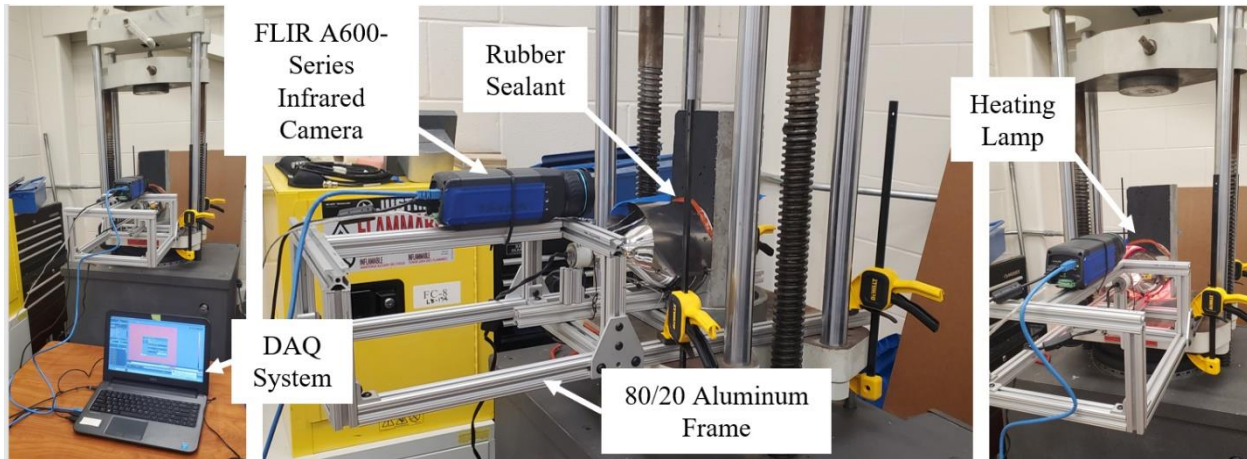


**Figure 55: Testing Setup**

### 5.3.3 Testing parameters

Like the ANSYS model, there was a 5-minute heating period where the lamp was turned on, and a 10-minute cooling period. Multiple runs were performed to compare the loaded and unloaded results. Due to inconsistent data, each test was run twice. Four tests of data were collected in this report, experiments 1 & 3 had no load applied, while experiments 2 & 4 had a constant 15 kips applied during the 15-minute runs. Each of these tests were performed on the same specimens, on the same day with a waiting period in between the tests to allow for the concrete to cool back down to ambient temperature.

Exp. 1	No Load
Exp. 2	15 Kips Applied (Concrete Stress = 755 psi)
Exp. 3	No Load
Exp. 4	15 Kips Applied (Concrete Stress = 755 psi)

### 5.3.4 Results

As previously mentioned, these tests were inconsistent and could not find conclusive results that there is a correlation between the stress applied and the thermal conductivity of the concrete. The results for experiments 1 & 2 can be seen in Figure 59 below. These different lines show the high and low temperatures during the 10-minute cool down period. The pink and red lines are at T=5 minutes while the blue and yellow lines are at T=15 minutes. Both experiments had very similar

high temperatures, while the lows varied by experiment. For these tests, the change in temperature was higher for the loaded specimen.

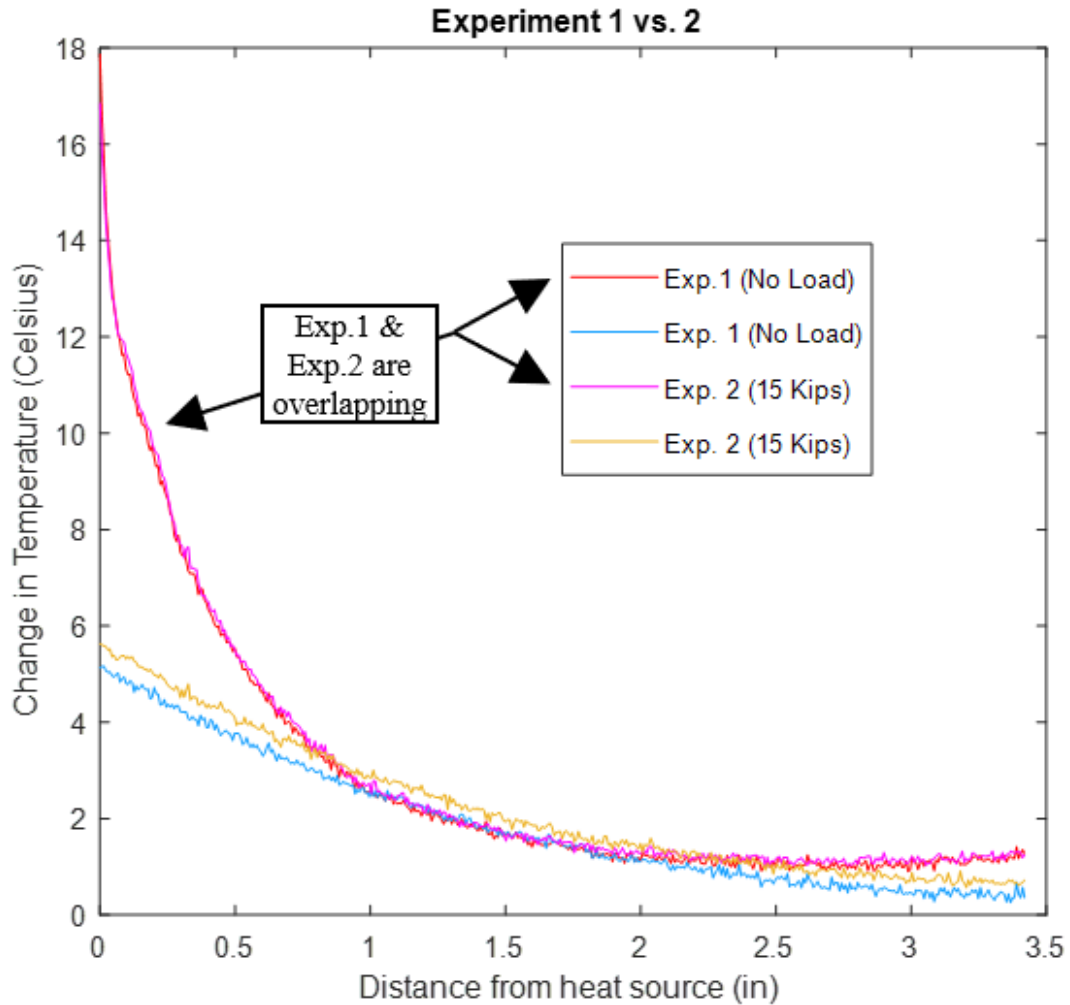


**Figure 56: Experiment 1 vs 2**

The results from experiments 3 & 4 are shown in Figure 60 below. Similar to the results from experiments 1 & 2 the high temperatures were the same for each experiment and the low were varied. The change in temperature for the low values was once again higher for the loaded specimen.

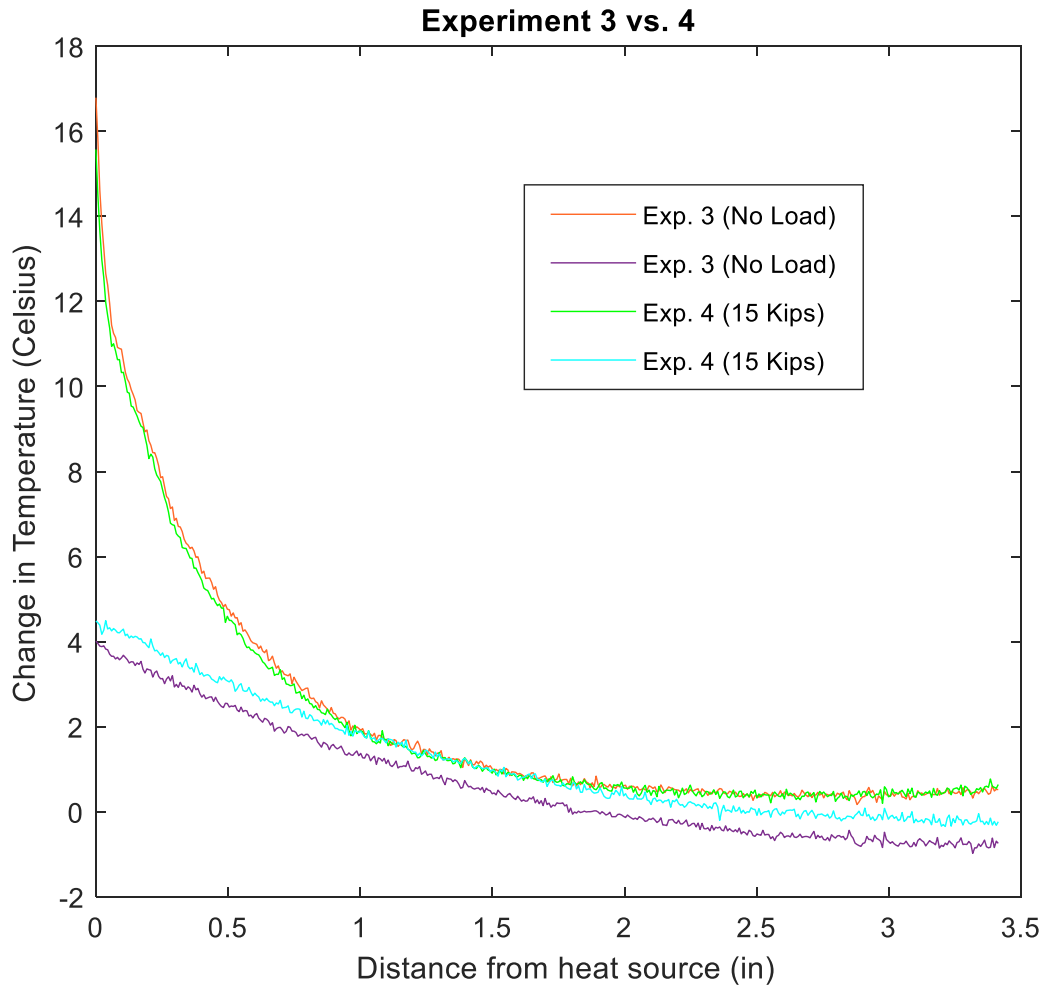


**Figure 57: Experiment 3 vs 4**

Data for experiments 1-4 is shown in Figure 61 below, and as previously mentioned, the high for each experiment is very similar while the lows are varied. It seems the lows for the loaded specimens are consistently higher, but the results are discouraging due to the differences between tests 1 & 3 and tests 2 & 4 as these experiments should match more closely due to the tests being performed the same. These tests were completed without moving the specimen and were analyzed along the same points of interest, because of this, the results for experiments 1 & 3 and 2 & 4 should be the same.

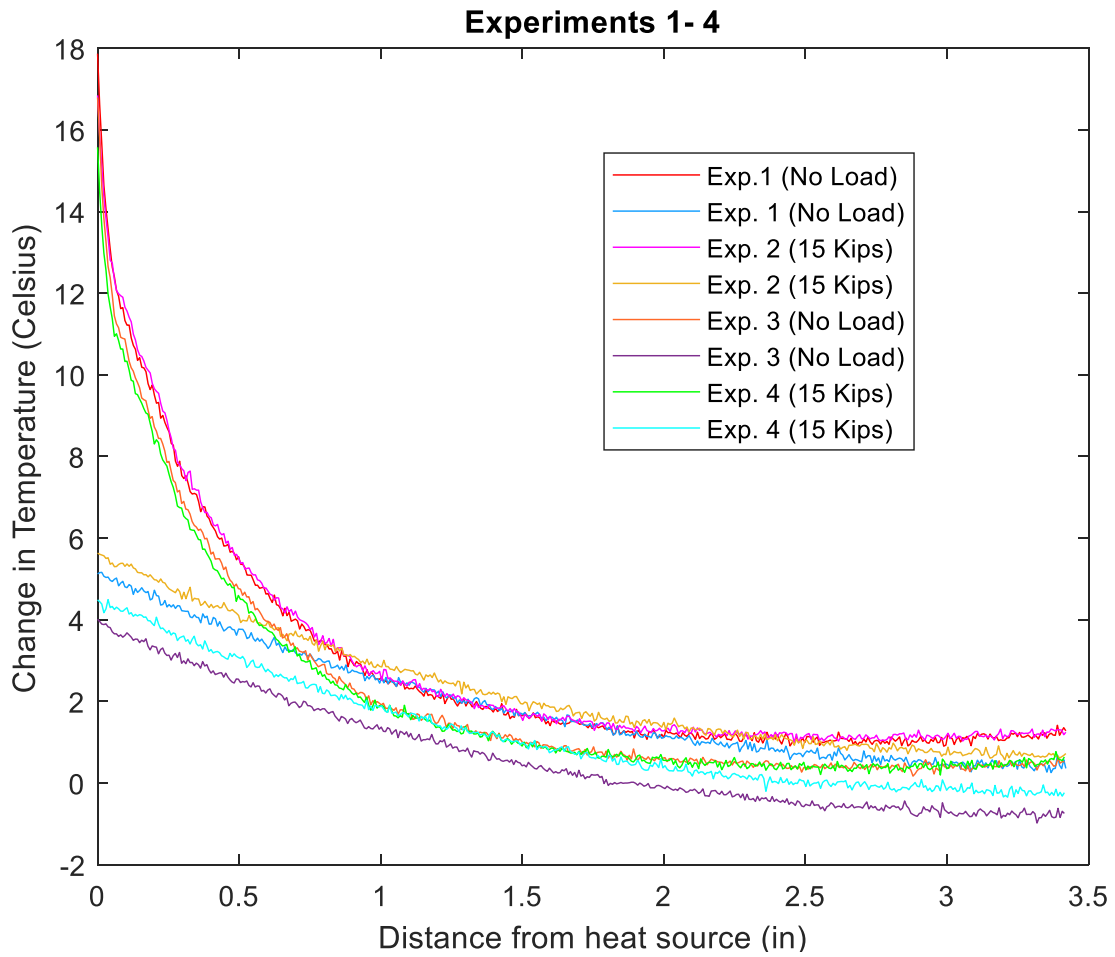


**Figure 58: Experiments 1-4**

Due to these results being inconsistent, a conclusive relationship could not be determined between the stress in the concrete and the thermal conductivity. More research on this subject should be performed in efforts to validate this relationship.

## **CHAPTER 6: CONCLUSION**

### **6.1 Summary of Findings**

This research was successful in identifying multiple NDE methods that would be adequate for inspecting PT bridges that use FFs. After exploring multiple NDE methods through a literature review, the three possible methods identified for further investigations were Visual Inspections, Radiography, and Thermoelasticity. This study found that visual inspections and radiography were both promising methods. The results for thermoelasticity were inconclusive. Visual inspection is a NDE method that will always be performed during FDOT's biennial inspections, but specific indicators unique to FF were identified. These indicators include unique cracking patterns and possible cap damage that would be experienced if strand or tendon failure were to occur. Radiography was also found to be an effective method on both internal and external tendons but is a costly method to perform. A deployment for the medical grade equipment costs approximately \$1150 (for 15 pictures, including technician travel costs) while a deployment of the industrial grade equipment was \$3300 (for 6 pictures, including technician travel costs). This method could detect voids and strand breakages but requires accessibility to the duct and cannot image through more than 12" of concrete for internal tendons. Thermoelasticity seemed to be a promising method due to its success in the mining industry but results in this study were inconsistent and could not find a correlation between thermal conductivity and stress.

### **6.2 Recommendations**

More research should be conducted on all three methods identified as there is not an abundant amount of research currently available on PT bridges that use FFs.

Visual inspections will be performed on current and future bridges that use FF and inspectors should take note and record any findings that they discover while performing these inspections. It



is possible that not all visual indicators were identified in this study. As more of these bridges are constructed, additional indicators could be identified.

Radiography proved to be an effective NDE method for both internal and external tendons, but more tests should be completed on this method. This is a very promising method that allows the inspector to have a clear visual of the possible defects found in the duct, but this study lacks results on FF filled internal ducts. Future studies on this topic should test on filled ducts, to determine the effectiveness of this equipment if employed in the field. The major downfall with this method is the high cost and clear accessibility to the ducts to take the images. Also, the industrial YXLON machine is only capable of imaging through 12” of concrete and requires a 30’ radius from the radiation source and the operator, meaning that in some cases the bridge may need to be shut down to perform this testing which is not ideal. But the low power POSKOM 20BT PXM would be able to image through anchorage caps throughout the bridge as long as a Type 5 protection detail is used. If the bridge needs a more in-depth inspection, the more powerful industrial equipment should be employed. If only the anchorage caps and external ducts need to be assessed, the low power medical x-ray equipment would suffice.

In this study, thermoelasticity was not found to be an effective NDE method for evaluating PT bridges that use FFs. As the results from testing were inconsistent, a correlation could not be found between the stress in the concrete and the thermal conductivity. The small-scale testing performed in this study was clearly unsuccessful, but more tests could prove effective in demonstrating the usefulness of this method.

### **6.3 Future Work**

Future work on this topic will include creating larger scale post-tensioned specimens to perform more testing on the various NDE methods. These specimens will be load tested, the visual

inspection of these specimens should confirm the expected indicators mentioned in this study. At this point, radiography has proven to be a promising method but due to the resources available, more radiography testing will not be performed in this study. Thermoelastic testing will be performed on these specimens to try and continue discovering a correlation between the stress and thermal conductivity, by using the natural diurnal cycles of the sun for the heating cycle.

There will be two different specimens, the first being an internal duct system while the other being an external duct specimen with two ducts. The drawings for these specimens can be seen in the Appendix.

## CHAPTER 7: REFERENCES

Hamilton, H. R., Rice, J. A., Brenkus, N. R., Abdullah, A. B. M., Bhatia, R., & Skelton, D.

(2017). Replaceable Unbonded Tendons for Post-Tensioned Bridges.

<https://rosap.ntl.bts.gov/view/dot/34819>

An FHWA special study: post-tensioning tendon grout chloride thresholds. U.S. Department of Transportation/Federal Highway Administration. (n.d.). Retrieved January 7, 2022, from

<https://www.fhwa.dot.gov/publications/research/infrastructure/structures/bridge/14039/005.cfm>

FDOT (2002). Post-Tensioning in Florida Bridges-Volume 1 of 10. Retrieved May 30, 2022,

from <https://www.fdot.gov/docs/default-source/structures/posttensioning/newdirectionsposttensioningvol1.pdf>

Azizinamini, A. (2018). Development of Quality Assurance and Quality Control System for Post Tensioned Segmental Bridges in Florida: Case of Ringling Bridge – Phase II Retrieved

from <https://fdotwww.blob.core.windows.net/sitefinity/docs/default-source/research/reports/fdot-bdv29-977-34-rpt.pdf>

FDOT (2021). Evaluation of Post-Tension Tendon Corrosion. Retrieved from

<https://cbs12.com/news/local/report-sheds-new-light-on-big-crack-in-roosevelt-bridge>

AASHTO LRFD Bridge Specifications

FDOT (2021). FDOT Structures Design Guidelines.

<https://fdotwww.blob.core.windows.net/sitefinity/docs/default-source/structures/structuresmanual/currentrelease/2021/vol1sdg.pdf>

Hurlebaus, S., Hueste, M., Karthik, M., & Terzioglu, T. (2016). Condition assessment of bridge

- post-tensioning and stay cable systems using NDE methods. Transportation Research Board of the National Academies. Retrieved from [http://onlinepubs.trb.org/onlinepubs/nchrp/docs/NCHRP14-28\\_FR.pdf](http://onlinepubs.trb.org/onlinepubs/nchrp/docs/NCHRP14-28_FR.pdf).
- Azizinamini, A. (2017). Non-destructive testing (NDT) of a segmental concrete bridge scheduled for demolition, with a focus on condition assessment and corrosion detection of internal tendons. Retrieved December 23, 2020, from <https://rosap.ntl.bts.gov/view/dot/32365>.
- Transportation Research Board. 1998. Durability of Precast Segmental Bridges: Final Report. Washington, DC: The National Academies Press. <https://doi.org/10.17226/6356>
- Azizinamini, A. (2012). Improved inspection techniques for steel prestressing /Post-tensioning strand No. BDK80 977-13) FDOT.
- Roustan, W., & Erblat, A. (2020, June 18). State of emergency declared over 'severe corrosion' on Roosevelt Bridge in Stuart. From <https://www.sun-sentinel.com/news/florida/fl-ne-stuartbridge-cracks-20200617-ax4hfrknqjbf7fdynchi3we3ze-story.html>.
- Detman, G., & Rodriguez, A. (2020, June 17). Roosevelt Bridge closed due to cracks, not in danger of 'imminent collapse'. From <https://cbs12.com/news/local/southbound-lanes-of-rooseveltbridge-in-stuart-closed-for-repairs>
- Demirci, A., Görgülü, K., & Durutürk, Y. S. (2004). Thermal conductivity of rocks and its variation with uniaxial and triaxial stress. International Journal of Rock Mechanics and Mining Sciences, 41(7), 1133-1138.
- Jin, L., Zhang, R., & Du, X. (2017). Computational homogenization for thermal conduction in heterogeneous concrete after mechanical stress. Construction and Building Materials, 141, 222-234.

## Acronyms

<b>PT</b>	Post-Tensioned
<b>FF</b>	Flexible Filler
<b>CG</b>	Cementitious Grout
<b>NDE</b>	Non-Destructive Evaluation
<b>NDT</b>	Non-Destructive Testing
<b>FDOT</b>	Florida Department of Transportation
<b>HDPE</b>	High Density Polyethene
<b>GPR</b>	Ground Penetrating Radar
<b>IRT</b>	Infrared Thermography
<b>ECT</b>	Electrical Capacitance Tomography
<b>MFL</b>	Magnetic Flux Leakage
<b>IE</b>	Impact Echo
<b>UST</b>	Ultrasonic Tomography
<b>USE</b>	Ultrasonic Echo
<b>SPV-UPV</b>	Sonic/Ultrasonic Pulse Velocity
<b>LFUT</b>	Low Frequency Ultrasound
<b>VT</b>	Visual Testing
<b>PPE</b>	Personal Protective Equipment
<b>NCHRP</b>	National Cooperative Highway Research Program
<b>FEA</b>	Finite Element Analysis

## Appendix

# General Notes:

## Acknowledgements:

Design for internal-duct specimen based on previous work by Dr. Consolazio.  
Design for external-duct specimen based on previous work by Dr. Hamilton and Dr. Rice

## Materials

Concrete shall be FDOT class VI  
f'c (28 day) = 8500 psi  
fci (release) = 6000 ksi

The same concrete mix shall be used for both beams.

Mild reinforcement shall be ASTM A615 grade 60 (fy 60 ksi)

Prestressing strand shall be ASTM A416 270 ksi Lo-Lax

Fabricator shall provide data sheets from concrete, strand, and rebar suppliers.

Fabricator shall provide report of strand stressing.

Fabricator shall provide material samples to ERAU/FDOT as follows:

(8) 6" dia x 12" cylinders from each concrete batch: (4) cylinders cure with girder, (4) lab cure

(8) 36" pieces of prestressing strands free from sand, dust, etc. Samples taken directly off of reel.

## Schedule

Fabrication is requested by end of April 2022. Shipping is anticipated by the end of May 2022.

Contact Carley Gonzalez at ERAU at least (1) week prior to stress, casting, detensioning, and shipping: 813-455-0349 or Gonzac46@my.erau.edu

Allow 24 hours minimum between placement of reinforcing and placement of concrete to allow of placement of research instrumentation.

Both beams shall be fabricated in the same stressing bed and at the same time.

All instrumentation will be applied by ERAU, contractor will coordinate scheduling at least one week prior to stressing, casting and detensioning

## Other

Fabricator will transport girders from the fabrication facility to:  
FDOT Structures Research Center  
2007 East Paul Dirac Drive  
Tallahassee, FL 32310

Delivery time to be coordinated with FDOT: Christina Freeman (850) 921-7100

Unless otherwise noted, fabrication of girders shall follow typical procedures and practices for FDOT bridge girders.

Cover beams with heavy tarp during curing.

Roughen top of beams to  $\frac{1}{4}$ " amplitude.

Inspections will be provided by on-site FDOT personnel and by ERAU.

No patch-work or finishing is required.

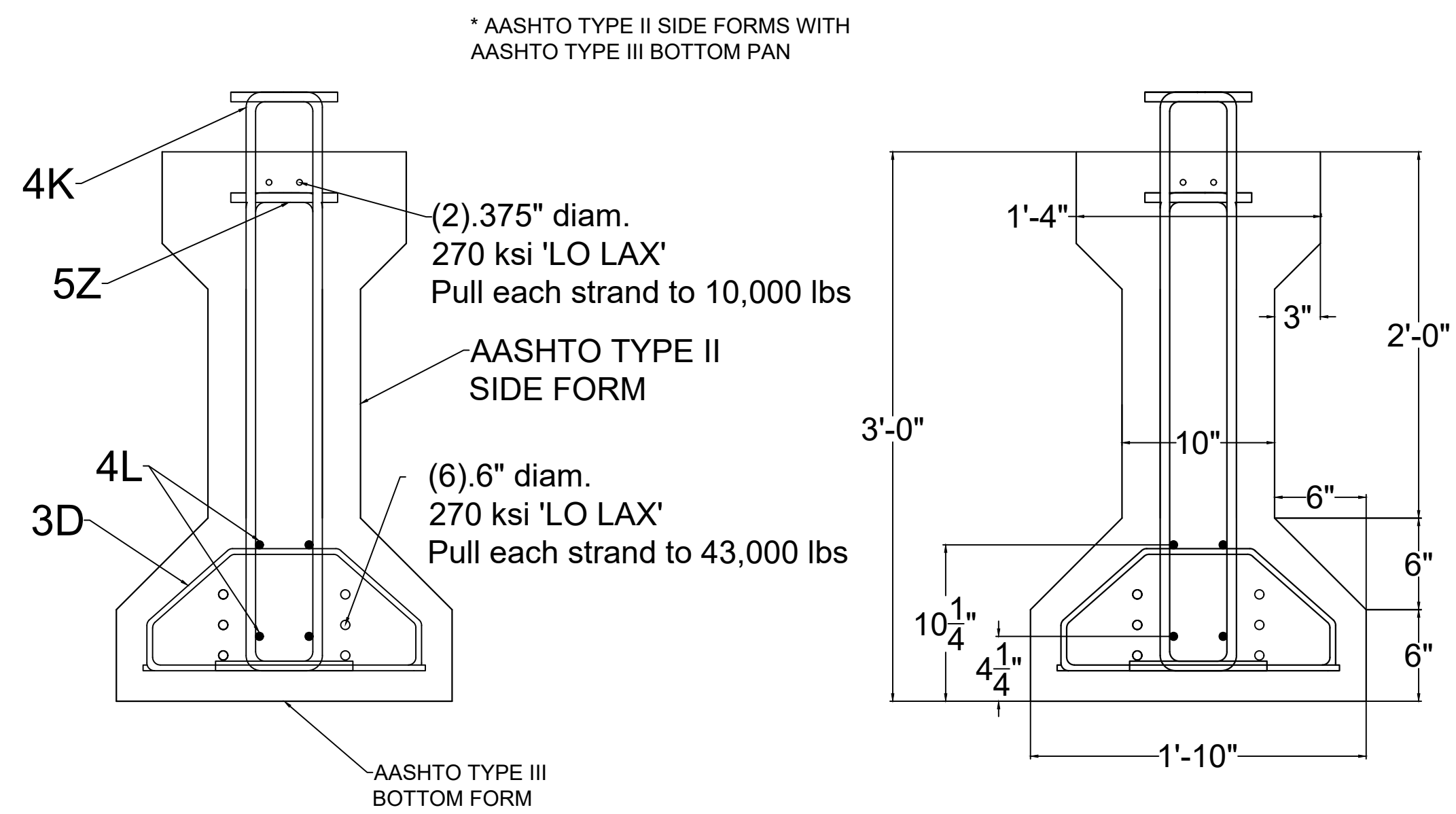
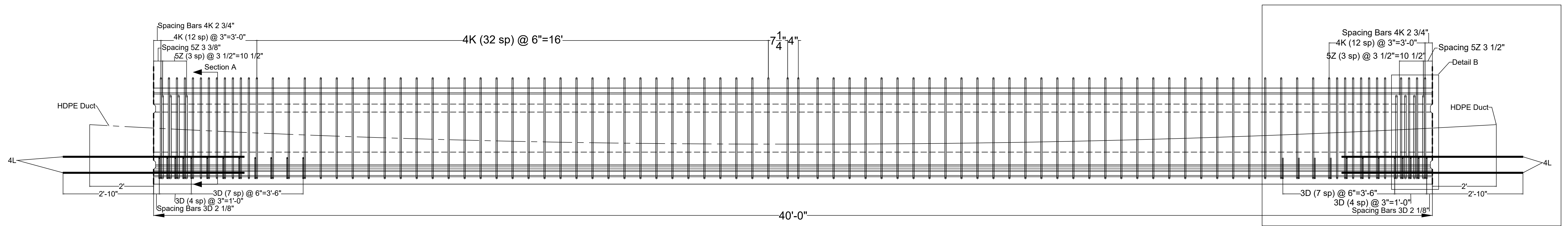
Construction shall be in accordance with FDOT Standard Specifications, January 2022

Production: Contact  
Carley Gonzalez  
(813) 455-0349  
at least 1 week prior to  
stressing, casting,  
detensioning, and  
shipping

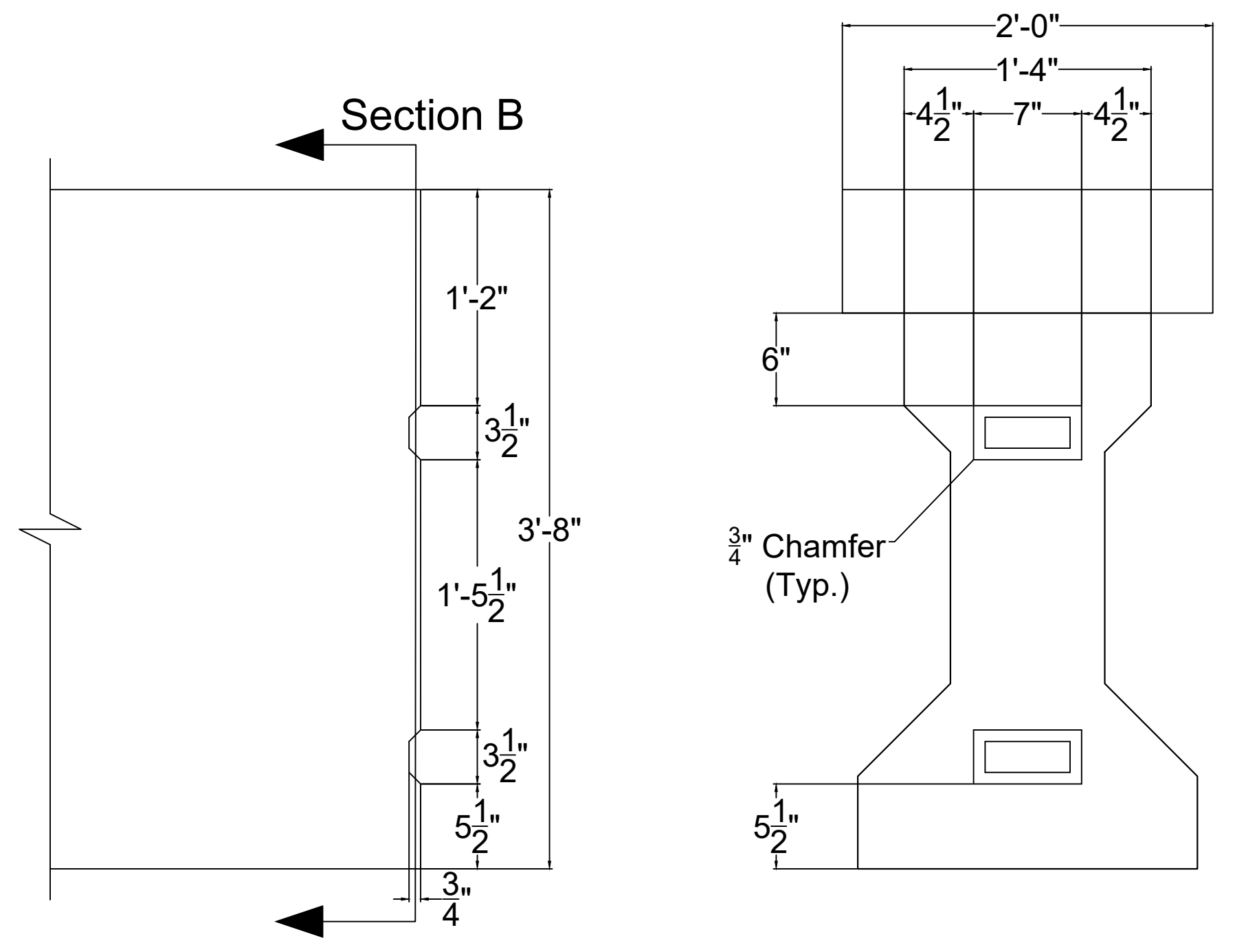
## SHEET INDEX:

- 1 GENERAL NOTES
- 2 SHEET INDEX
- 3 INTERNAL SPECIMEN - GEOMETRY & REINFORCEMENT
- 4 INTERNAL SPECIMEN PRETENSIONING
- 5 DRAPING PROFILE INTERNAL SPECIMEN
- 6 EXTERNAL SPECIMEN
- 7 EXTERNAL SPECIMEN PRETENSIONING
- 8 BEAM REINFORCEMENT SUMMARY
- 9 DECK REINFORCEMENT DETAIL
- 10 INTERNAL SPECIMEN END BLOCK DETAIL
- 11 EXTERNAL SPECIMEN END BLOCK DETAIL
- 12 END BLOCK REINFORCEMENT SUMMARY
- 13 EXTERNAL SPECIMEN DEVIATOR BLOCK DETAIL
- 14 DRAPING PROFILE EXTERNAL SPECIMEN
- 15 TESTING SETUP
- 16 INTERNAL INSTRUMENTATION PLAN
- 17 EXTERNAL INSTRUMENTATION PLAN
- 18 MONO-TENDON STRESSING PLAN
- 19 INTERNAL FILLER INJECTION PLAN
- 20 EXTERNAL FILLER INJECTION PLAN
- 21 YARD PLACEMENT





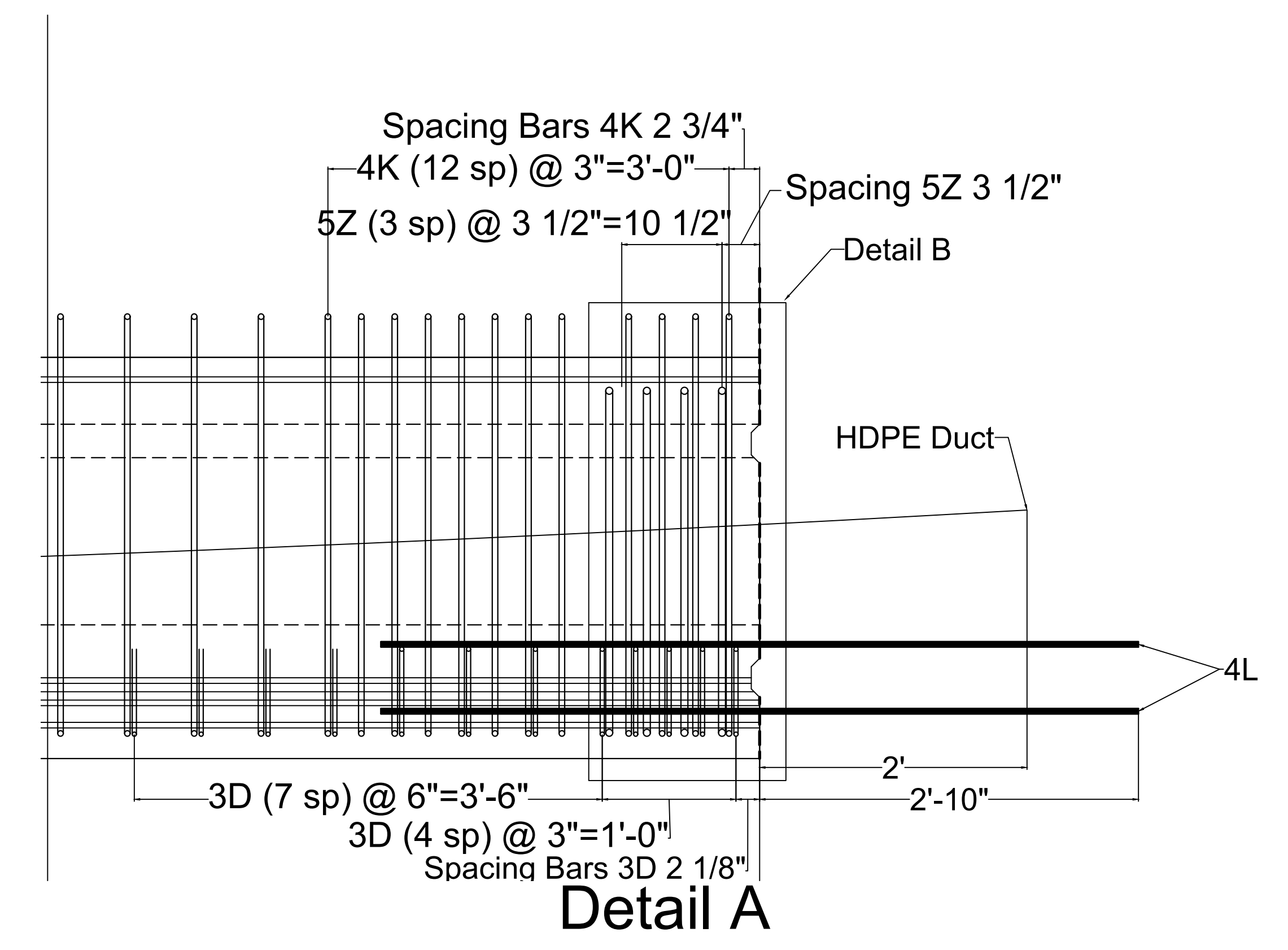
**Section A**



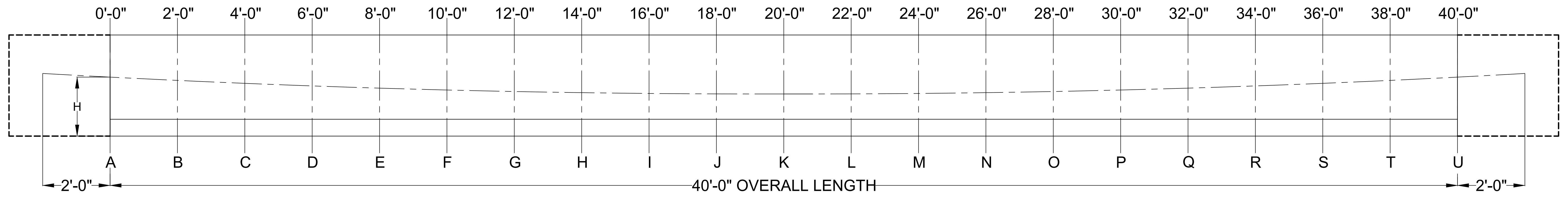
**Detail B**

**Section B**

**Shear Keys  
connecting to End  
Blocks**

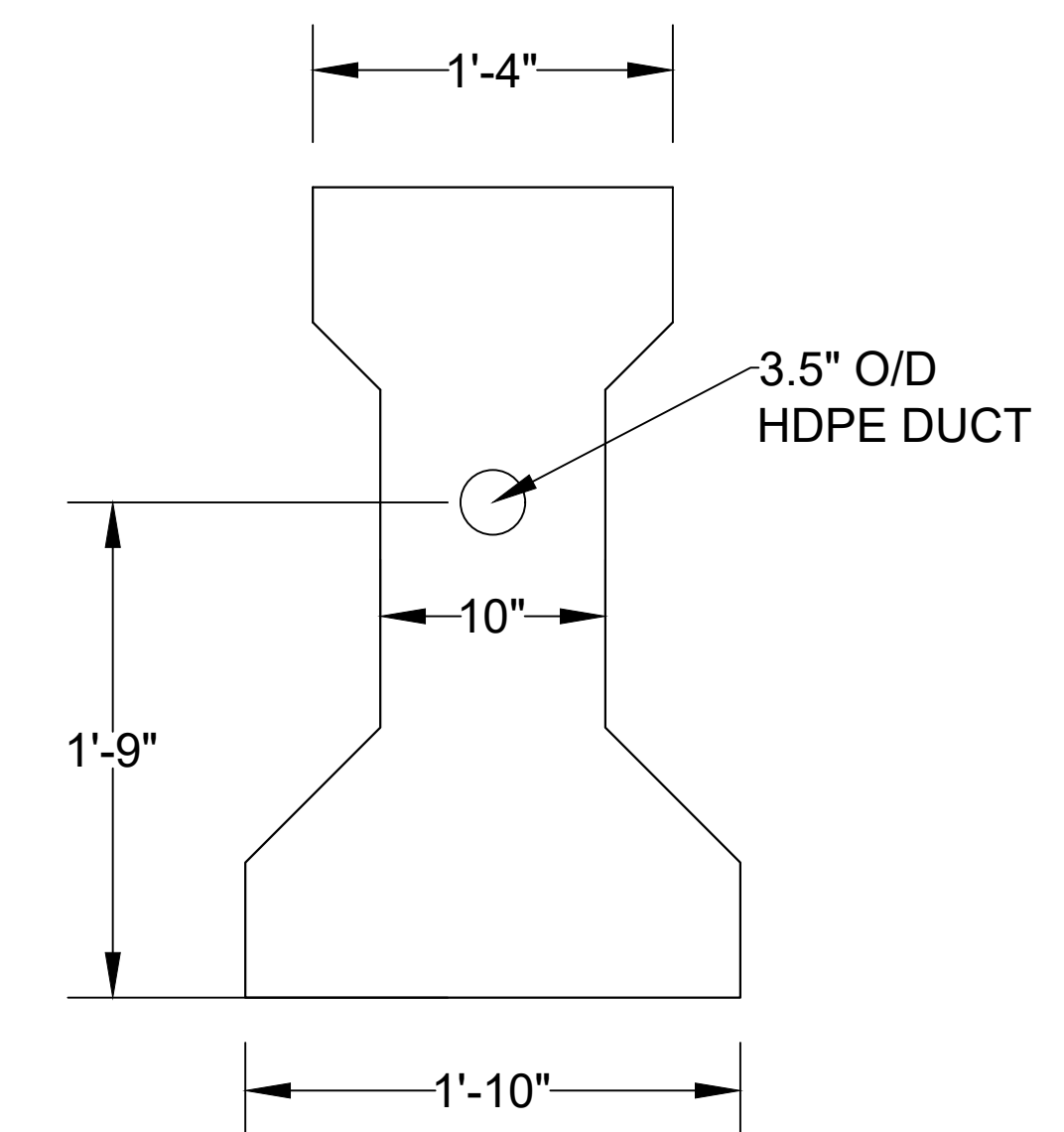


BEAM REINFORCEMENT SUMMARY			
NAME	SIZE	QTY.	LENGTH
4K	#4	92	4'-2"
5Z	#5	8	3'-7"
4L	#4	8	5'-8"
3D	#3	48	3'-3 1/4"



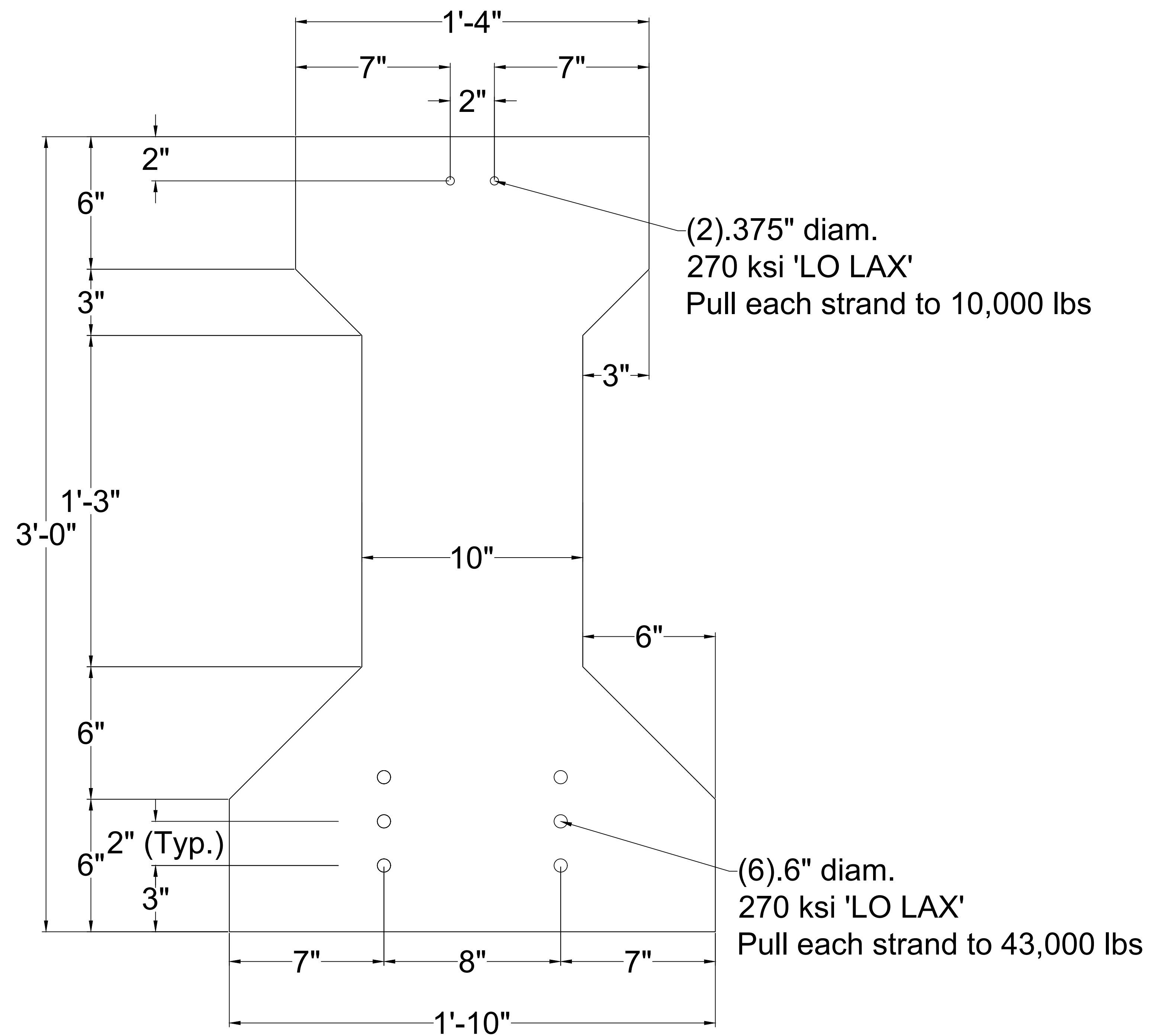
SECTION	A	B	C	D	E	F	G	H	I	J	K
DISTANCE FROM END OF GIRDER	0'-0"	2'-0"	4'-0"	6'-0"	8'-0"	10'-0"	12'-0"	14'-0"	16'-0"	18'-0"	20'-0"
H	1'-9"	1'-7 <sup>3</sup> / <sub>4</sub> "	1'-6 <sup>3</sup> / <sub>4</sub> "	1'-6"	1'-5"	1'-4 <sup>1</sup> / <sub>2</sub> "	1'-3 <sup>3</sup> / <sub>4</sub> "	1'-3 <sup>1</sup> / <sub>2</sub> "	1'-3 <sup>1</sup> / <sub>4</sub> "	1'-3"	1'-3"

SECTION	L	M	N	O	P	Q	R	S	T	U
DISTANCE FROM END OF GIRDER	22'-0"	24'-0"	26'-0"	28'-0"	30'-0"	32'-0"	34'-0"	36'-0"	38'-0"	40'-0"
H	1'-3"	1'-3 <sup>1</sup> / <sub>4</sub> "	1'-3 <sup>1</sup> / <sub>2</sub> "	1'-3 <sup>3</sup> / <sub>4</sub> "	1'-4 <sup>1</sup> / <sub>2</sub> "	1'-5"	1'-6"	1'-6 <sup>3</sup> / <sub>4</sub> "	1'-7 <sup>3</sup> / <sub>4</sub> "	1'-9"

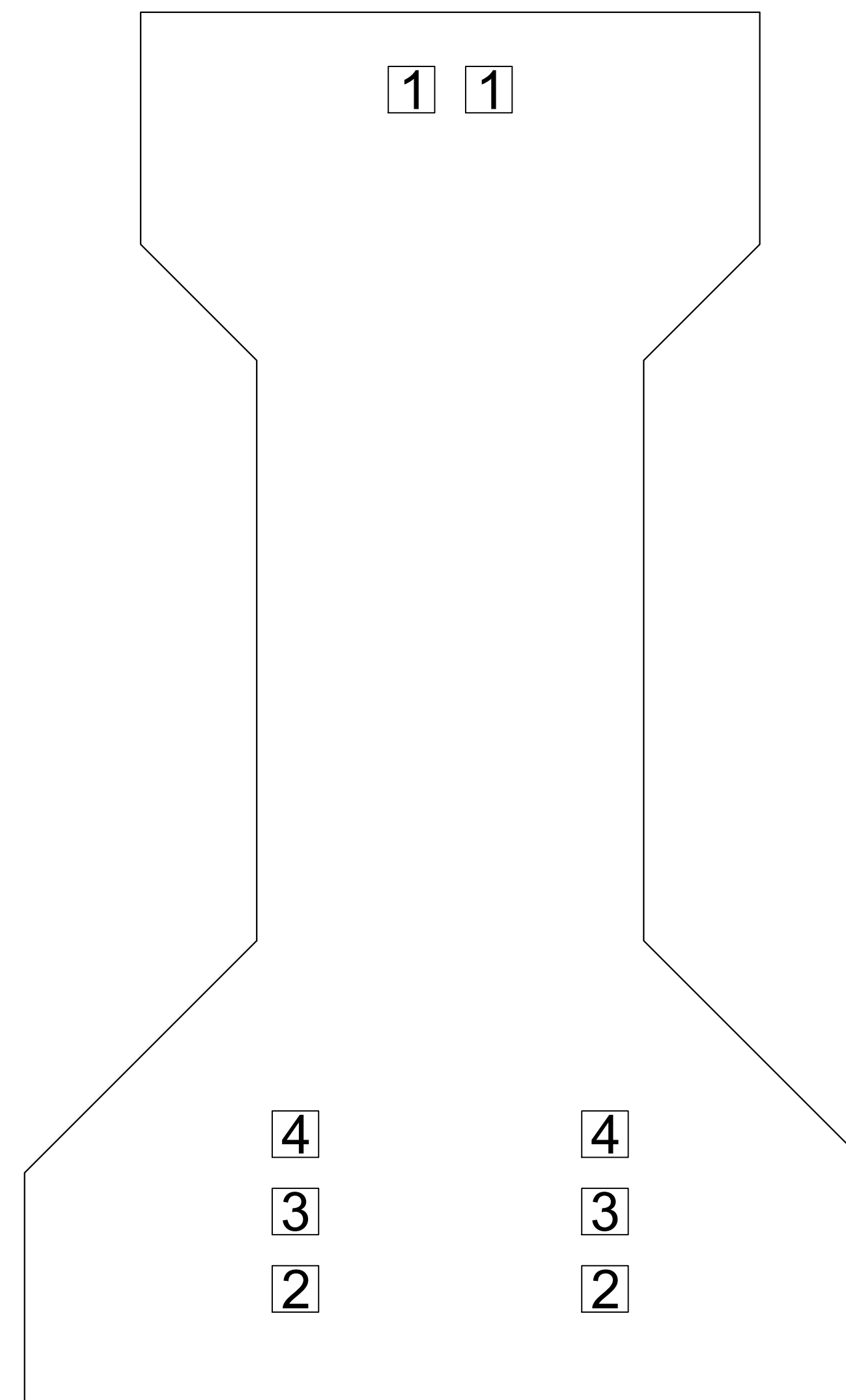


SECTION A

\*SEE SHEET 9 FOR CAST-IN-PLACE DECK DETAIL



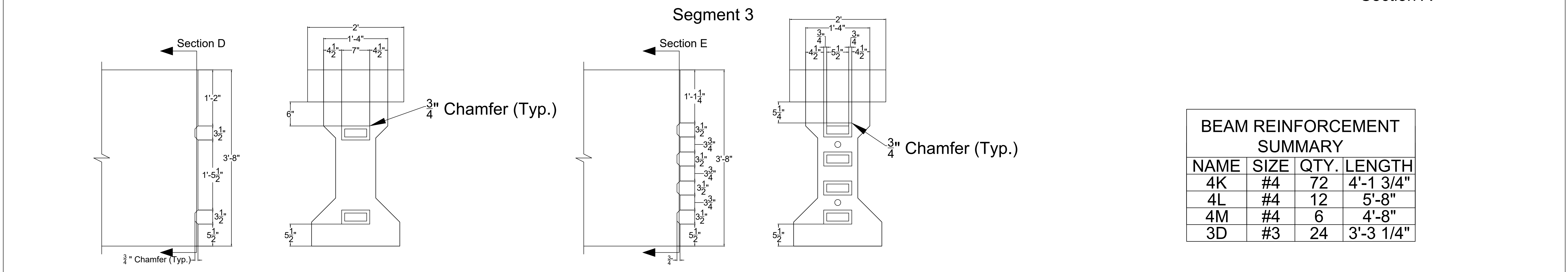
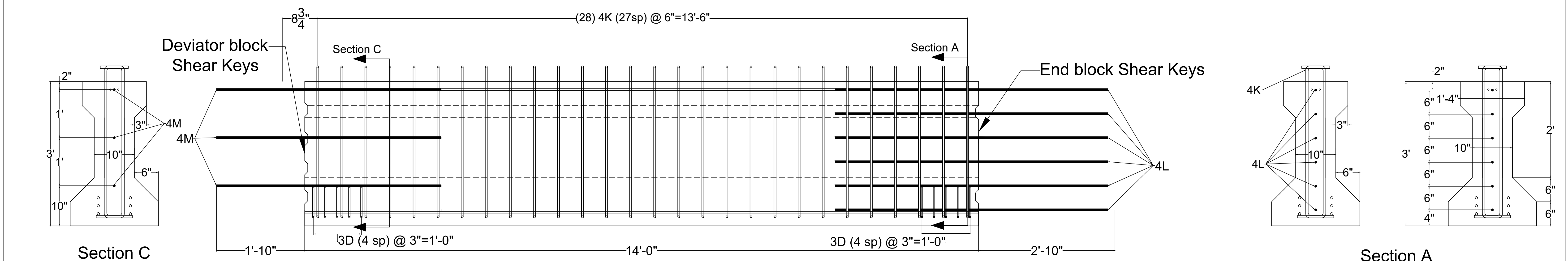
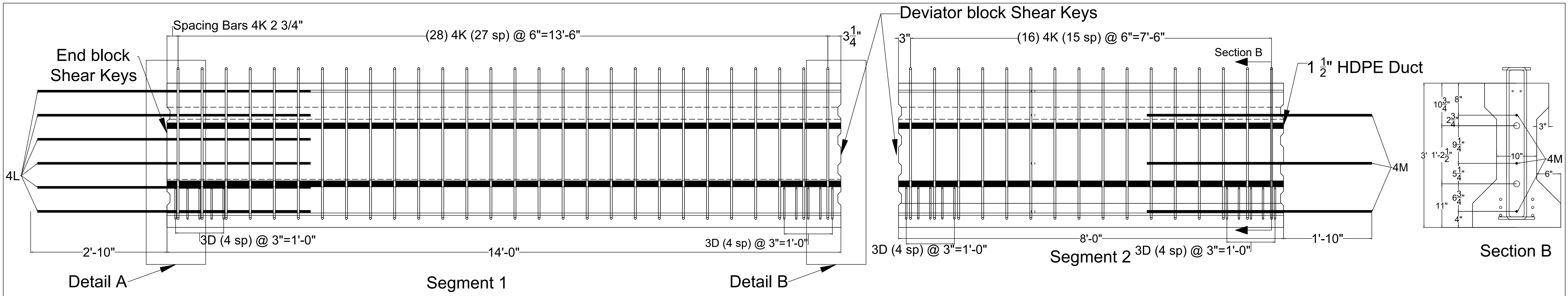
**Strand Pattern & Pretensioning**



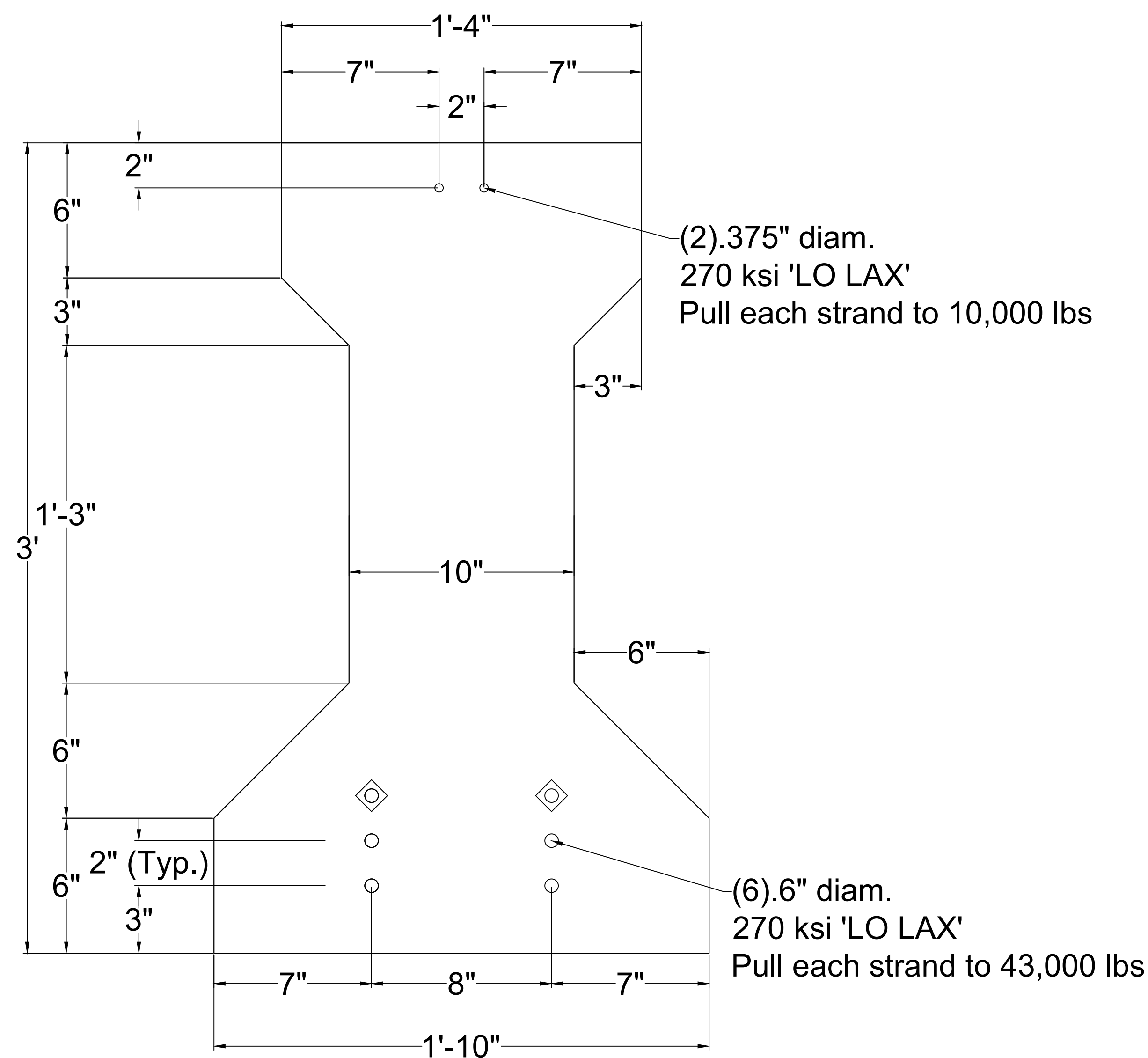
**Detensioning Sequence**

**SHIELDING LEGEND**

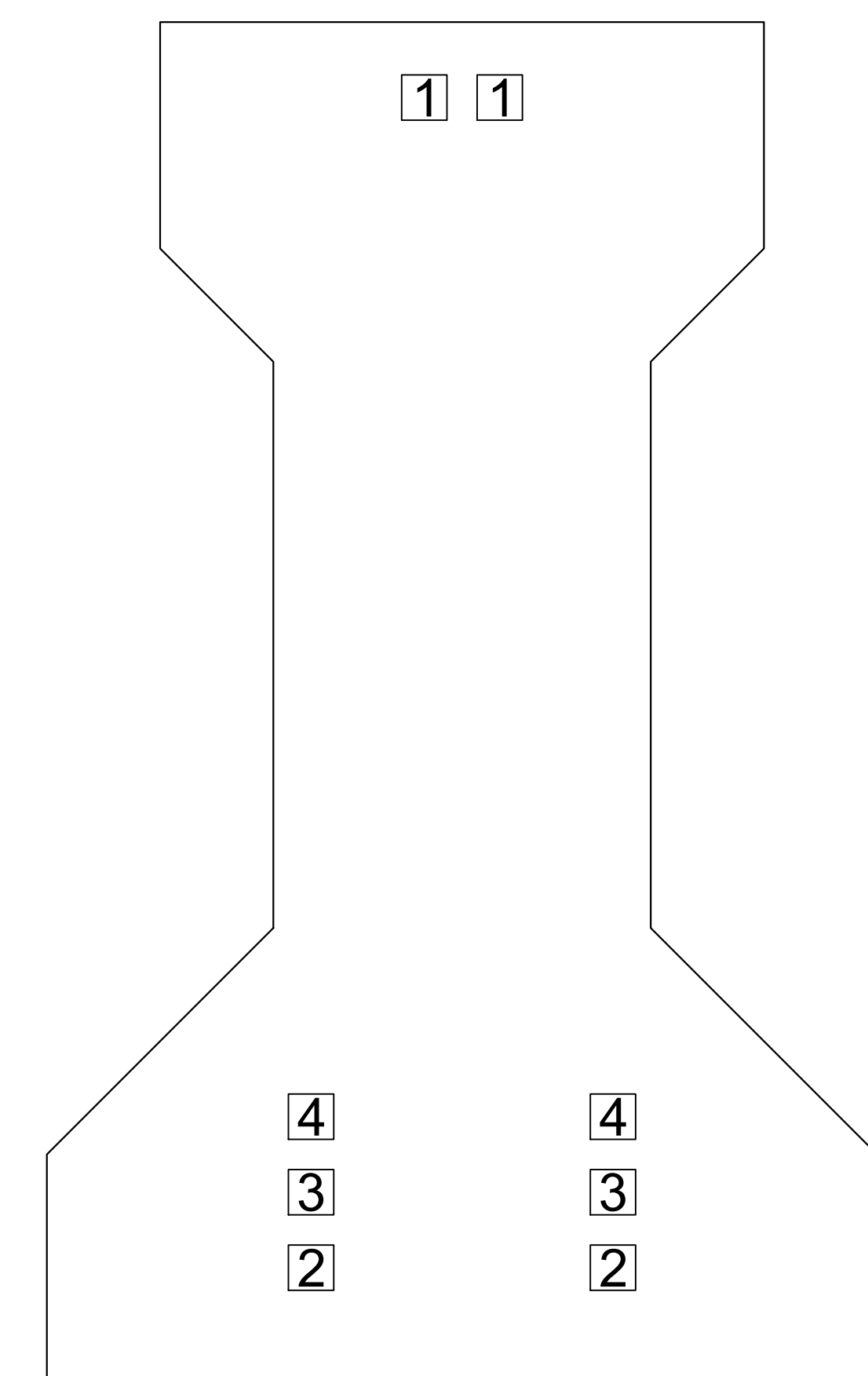
○ NONE REQUIRED



BEAM REINFORCEMENT SUMMARY			
NAME	SIZE	QTY.	LENGTH
4K	#4	72	4'-1 3/4"
4L	#4	12	5'-8"
4M	#4	6	4'-8"
3D	#3	24	3'-3 1/4"



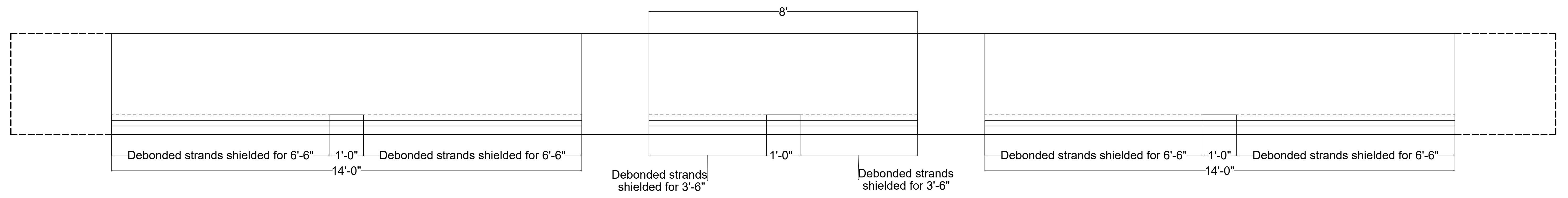
**Strand Pattern & Pretensioning**

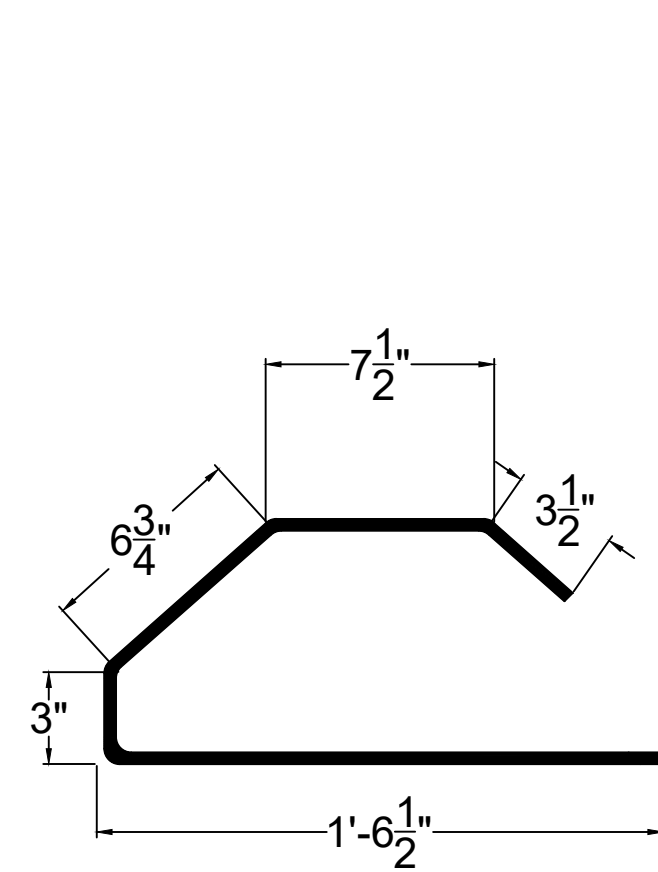


**Detensioning Sequence**

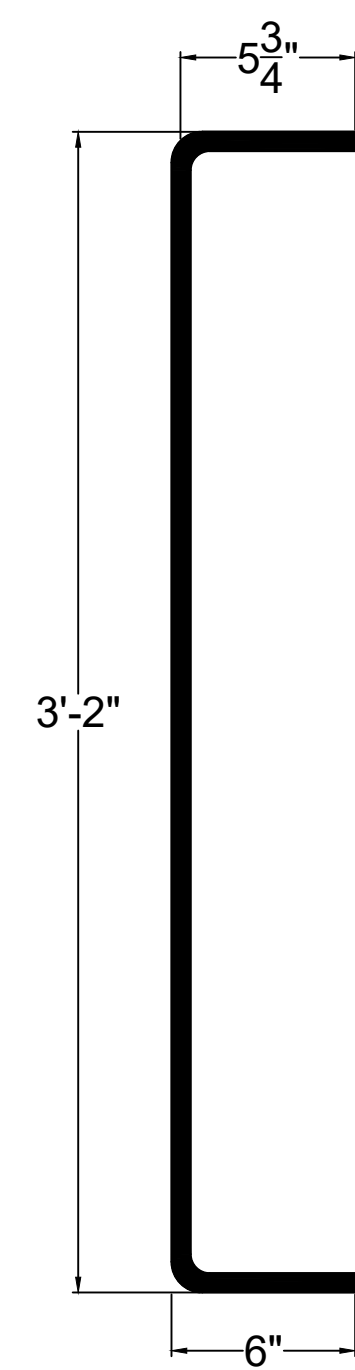
**SHIELDING LEGEND**

- NONE REQUIRED
- ◊ DEBONDED EXCEPT FOR MIDDLE 1' OF SEGMENT

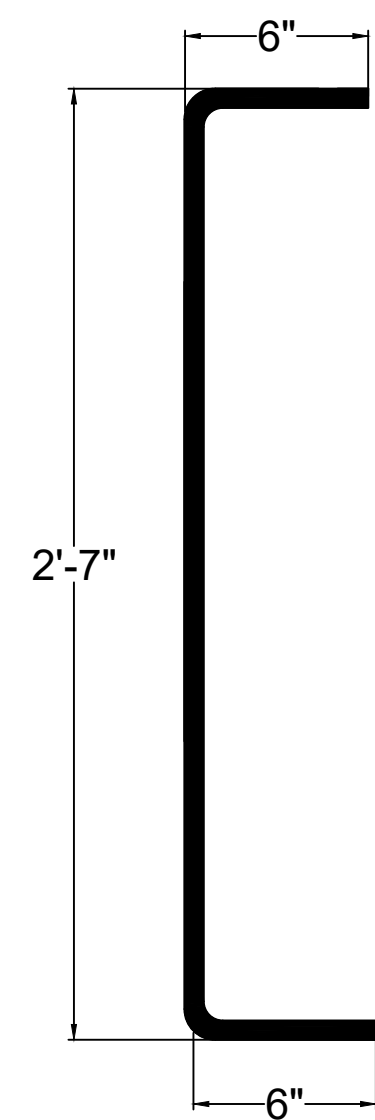




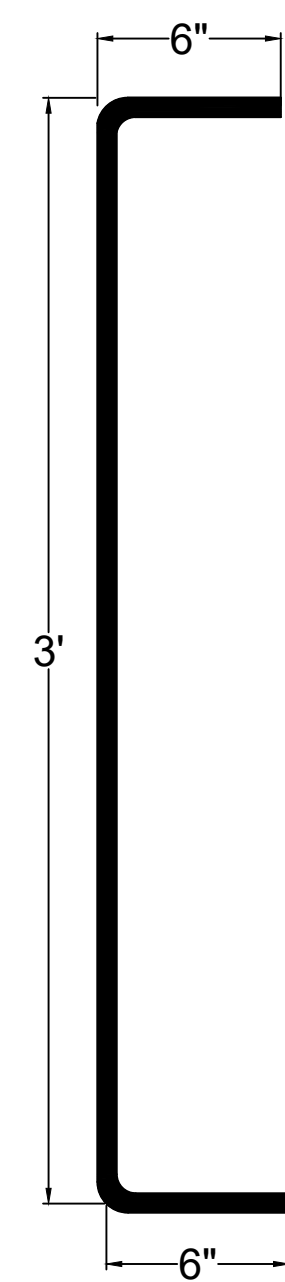
3D



4K



5Z



5K

## External Specimen

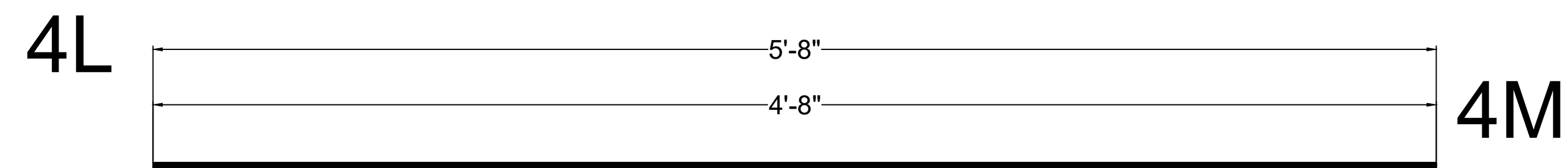
### BEAM REINFORCEMENT SUMMARY

NAME	SIZE	QTY.	LENGTH
4K	#4	71	4'-1 3/4"
4L	#4	12	5'-8"
4M	#4	6	4'-8"
3D	#3	24	3'-3 1/4"

## Internal Specimen

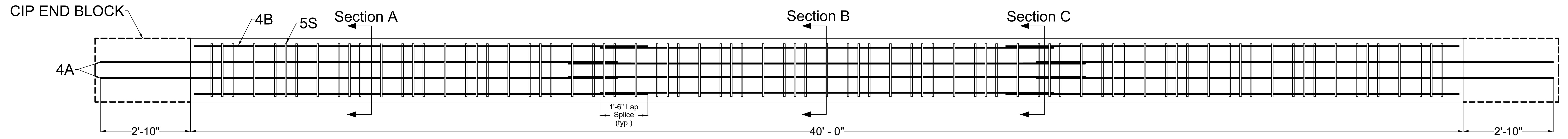
### BEAM REINFORCEMENT SUMMARY

NAME	SIZE	QTY.	LENGTH
3D	#3	48	3'-3 1/4"
4K	#4	92	4'-2"
4L	#4	8	5'-8"
5Z	#5	8	3'-7"

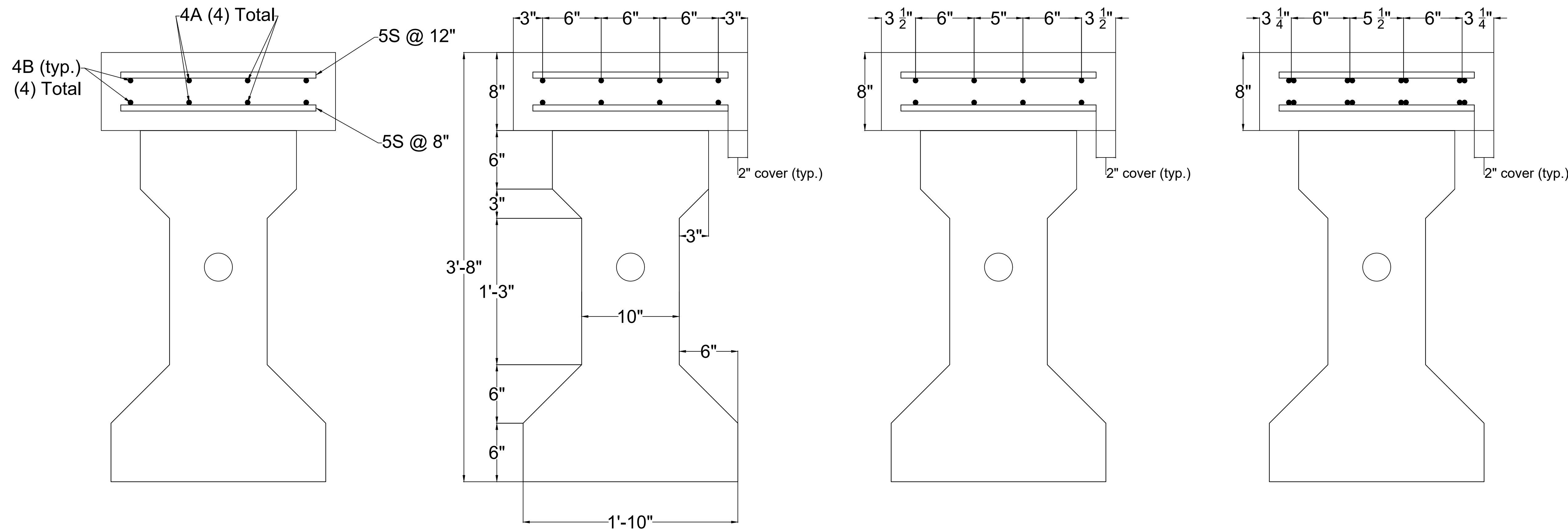


4L

4M



DECK TOP VIEW



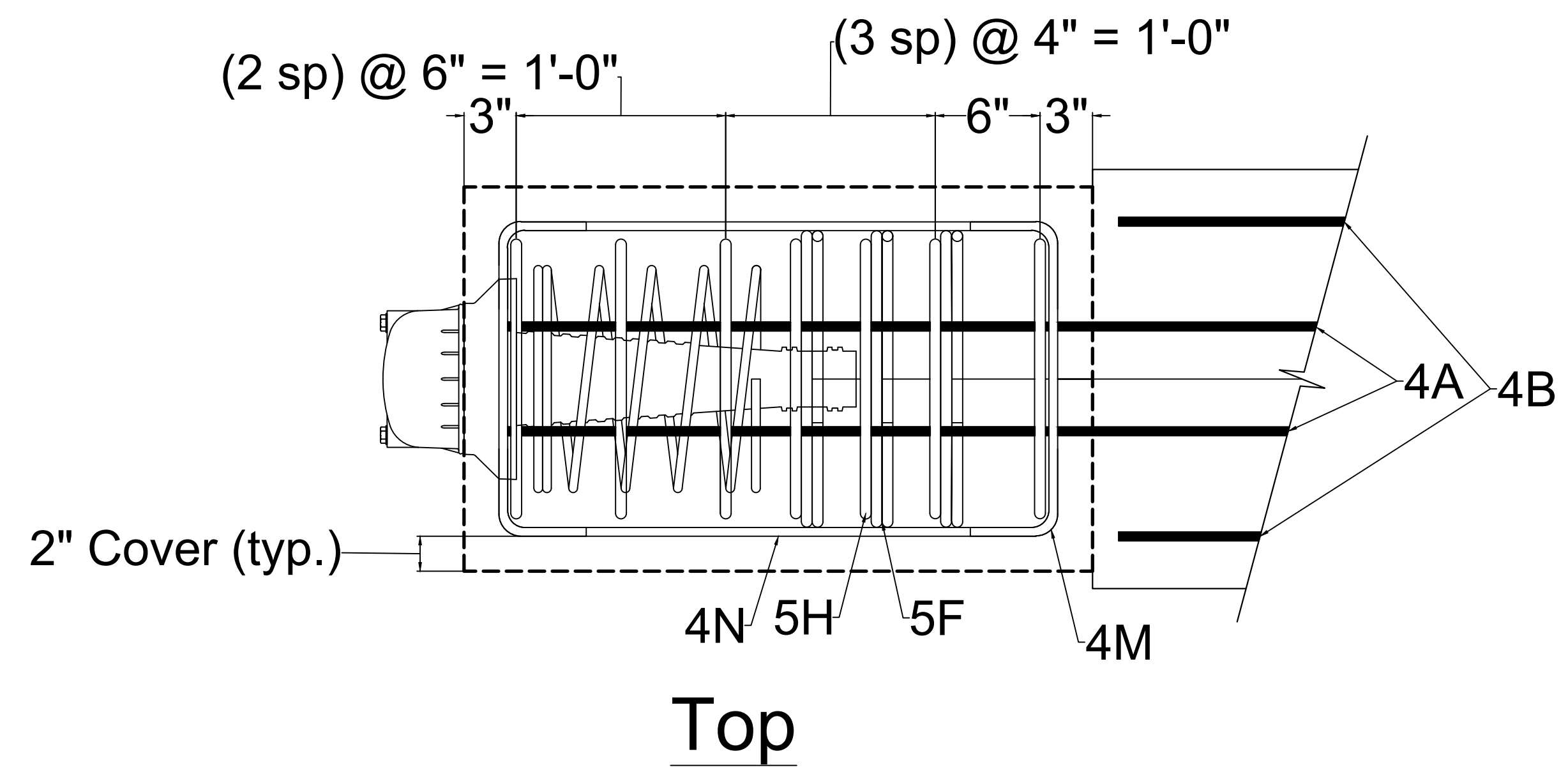
SECTION A

SECTION B

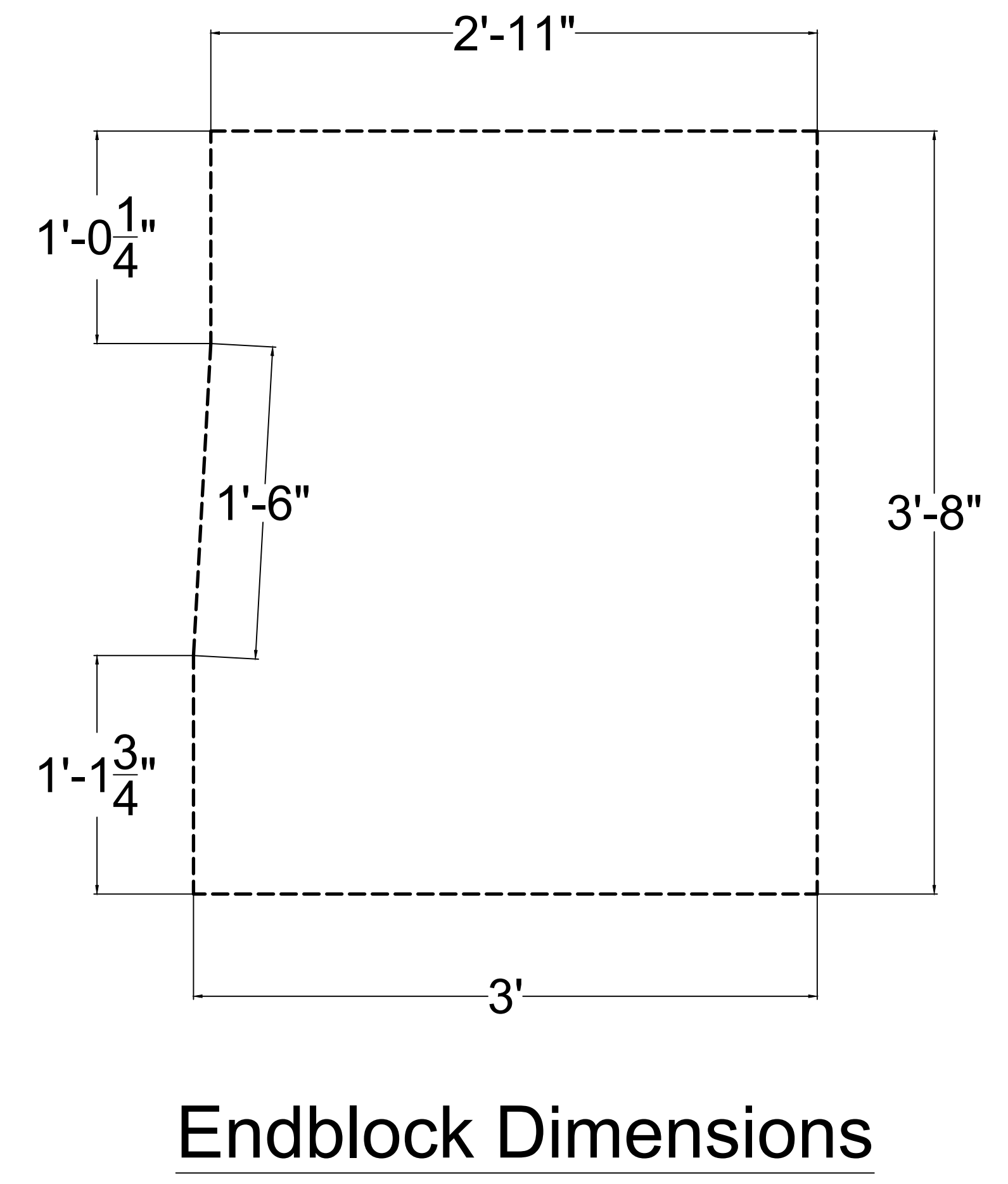
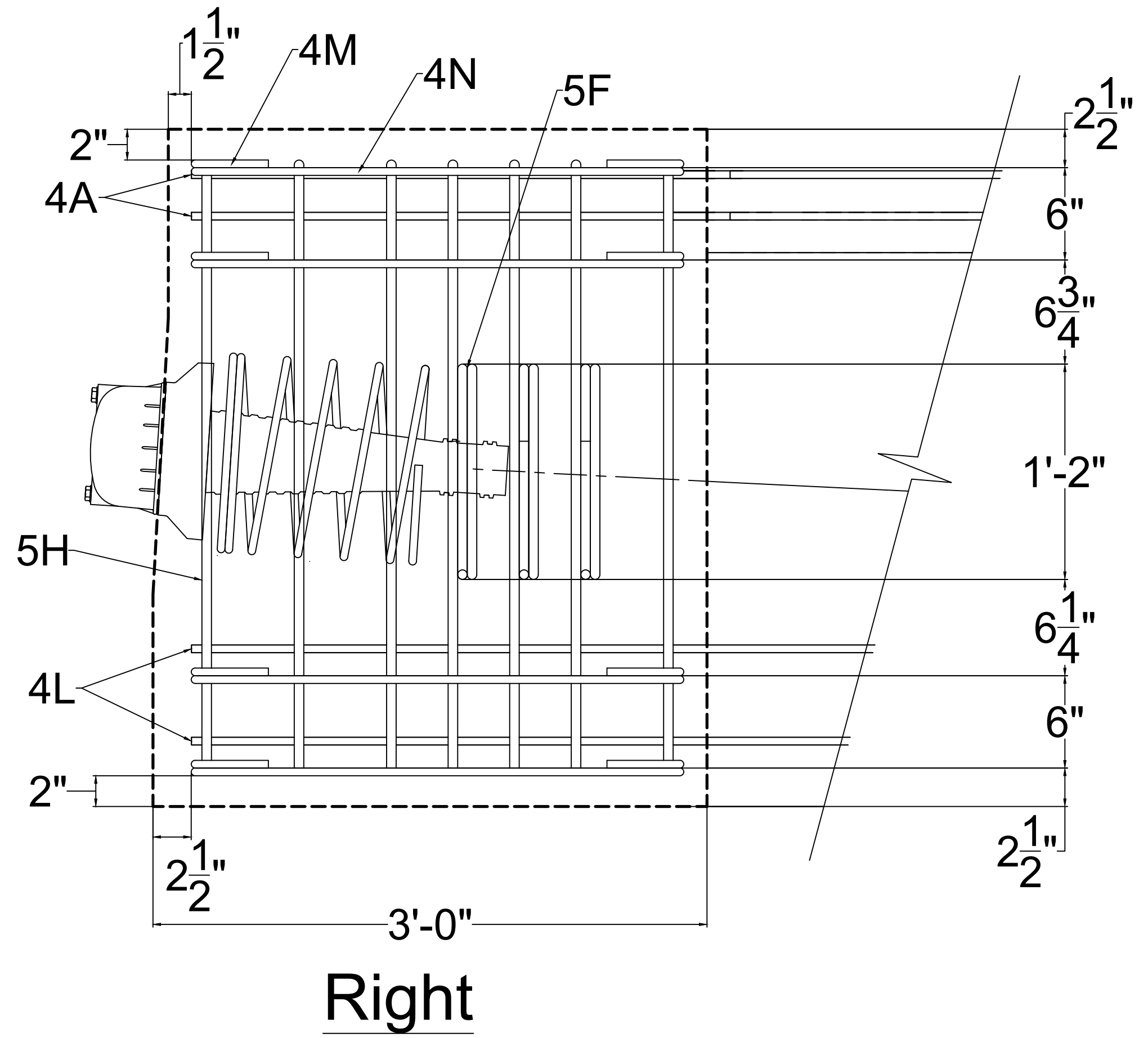
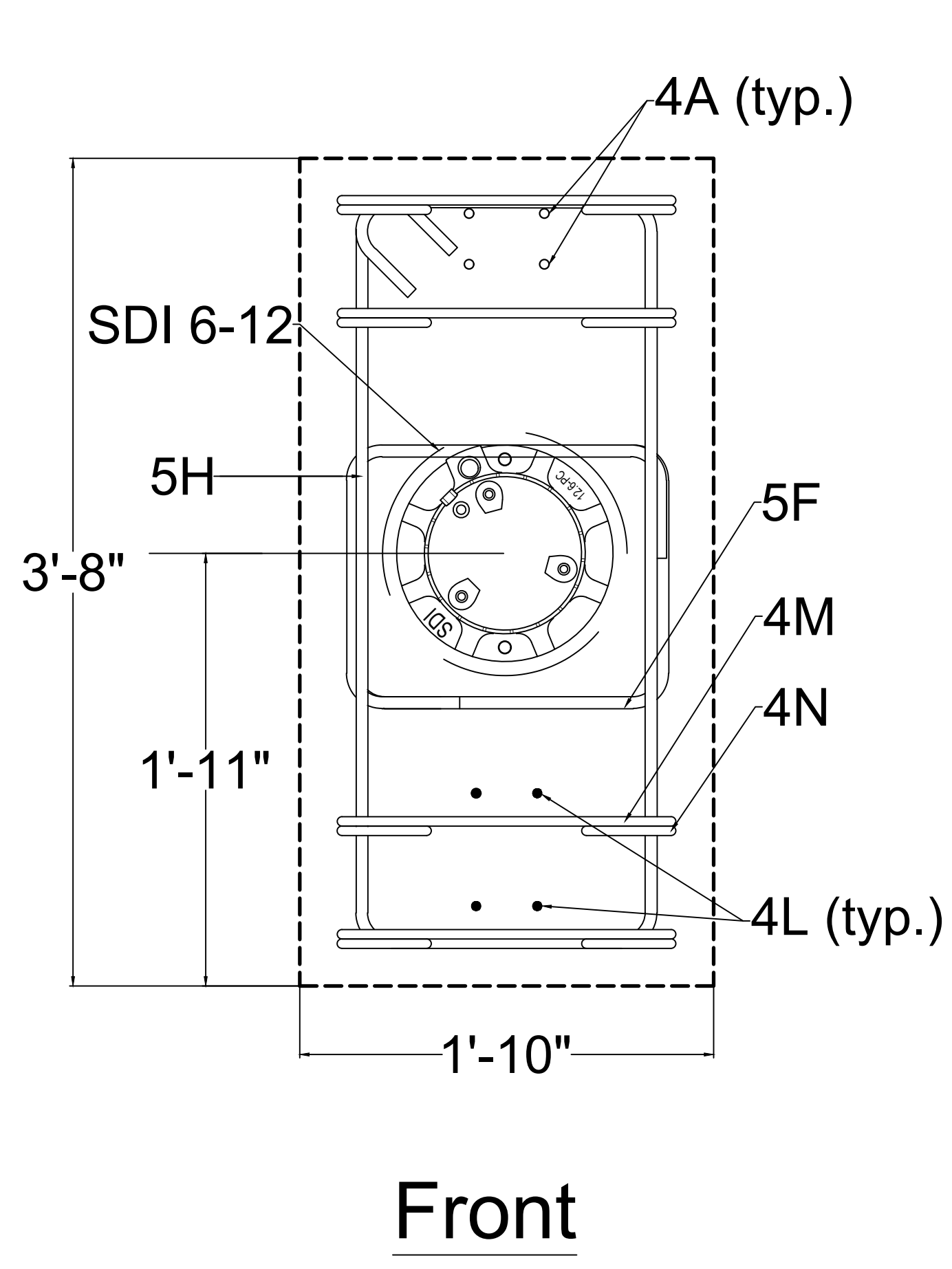
SECTION C

DECK REINFORCEMENT SUMMARY (2 REQUIRED)			
NAME	SIZE	QTY.	LENGTH
4A	#4	12	16'-3"
4B	#4	12	14'-3"
5S	#5	98	1'-8"

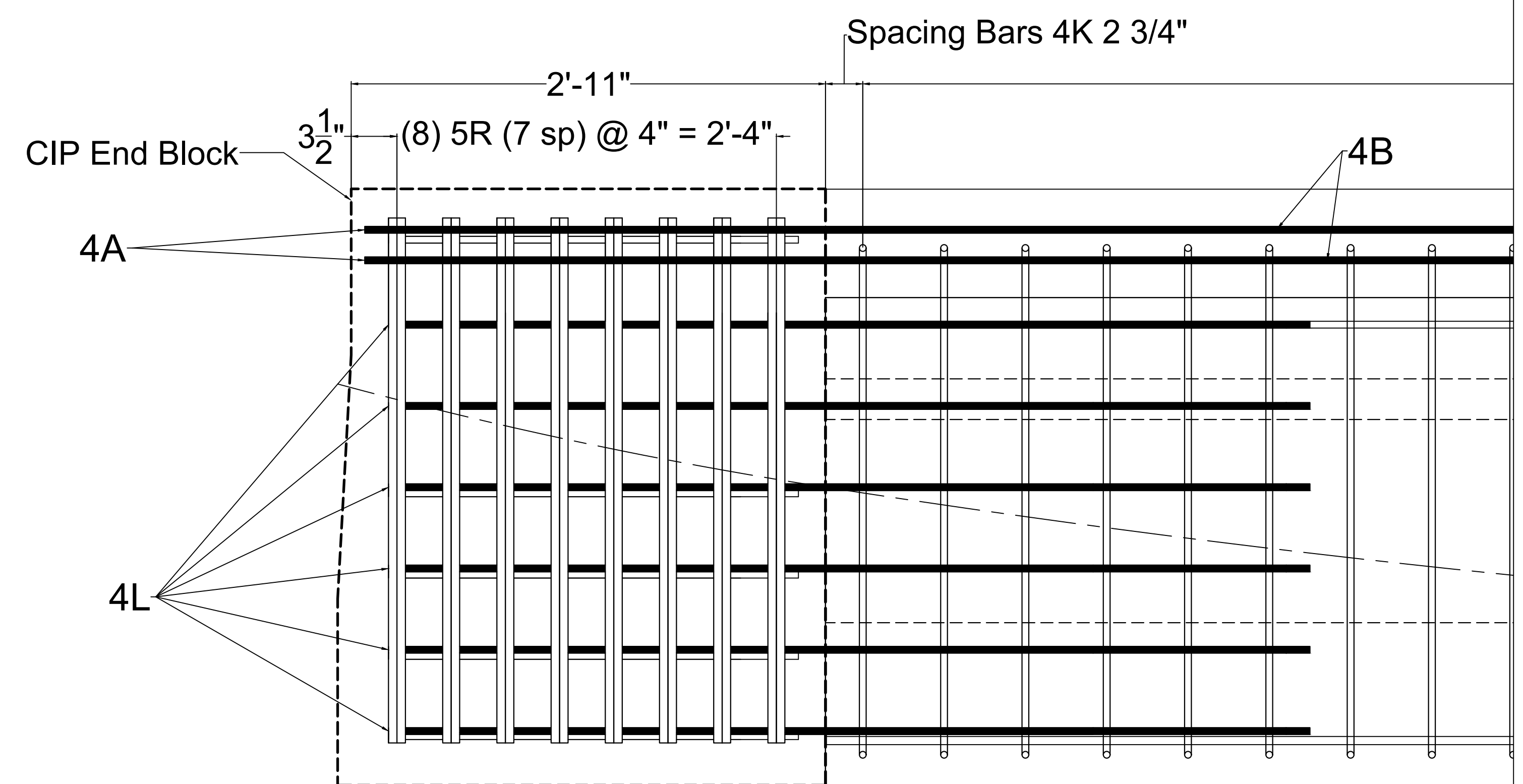
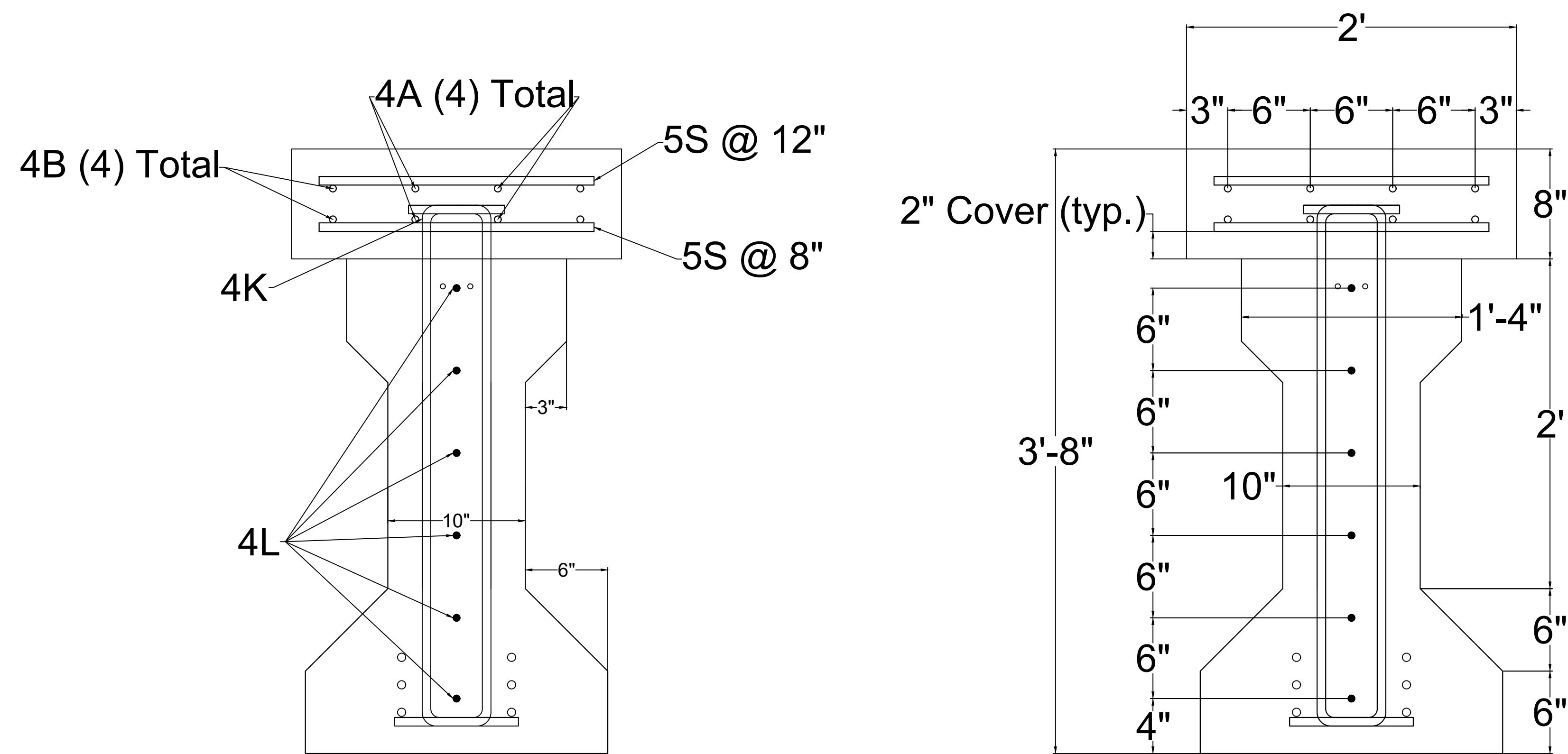
\*BEAM REINFORCEMENT EXCLUDED FOR CLARITY



END CAP REINFORCEMENT SUMMARY			
NAME	SIZE	QTY.	LENGTH
4M	#4	16	2'-4"
4N	#4	16	3'-6"
5F	#5	12	3'-7"
5H	#5	14	10'-3"

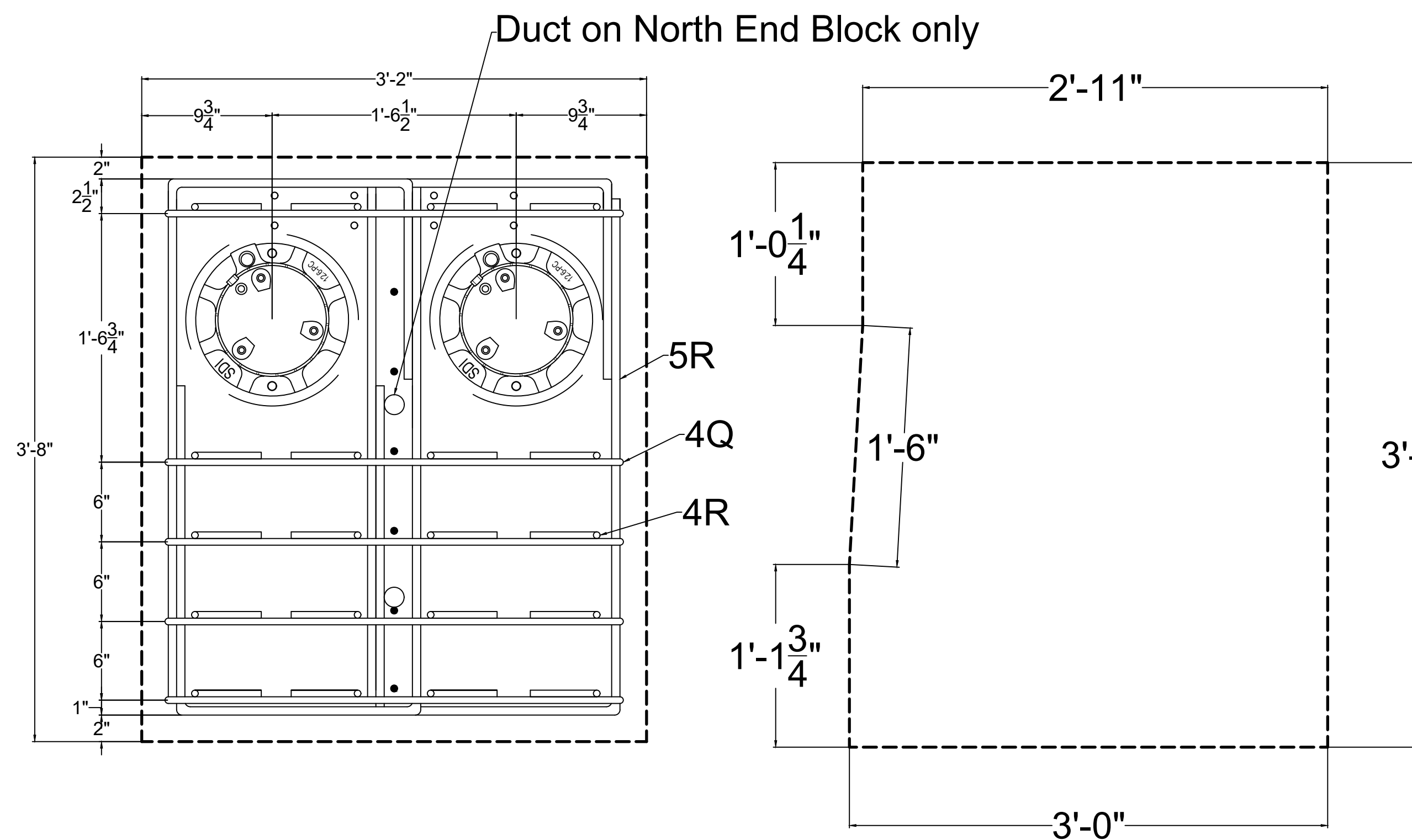






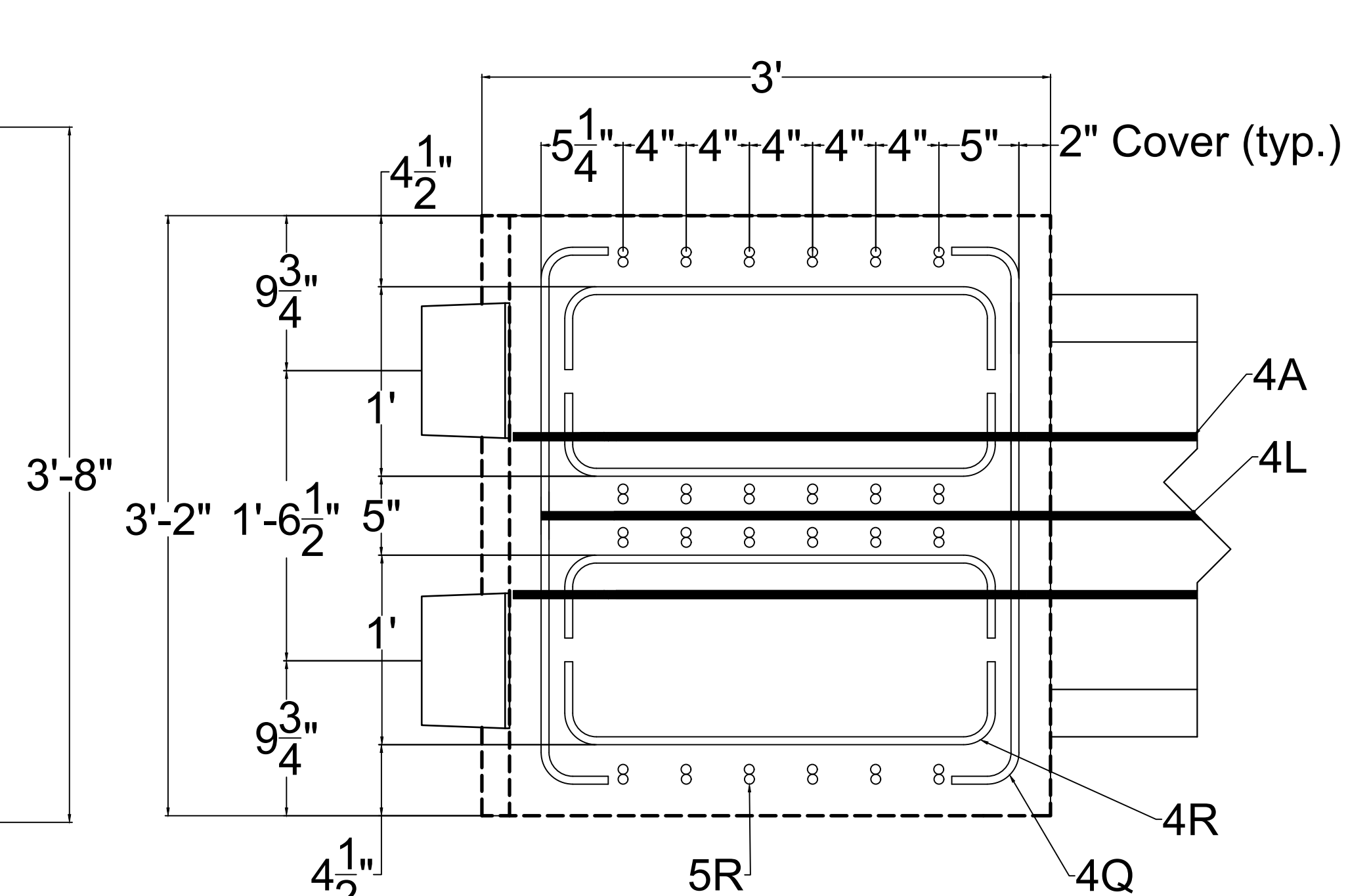
**Beam Cross-Section**

\*4Q not shown for clarity



**End Block Front View**

**Endblock Dimensions**



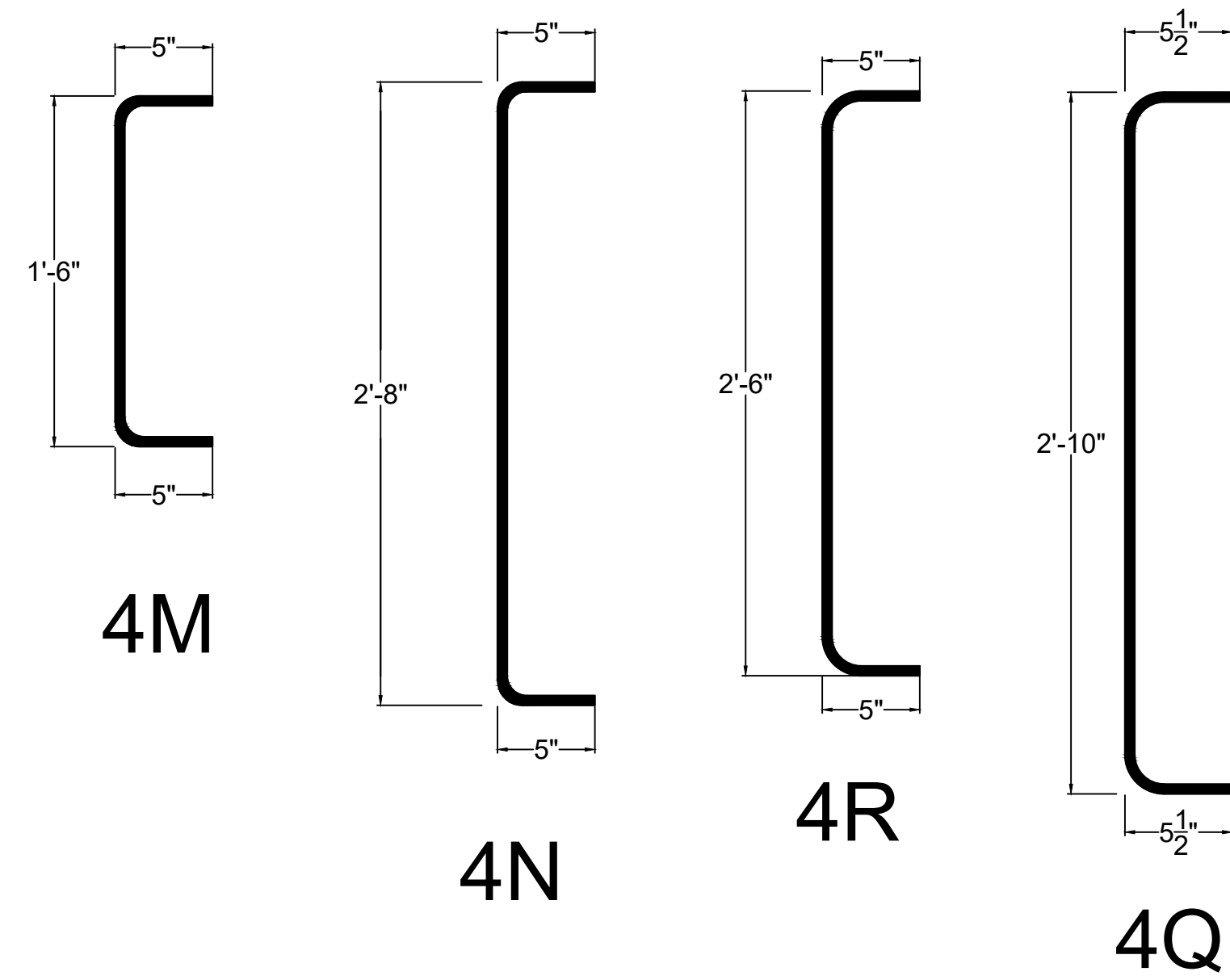
**End Block Top View**

**END CAP REINFORCEMENT SUMMARY**

NAME	SIZE	QTY.	LENGTH
5R	#5	60	5'-11"
4R	#4	40	3'-4"
4Q	#4	20	3'-9"

## External Specimen

## Internal Specimen



END CAP REINFORCEMENT SUMMARY

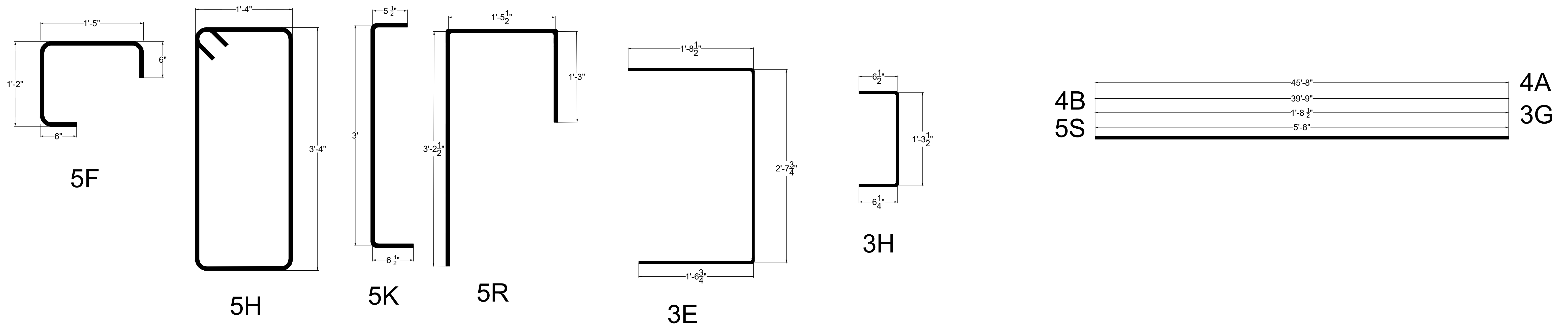
NAME	SIZE	QTY.	LENGTH
4A	#4	4	45'-8"
4B	#4	4	39'-9"
4Q	#4	20	3'-9"
4R	#4	40	3'-4"
5R	#5	64	5'-11"
5S	#5	98	1'-8"

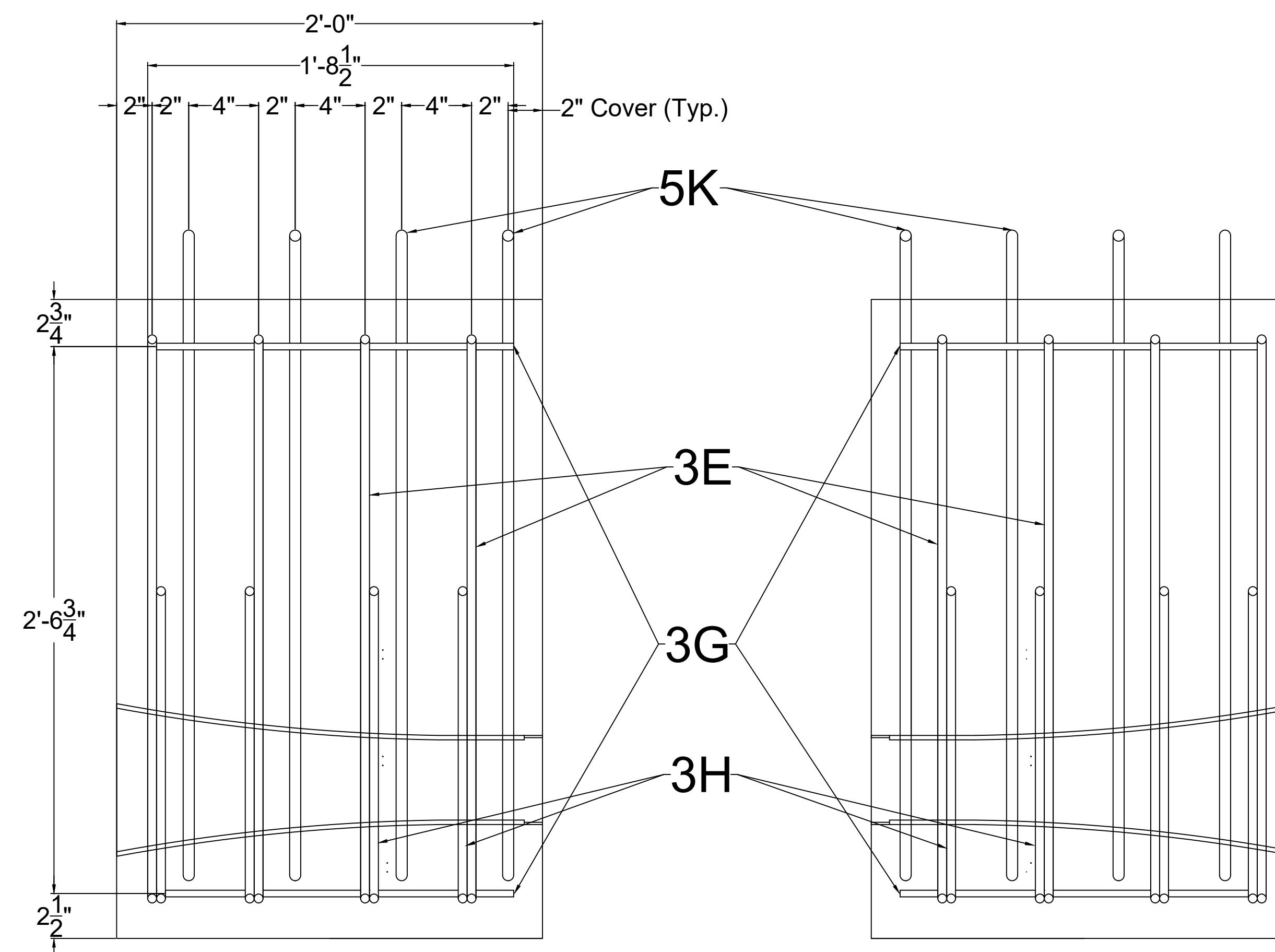
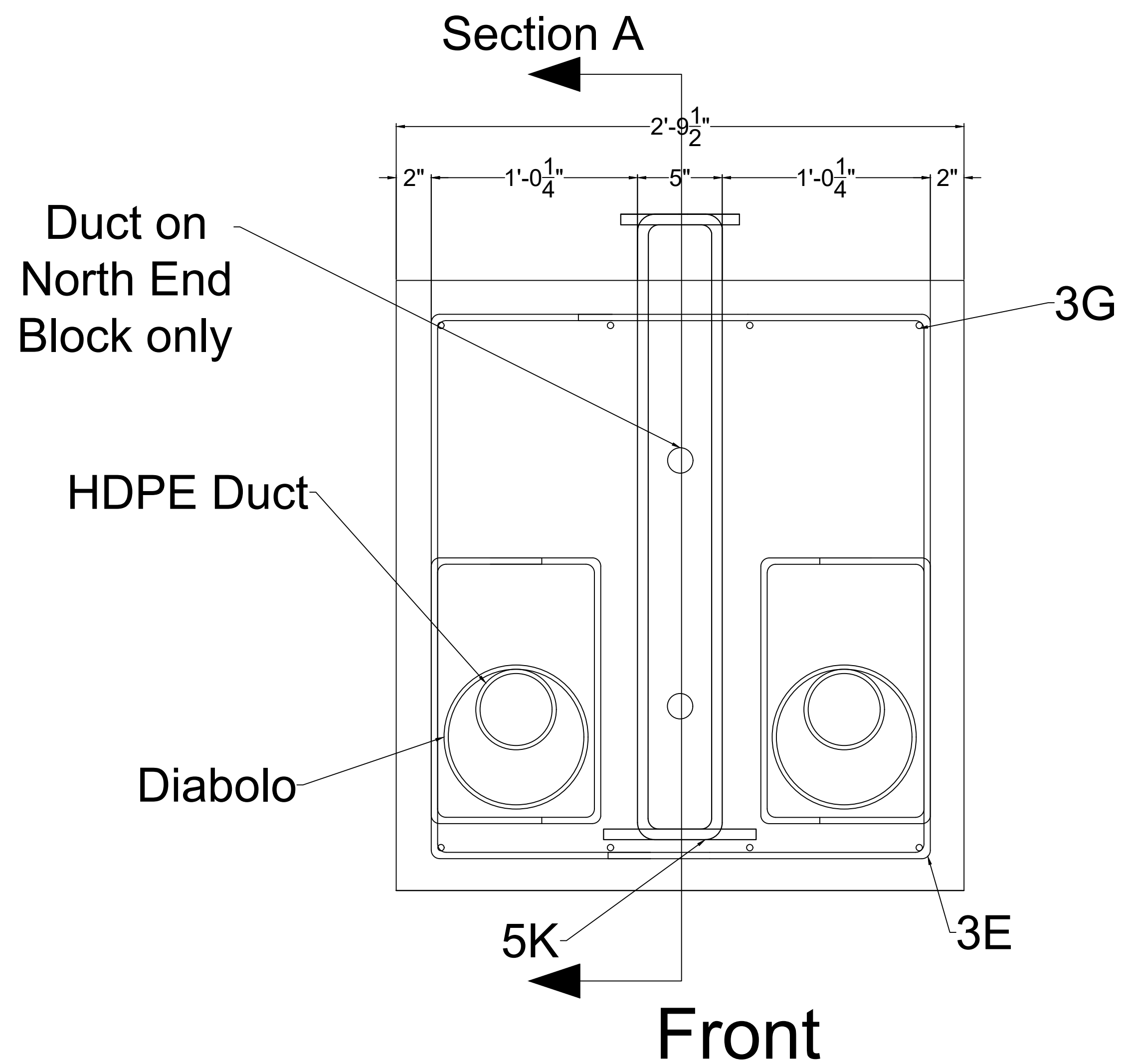
DEVIATOR BLOCK REINFORCEMENT SUMMARY

NAME	SIZE	QTY.	LENGTH
5K	#5	16	4'-0"
3E	#3	16	5'-11"
3G	#3	8	1'-8 1/2"
3H	#3	32	2'-4 1/4"

END CAP REINFORCEMENT SUMMARY

NAME	SIZE	QTY.	LENGTH
4M	#4	16	2'-4"
4N	#4	16	3'-6"
5F	#5	12	3'-7"
5H	#5	14	10'-3"
4A	#4	4	45'-8"
4B	#4	4	39'-9"
5S	#5	98	1'-8"

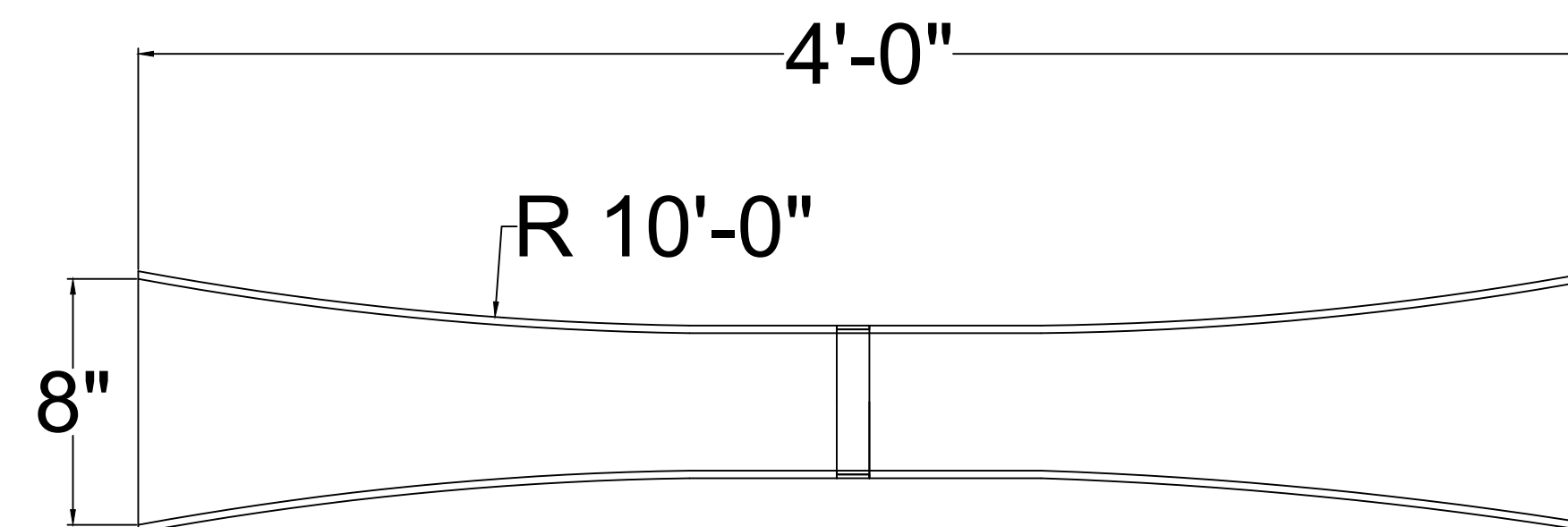




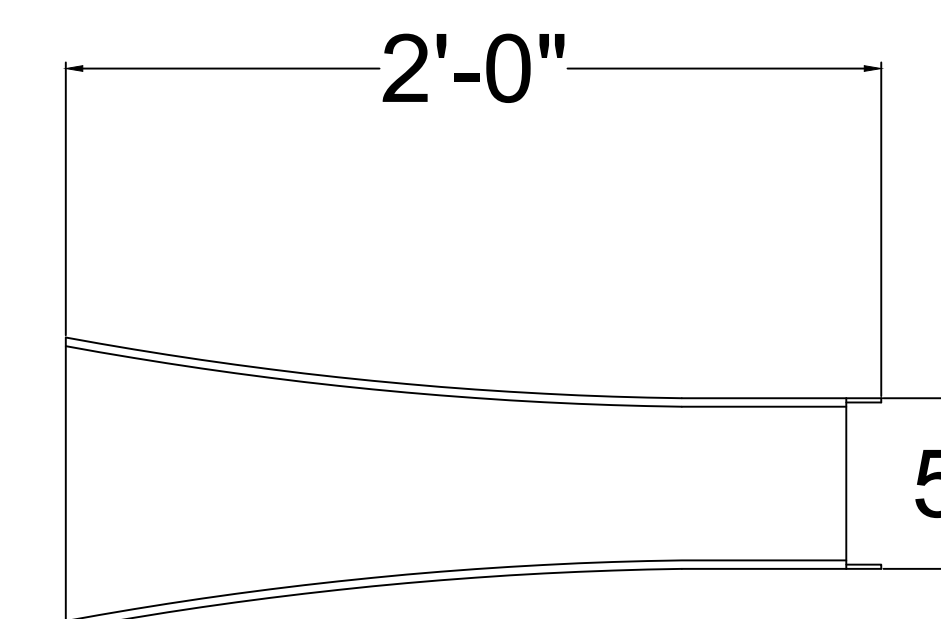
Section A

\*ERAU will 3D print Diabolo's

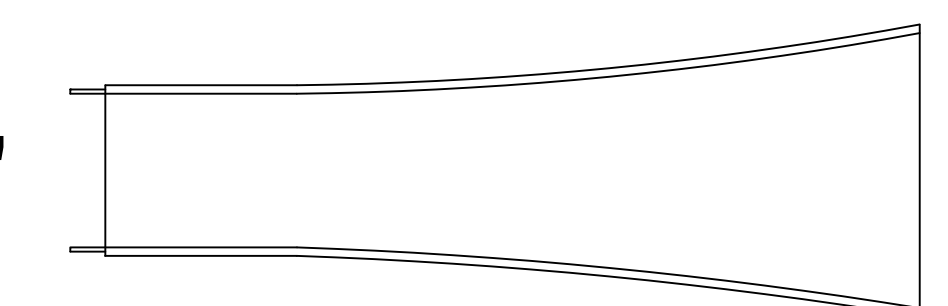
DEVIATOR BLOCK REINFORCEMENT SUMMARY			
NAME	SIZE	QTY.	LENGTH
5K	#5	16	4'-0"
3E	#3	16	5'-11"
3G	#3	8	1'-8 1/2"
3H	#3	32	2'-4 1/4"



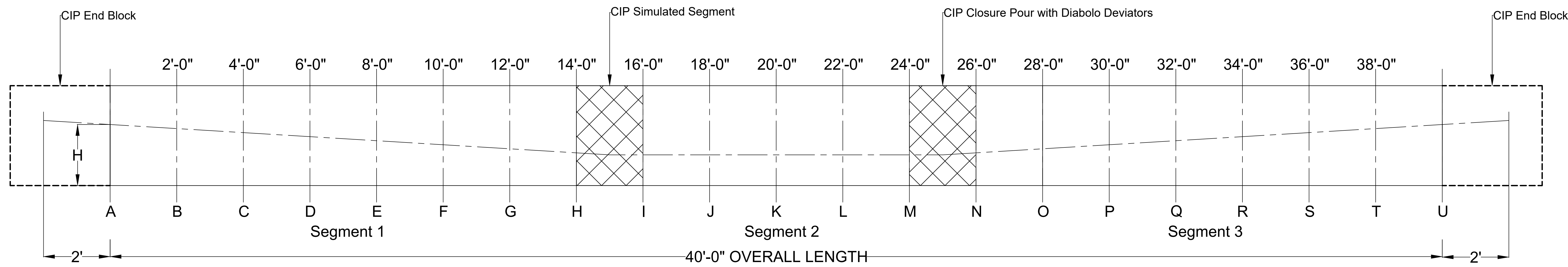
DIABOLO ASSEMBLY



FEMALE DIABOLO

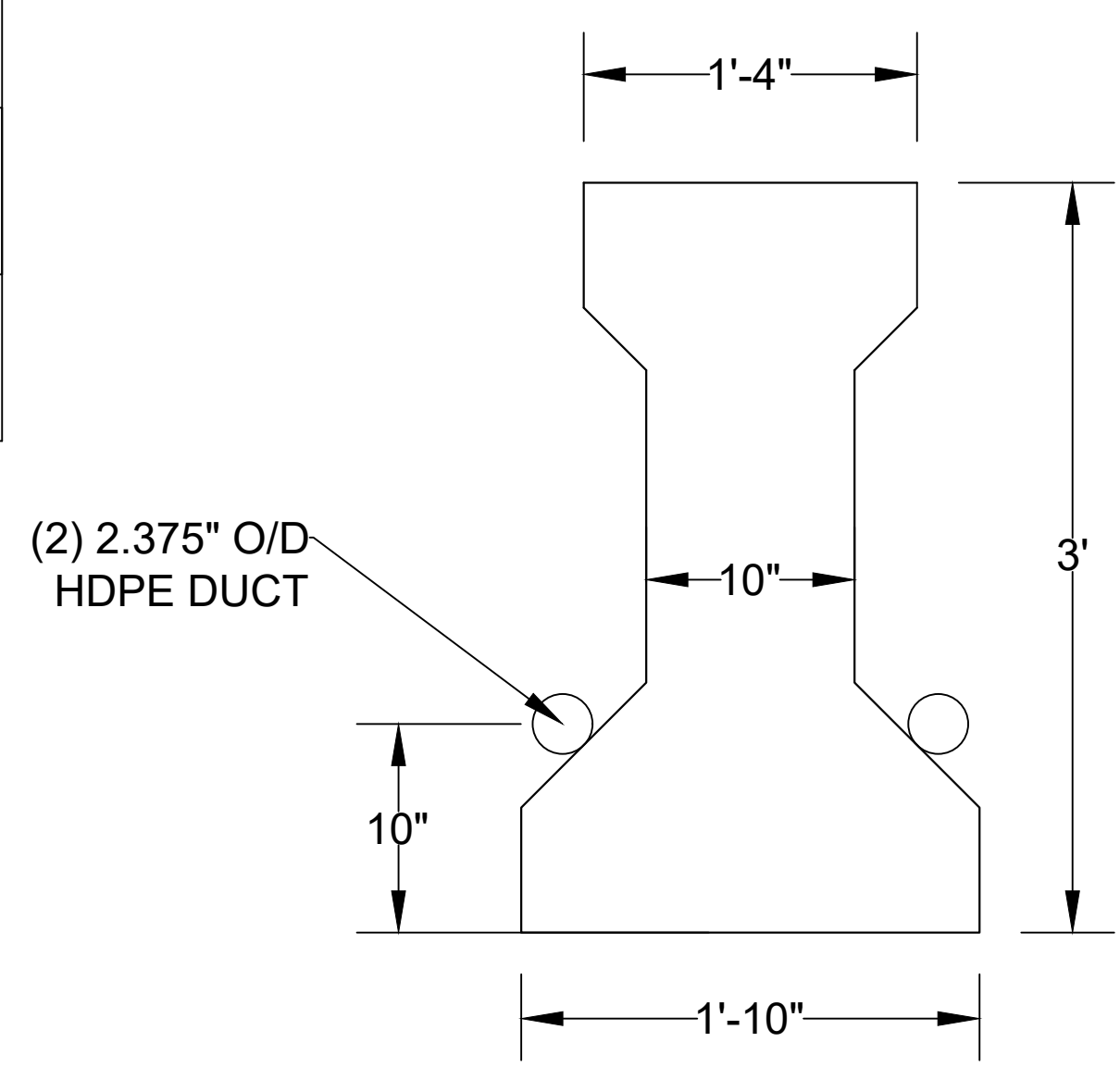


MALE DIABOLO

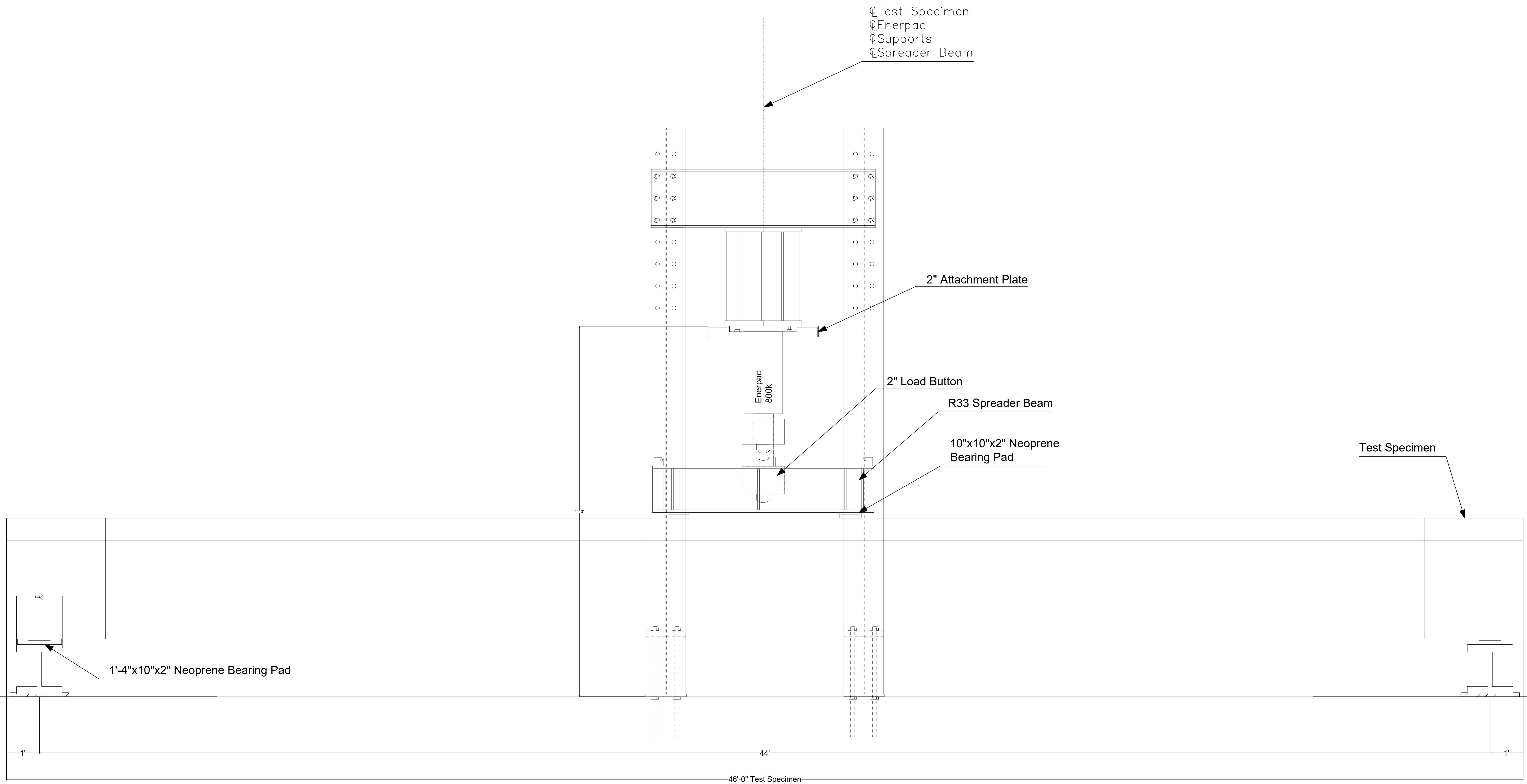


SECTION	A	B	C	D	E	F	G	H	I	J	K
DISTANCE FROM END OF GIRDER	0'-0"	2'-0"	4'-0"	6'-0"	8'-0"	10'-0"	12'-0"	14'-0"	16'-0"	18'-0"	20'-0"
H	1'-10"	1'-8 1/2"	1'-7"	1'-5 3/4"	1'-4 1/4"	1'-2 3/4"	1'-1 1/4"	11 3/4"	10"	10"	10"

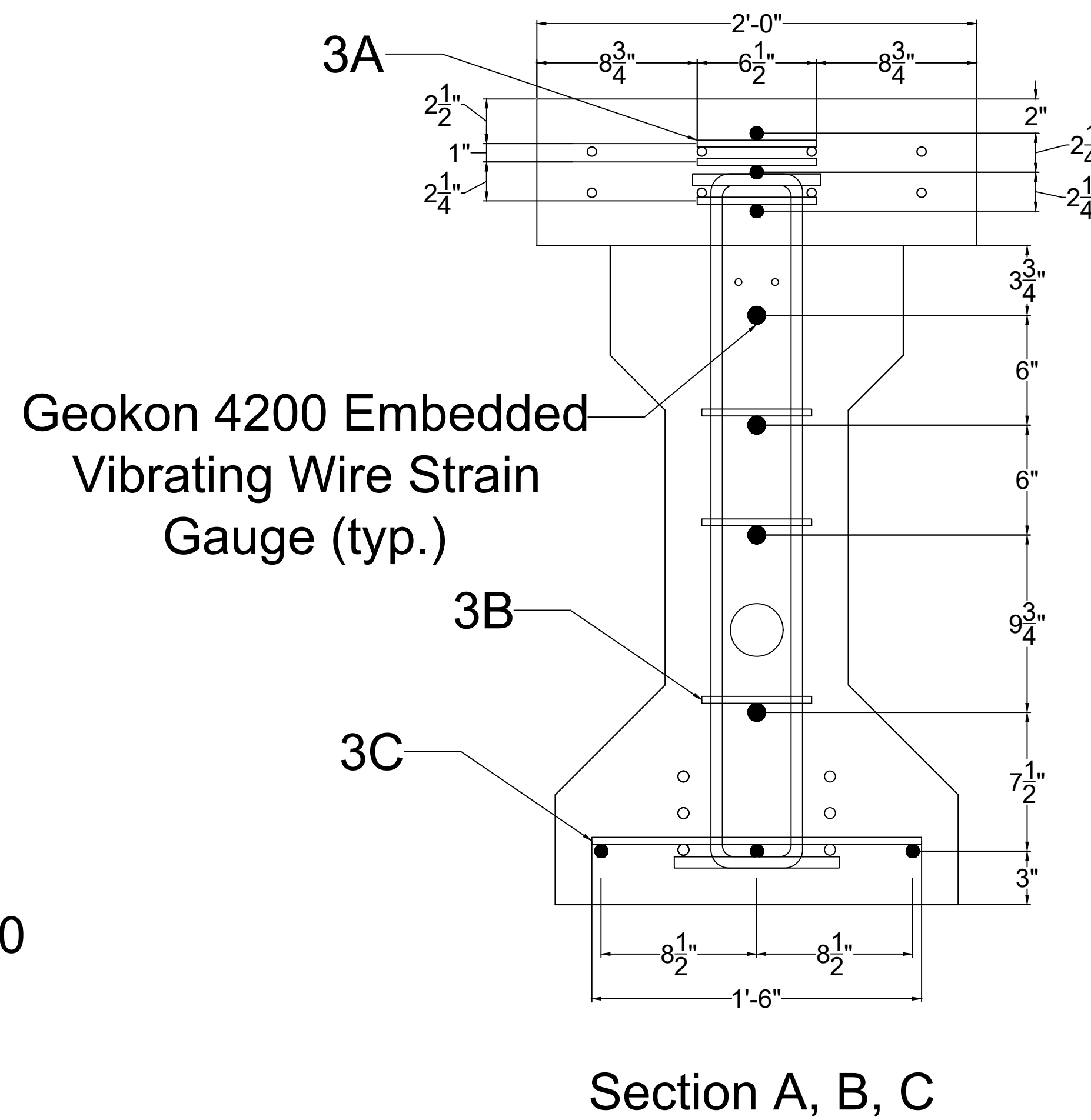
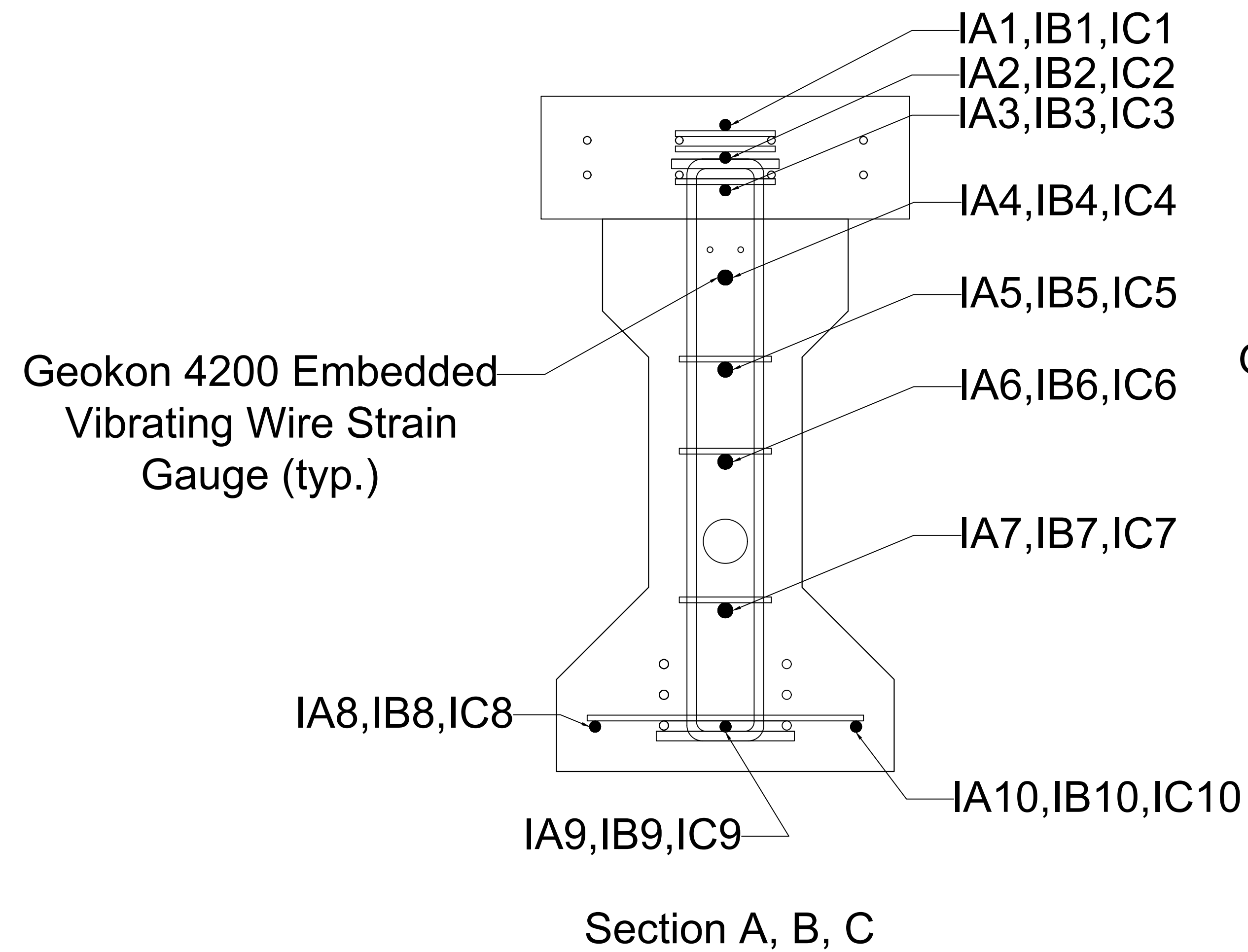
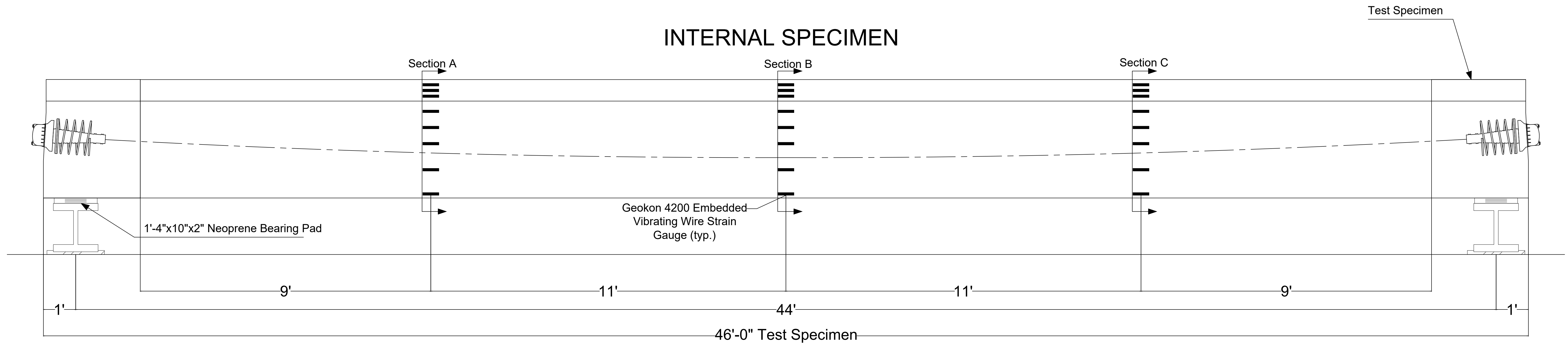
SECTION	L	M	N	O	P	Q	R	S	T	U
DISTANCE FROM END OF GIRDER	22'-0"	24'-0"	26'-0"	28'-0"	30'-0"	32'-0"	34'-0"	36'-0"	38'-0"	40'-0"
H	10"	10"	11 3/4"	1'-1 1/4"	1'-2 3/4"	1'-4 1/4"	1'-5 3/4"	1'-7"	1'-8 1/2"	1'-10"



SECTION K



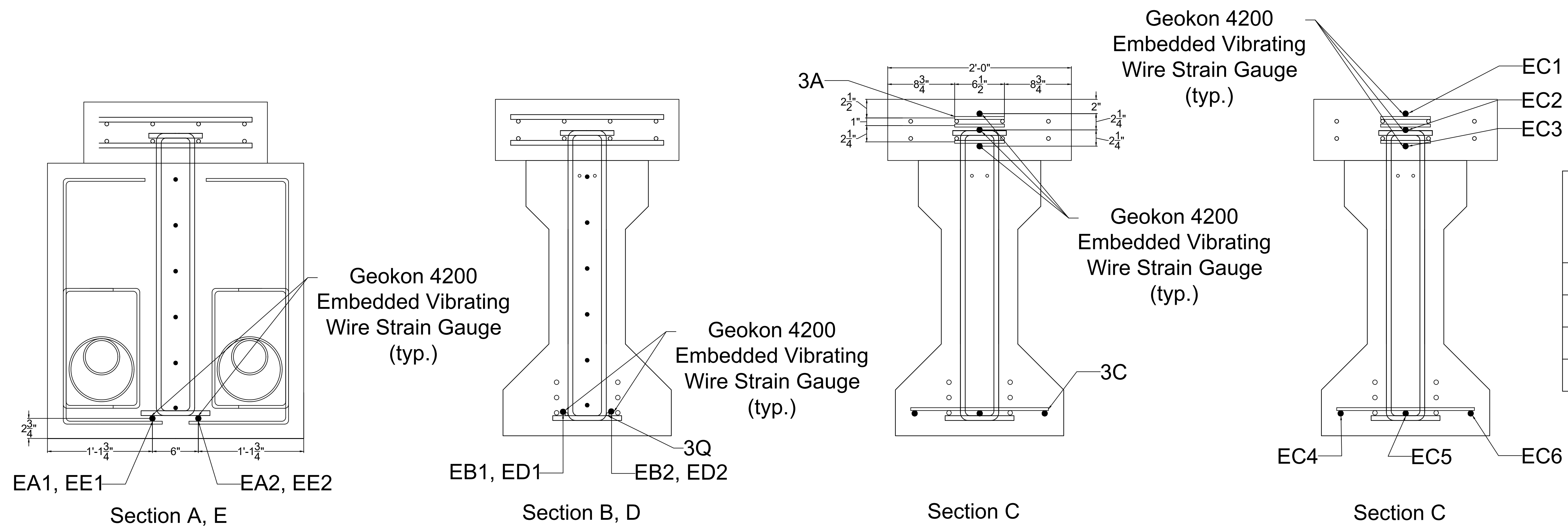
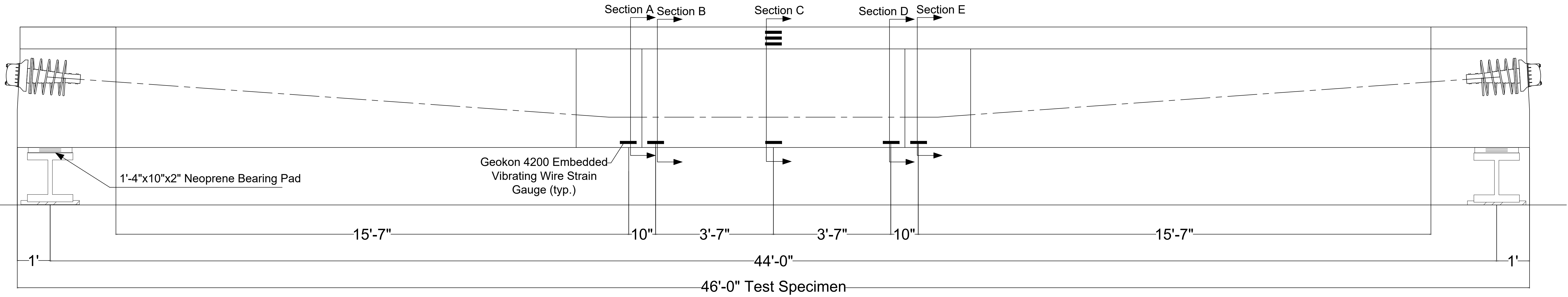
# INTERNAL SPECIMEN



## REINFORCEMENT SUMMARY

NAME	SIZE	QTY.	LENGTH
3A	#3	18	6 1/2"
3B	#3	18	6"
3C	#3	6	1'-6"

# EXTERNAL SPECIMEN



REINFORCEMENT SUMMARY			
NAME	SIZE	QTY.	LENGTH
3A	#3	6	6 1/2"
3Q	#3	2	10"
3C	#3	2	1'-6"

**FLEXURAL CAPACITY OF CONCRETE ELEMENTS  
WITH UNBONDED AND BONDED PRESTRESSING**

**Stressing (post-tensioning) Internal and External Specimen**

All beam specimens will be post-tensioned after their concrete endblocks reach the specified compressive strength. The hardware needed for the post-tensioning stage is listed in Table 1. Figure 1 shows the strand layout in the anchor heads. Target PT force corresponds to 75% of fpu. Table 2 presents the jacking forces and corresponding pressures on the multi-strand jack for the PT tendon.

Table 1. Required hardware for post-tensioning of internal & external beam specimen

Beam specimen	0.6-in. PT strands			Dead end	Live end
	No. of tendons	No. of strands/tendon	Length of strands (ft)		
INTERNAL	1	12	50	(1) alignment washer set (1) load cell (1) wedge plate/anchor head (12) wedges	(1) multi-strand jack (1) jack stressing plate (1) wedge plate/anchor head (12) wedges
EXTERNAL	2	6	50	(2) alignment washer set (2) load cell (2) wedge plate/anchor head (12) wedges	(2) multi-strand jack (2) jack stressing plate (2) wedge plate/anchor head (12) wedges

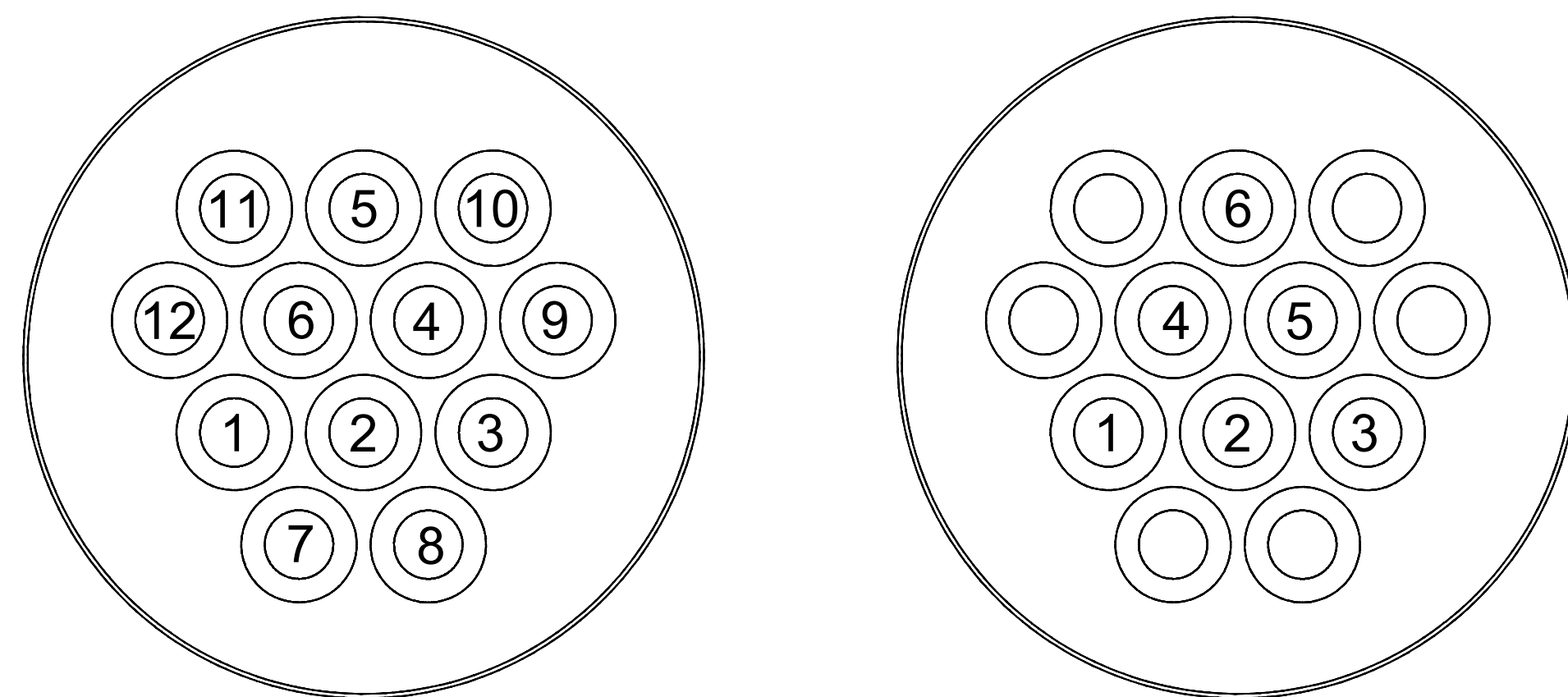


Figure 1. Layout of prestressing strands in post-tensioning anchor heads for Internal and External specimen

Post-tensioning procedure:

1. Push prestressing strands by hand into PT duct following the layouts provided in Figure 1 and preventing twisting of the strands. Use a cap at the end of the beam to prevent scratching.
2. Install alignment washer and load cell on dead end, using crane.
3. Install wedge plate on dead end (0° rotation pattern).
4. Install wedge plate on live end (0° rotation pattern).
5. Install wedges on strands at both ends of the specimen.
6. Set data acquisition to 2 Hz for the load cell.
7. Hoist the multi-strand jack into position for stressing the live end while ensuring proper alignment of the strands between the wedge plate and jack.
8. Use multi-strand jack at the live end to cinch load cell and washers into place.
9. Stress multi-strand jack to 5% of Pjack.
10. Stress multi-strand jack to 20% of Pjack and mark the initial elongation on the strands.
11. Continue stressing strands with increments of 20% of Pjack, mark and measure elongation on the strands.
12. Complete the jack stressing to stress multi-strand jack to 100% of Pjack, mark and measure the final elongation.

\* The external specimen tendons will be incrementally post-tensioned

		% of Pjack	5%	20%	40%	60%	80%	100%
Internal Specimen	Force (kip)		12	48	96	144	192	240
	Pressure (psi)	Master Gage						
		Gage A						
		Gage B						
External Specimen	Force (kip)		6	24	48	72	96	120
	Pressure (psi)	Master Gage						
		Gage A						
		Gage B						

\* Gauge pressure is TBD based on characteristics of multi-strand post tensioning jack



## Vacuum assist Injection of Civetex Wax into Internal Specimen

### Targets

Temp = between 212 deg F and 240 deg F

Tendon volume = 15 gal

Tendon volume + waste = 17 gal

Velocity = 40 - 70 ft/min

Flow = 15 gpm

Max pressure (at inlet) = 75 psi

Max pressure (at pump) = 145 psi

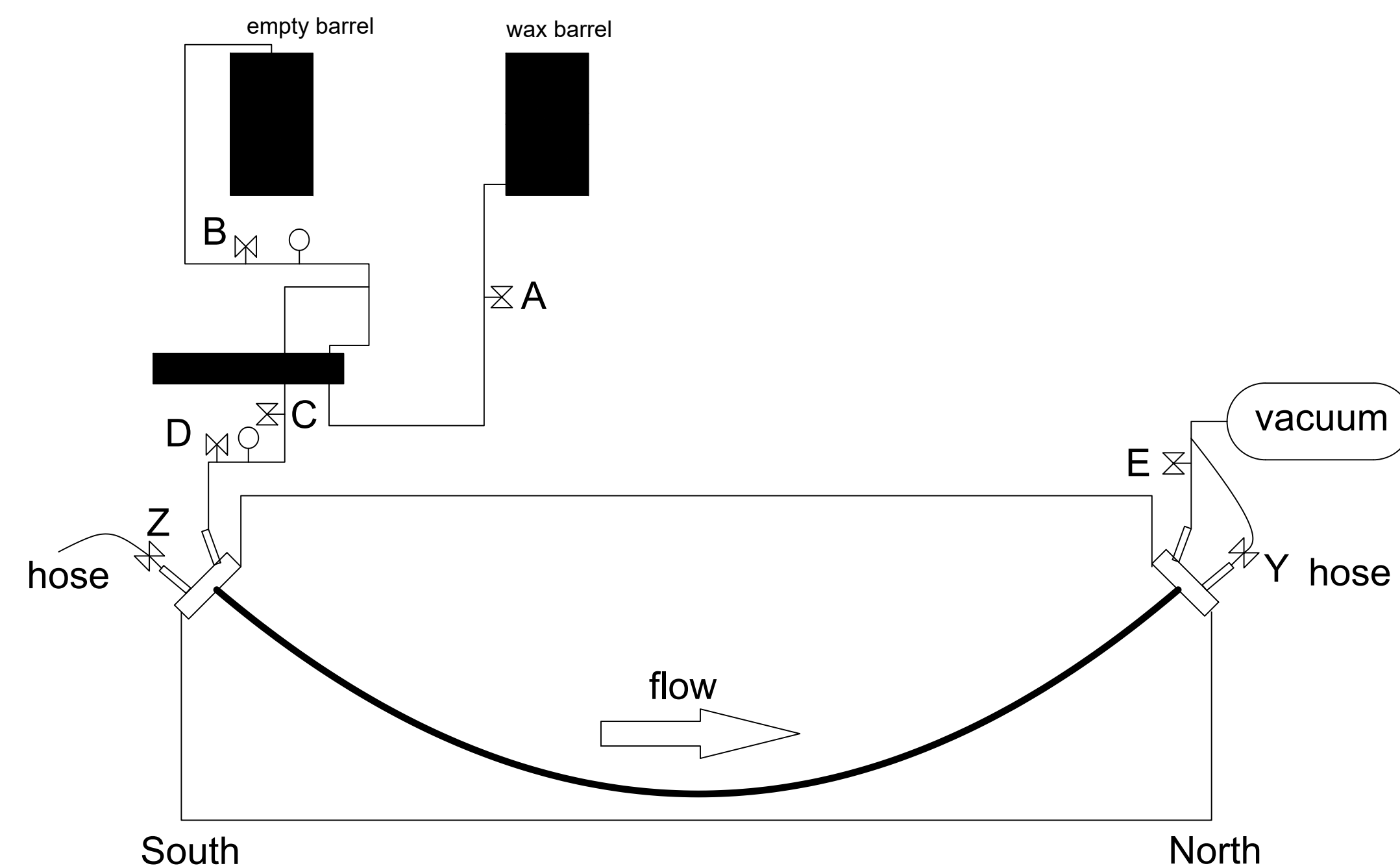


Figure 1—Schematic of set up for vacuum injection

### 1.1 Pre injection:

1. Air test: Increase tendon pressure with pump to 50 psi. Accept the test if pressure drop is less than 25 psi in 1 minute.
2. Vacuum test: Vacuum pump to 90% vacuum and stop the pump. Wait one minute. If the loss of vacuum after 1 minute exceeds 10%, repair leaks and repeat test, as necessary.
3. Heat filler to between 212 deg F and 240 deg F. Occasionally stir the filler material to ensure uniform temperature.
4. Ensure that all hoses are clear and preheated.
5. Position video cameras and LED lights at each of the windows to record injection.
6. Position personnel at both ends with buckets and wet towels. Personnel should be visible to the pump operator.

### 1.2 Injection:

1. Position drums adjacent to pump.
2. Place return line in empty barrel.

3. Connect discharge line to the pump. Leave the outlet end of the discharge line open.
4. Preheat the pump to 250° F.
5. Start data acquisition system and begin video recording.
6. Begin pulling a vacuum. Target vacuum: 28 in. Hg.
7. Before connecting the discharge line to the inlet valve, start the pump and discharge 2 gallons into a clean container. Make sure hose is discharging WAX, NO AIR.
8. Connect discharge line to inlet valve.
9. Open in line valves. Make sure cap valves are CLOSED.
10. Open discharge line valves and throttle pump to 10 on dial. Inject filler continuously at approximately 15 gpm.
11. When filler is noted in the discharge line, close outlet valve before filler enters vacuum pump.
12. Close inlet valve and stop pump. Lock in pressure = 30 - 45 psi.
13. Disconnect discharge line and reverse pump to pull filler from injection hose and deliver back into drum. Disconnect hoses and clean.

IR Readings	Temperature (F)
Start temp, barrel:	
Concrete surf temp:	
End temp, barrel:	

\*From IWC project by Dr. Hamilton & Dr. Consolazio

\*This Injection plan will be adequate for the internal and external beam specimens

Number of Tendons	Number of Strands/Tendon	Length of Duct	Volume of Duct (in <sup>3</sup> )	Volume of Strands (in <sup>3</sup> )	Volume of Filler (gal)
1	12	44'	5079.95	1791.46	15

## Vacuum assist Injection of Civetea Wax into External Specimen

### Targets

Temp = between 212 deg F and 240 deg F

Tendon volume = 6 gal

Tendon volume + waste = 8 gal

Velocity = 40 - 70 ft/min

Flow = 15 gpm

Max pressure (at inlet) = 75 psi

Max pressure (at pump) = 145 psi

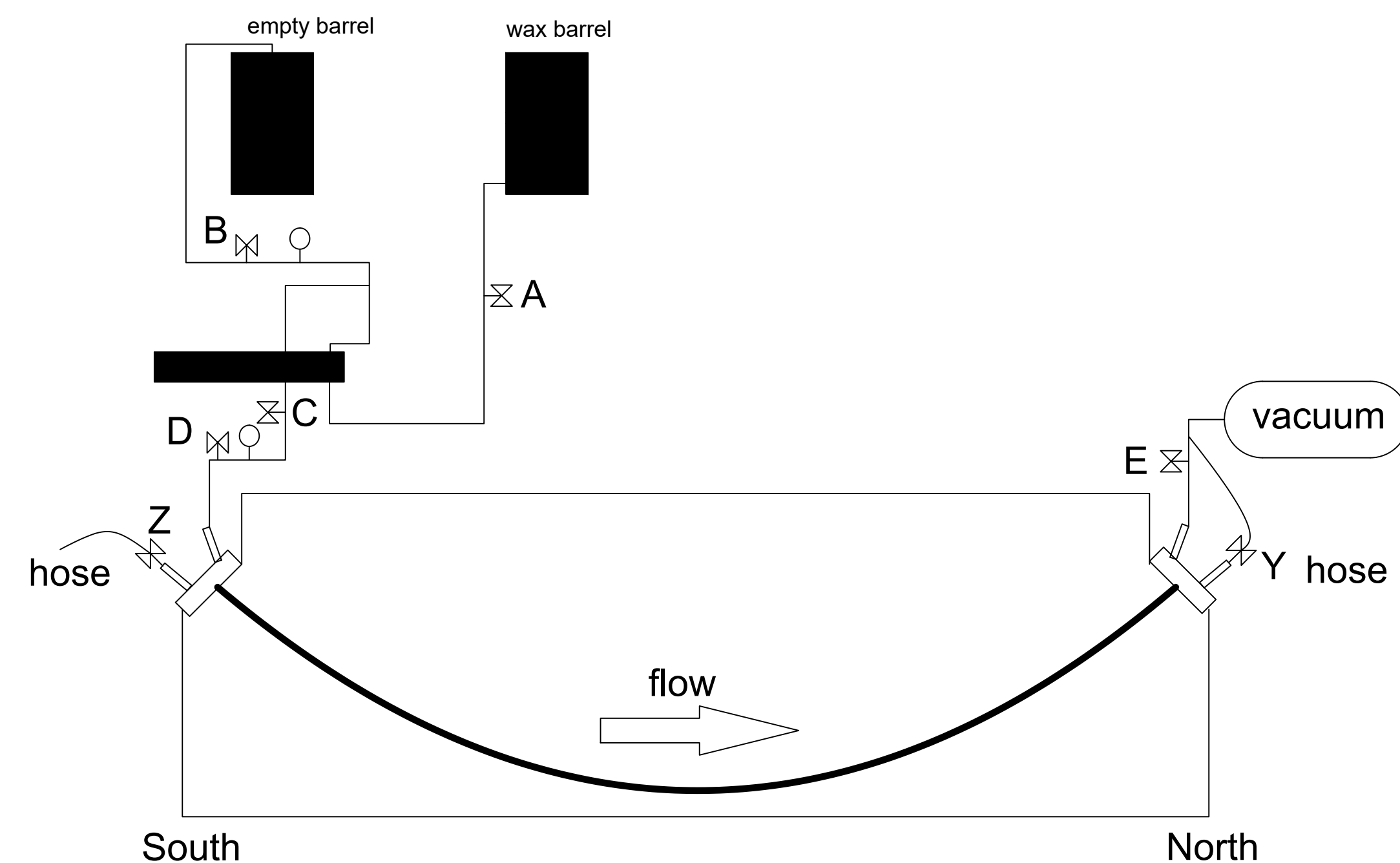


Figure 1—Schematic of set up for vacuum injection

### 1.1 Pre injection:

1. Air test: Increase tendon pressure with pump to 50 psi. Accept the test if pressure drop is less than 25 psi in 1 minute.
2. Vacuum test: Vacuum pump to 90% vacuum and stop the pump. Wait one minute. If the loss of vacuum after 1 minute exceeds 10%, repair leaks and repeat test, as necessary.
3. Heat filler to between 212 deg F and 240 deg F. Occasionally stir the filler material to ensure uniform temperature.
4. Ensure that all hoses are clear and preheated.
5. Position video cameras and LED lights at each of the windows to record injection.
6. Position personnel at both ends with buckets and wet towels. Personnel should be visible to the pump operator.

### 1.2 Injection:

1. Position drums adjacent to pump.
2. Place return line in empty barrel.

3. Connect discharge line to the pump. Leave the outlet end of the discharge line open.
4. Preheat the pump to 250° F.
5. Start data acquisition system and begin video recording.
6. Begin pulling a vacuum. Target vacuum: 28 in. Hg.
7. Before connecting the discharge line to the inlet valve, start the pump and discharge 2 gallons into a clean container. Make sure hose is discharging WAX, NO AIR.
8. Connect discharge line to inlet valve.
9. Open in line valves. Make sure cap valves are CLOSED.
10. Open discharge line valves and throttle pump to 10 on dial. Inject filler continuously at approximately 15 gpm.
11. When filler is noted in the discharge line, close outlet valve before filler enters vacuum pump.
12. Close inlet valve and stop pump. Lock in pressure = 30 - 45 psi.
13. Disconnect discharge line and reverse pump to pull filler from injection hose and deliver back into drum. Disconnect hoses and clean.

IR Readings	Temperature (F)
Start temp, barrel:	
Concrete surf temp:	
End temp, barrel:	

\*From IWC project by Dr. Hamilton & Dr. Consolazio

\*This Injection plan will be adequate for the internal and external beam specimens

Number of Tendons	Number of Strands/Tendon	Length of Duct	Per Tendon		
			Volume of Duct (in <sup>3</sup> )	Volume of Strands (in <sup>3</sup> )	Volume of Filler (gal)
2	6	44'	2339.11	895.73	6

Printed map

Write a description for your map.

